A Novel Dual-Functionalized Polycaprolactone : Synthesis, Surface Properties, and Its Controlled Release

張, 宇澄

https://doi.org/10.15017/1931870

出版情報：九州大学, 2017, 博士（工学）, 課程博士
バージョン：
権利関係：

A Novel Dual-Functionalized Polycaprolactone: Synthesis, Surface Properties, and Its Controlled Release

Yucheng Zhang

-Contents-

Chapter 1

Introduction

1.1. Polycaprolactone and its functionalization

Polycaprolactone (PCL) is one of the earliest kinds of polyester which was synthesized by Carothers' group in the early 1930s.[1] The ester groups in PCL endow it with a complete degradability.[2] PCL is a semi-crystalline polymer, and its crystallinity tends to decrease as the molecular weight increases. In recent years, attentions were drawn to PCL in tissue engineering, owing to their numerous advantages over other biopolymers.[3] These advantages include tailorable degradation kinetics, ideal mechanical properties, ease of shaping and manufacture, and drug capacity.[2] In addition, a number of drug delivery devices consisting of PCL already have FDA approval and CE Mark registration, which enables a faster avenue to market.[4]

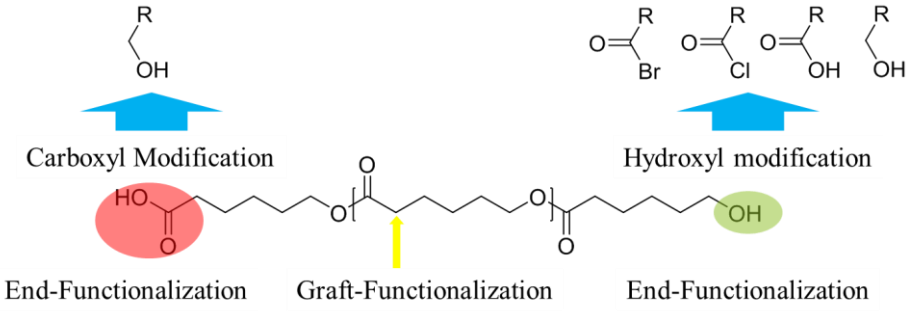

Figure 1.1. End-functionalization and graft-modification for PCL.

Although PCL is already applied in different biomedical applications, it has several drawbacks due to its undesirable inherent properties including slow degradation rate, poor blood compatibility, and hydrophobicity. The modification of PCL is an appealing approach for this material to obtain particular properties. Generally, the modification of PCL contains end-functionalization and graft-modification.[5] As shown in Figure 1.1, the terminal groups of PCL are hydroxyl or carboxyl group, which are determined by the polymerization methods. The end-functionalization could achieve via acylation (for hydroxyl groups) and esterification (for carboxyl groups). Two examples are shown in Figure 1.2, the macroinitiators of atom transfer radical polymerization (ATRP) and reversible addition-fragmentation chain transfer

polymerization (RAFT) are prepared from hydroxyl-terminated PCL via acylation and esterification, respectively. The further polymerization is able to obtain a well-designed copolymer. The graft-modification refers to the modification of PCL main chain, which is more desirable, since this approach is able to tailor the properties, including crystallinity, hydrophilicity, biodegradation rate, adhesion, and mechanical properties.[6] The common strategy of PCL graft-modification contains atom transfer radical addition (ATRA) and "click" reaction (Figure 1.3).[7] Both of them need a chloride substituted PCL segment which can be prepared by the random/block copolymerization with the monomer of α-chloride-ε-caprolactone (α-Cl-ε-CL).[8]

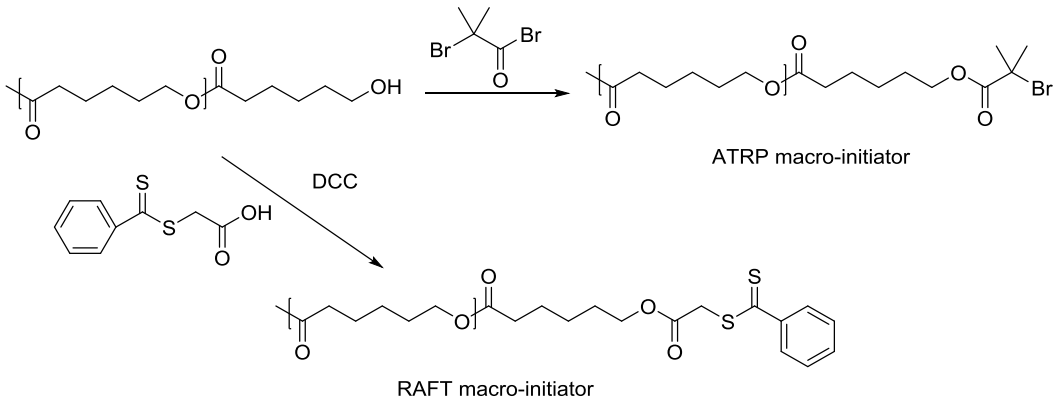

Figure 1.2. Synthesis of PCL-based ATRP macroinitiator and RAFT macroinitiator.

ATRA is based on the haloalkane-methacrylate addition. The reaction is performed with the presence of copper/ligand catalyst system which is similar to ATRP catalyst system (Figure 1.3).[9] This reaction can modify PCL with an acceptable conversion rate. However, the undesirable reduction of chloride units is regarded as drawbacks of this method.[7] Since ATRA is based on radical mechanism, the termination of radical including cross-linking and quenching induces the reduction of chloride units and increases the polydispersity index (PDI) of the resultant polymer (Figure 1.4).[9] "Click" reaction is based on copper-catalyzed 1,3-Huisgens cycloaddition between azides and alkynes. This method has several advantages, such as fast kinetics, mild condition, low

toxicity catalysis, and quantificational reaction.[8] However, the nitrine-based polymer or material is quite unstable and dangerous, and the reduction of azides units easily occurs during the storage.

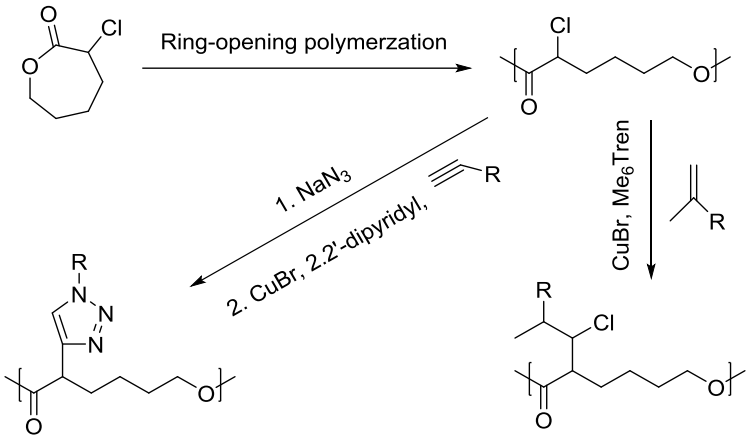

Figure 1.3. Methods of graft-modification for α-substituted PCL.

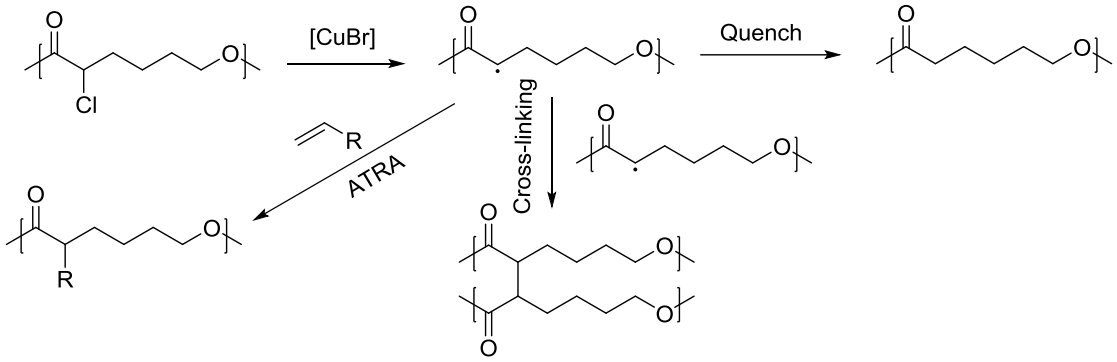

Figure 1.4. Potential side reaction of ATRA.

1.2. Anti-fouling properties and phosphocholine modification

Fouling is used to describe the phenomenon that biological molecules non-specifically adsorb onto the surface of biomaterials on their surfaces, resulting in the reduced performance of such material. Hence, a lot of research has been put forward to realize an anti-fouling surface, and summarized in Table 1.1.[10]

The human tissue- and fluid-covered surface are considered as the best method since the implanted materials with this coating are recognized as normal tissues without any further pathological changes.[20] However, the complicated procedure and long manufacturing period make

it difficult for the extensive application. Although hydrophobic surface shows favorable performance *in vitro* test, the *in vivo* effectiveness still remains doubtful.[13,14] The therapeutic eluting surface is a temporary method for the anti-fouling property.[19] After the complete drug release, the surface undergoes fouling again. The denaturation of biomolecules is the main shortage for biomolecules functionalization method.[18] Although the use of chitosan which is cationic charged natural polymer exhibits good anti-fouling properties, however, other materials give even worse results.[17] The hydrophilic surface benefits from the strong hydration effect which increases the energetic penalty of removing surface binding water for protein attachments. Although zwitterionic-charged surface shares similar principle with a hydrophilic surface, a stronger hydrophilicity and water-binding effect suggested that this method is more promising.[15,16]

Table 1.1. Different Methods to Obtain Anti-fouling Surface

Modification	Approach	Typical example	Reference
Hydrophilic	Hydration layer	PEG[a]	11, 12
Hydrophobic	Repel the attachment of fouling	Fluorocarbon	13, 14
Zwitterionic	Hydration layer	PC, PMAPS[b]	15, 16
Cationic	Broad-spectrum antimicrobial activity	Chitosan	17
Biomolecules	Create a barrier between fouling and device surface	Peptides and Heparin	18
Therapeutic eluting	Localized drug release	Anti-proliferative drug	19
Human tissues covered	"Coating" of healthy cell		20

[a]PEG is the abbreviation of poly(ethylene oxide); [b]PC is phosphorylcholine and PMAPS is poly(3-[dimethyl(2′-methacryloyloxyethyl)ammonio]propanesulfonate).

During the last two decades, the excellent performance of phosphorylcholine (PC) modification is gradually recognized by researchers.[21] PC presents at the end of phospholipids and

the exterior surfaces of cell membranes.[21,22] The PC-conjugations have been widely accepted as an effective mean to improve the anti-fouling property for different polymers and surfaces.[23,24] Notably, the commercialization of polymerizable PC-based monomer with high purity and polymerization activities, 2-methacryloyloxyethyl phosphorylcholine (MPC), has stimulated the expansive research of this material.[24] Surface modification using PMPC brush showed incredible anti-fouling property and biocompatibility. Brash et al. reported the most significant values: less than 5 ng/cm^2 for fibrinogen adsorption from the plasma and whole blood using a high density "graft-from" PMPC-based polymer brush.[25]

1.3. Surface functionalization and catechol groups

With rapid medical technological advances, a lot of implant devices were introduced to different surgeries including sensory, neurological, cardiovascular, orthopedic, contraception, cosmetic, and organs.[17] Since they directly contact with human tissue and body fluid, the biocompatibility of such material is extremely important.[26] Although the preparation of biocompatible materials with suitable mechanical properties, shape, and size is difficult, new method focusing on the tailoring the surface properties without changing of mechanical properties has received increasing attention. This method can minimize the impact on the mechanical properties of different devices and endow the modified device with desirable surface properties.[27]

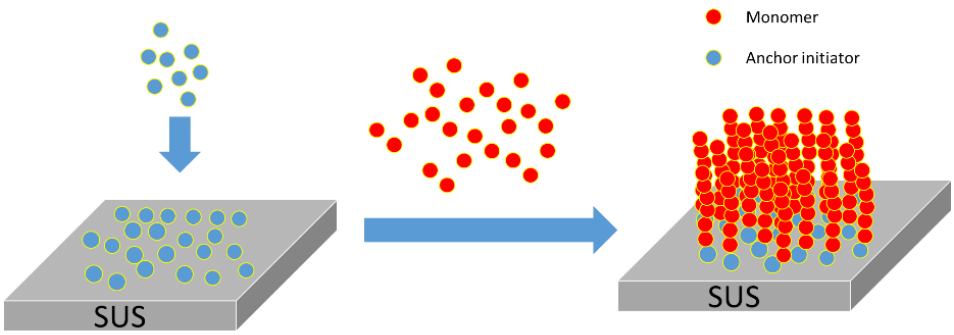

Figure 1.5. "Graft-from" method for surface modification.

The surface functionalization contains “graft-to” method (Figure 1.5) and “graft-from” method (Figure 1.6).[28] In “grafting-from” method, a molecule with initiator was firstly immobilized onto the surface. The further polymerization modifies the surface by selective functional monomers. This method is preferential to get high density and/or high thickness layer.[28,29] Since this method involves in-situ polymerization, the size, and shape of the samples are restricted, the chemical inertness is necessary to avoid the undesirable changes, and the experiment condition and solution selection should be careful to avoid the introduction of toxicity compounds.[30]

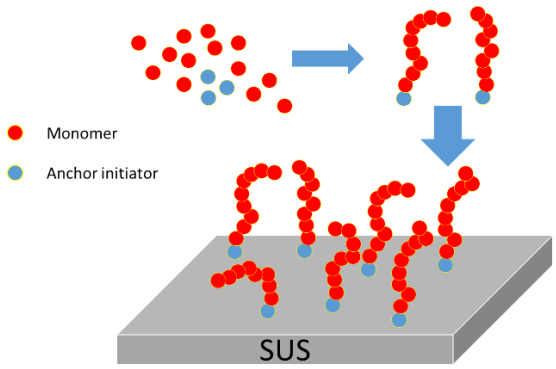

Figure 1.6. “Graft-to” method for surface modification.

The “grafting-to” method is the functionalization of surfaces using a well-designed polymer with anchor groups. This approach involves a simple dip-and-risen procedure, which is the cost-effective and ease of size. Moreover, the molecular weight distributions, special structure, and functionalities can be easily controlled by a well-designed synthesis strategy of the polymer with anchor groups. However, the grafting density and thickness of resultant films are lower than that obtained from “graft-from” method.[29]

Anchor groups which immobilize the surface modifier onto the substrate, play an important role in both “graft-from” and “graft-to” methods. Table 1.2 summarized some anchor groups utilized to immobilize the molecule or polymer onto varied substrates.

Table 1.2. Anchor Groups in Surface Modification

Anchor group	Surface	Driven Force	Reference
Fatty Acids	Metal surface	Electrovalent bond	31, 32
Organosilicon	Hydroxylated surface[a]	Formation of polysiloxane	33, 34
Organosulfur	Metal surface[b]	Formation of multiple bonds	35
Phosphoric acid	Metal oxide surface	Bonding with surface hydroxyl group	36, 37
Catechol	Metal oxide surface	Complicated interactions[c]	38

[a]Hydroxylated surface includes SiO_2, Al_2O_3, quartz, glass, mica, etc.; [b]Matal surface includes Ag, Cu, Pt, Hg, Au, etc.; [c]Catechol groups show strong adhesion properties including hydrogen bonding, metal/metal oxide coordination, and oxidative cross-linking.

Organosilicon and organosulfur are available for silicon-based material and precious metal, respectively.[33-35] Other methods are suited for the stainless steel, titanium, iron, and aluminum which are widely used in the biomedical device.[31,36-37] Some comprehensive research showed phosphoric acid possesses the strongest adhesion, but the internet acidity for phosphoric acid leads to the corrosion of the metal surface.[37] The fatty acids with the weakest adhesion is only applied in few fields.[8] Catechol modification with non-acid, flexible preparation, and good solubility has received increasing attention.[39] Catechol groups which exist in holdfast proteins of marine mussels, are the reason why such animals can adhere to the wet rock or ships.[40] The most adhesive proteins isolated from mussel (Mytilus sp.) holdfasts (byssus), mfp-3 and mfp-5 are catechol-rich.[40] A growing evidence implies that the catechol modification endows various natural and synthetic polymers with wet adhesion.[41] Some theory has been put forward to explain the mechanism of catechol adhesion, such as catechol-mediated bidentate hydrogen bonding, metal/metal oxide coordination, or oxidative cross-linking (Figure 1.7 showed the mechanisms of crosslinking of

catechol groups).[42] Although the mechanism of these adhesion properties still remains controversial, broadly applicable research has sufficiently supported its excellent adhesion property of this material.

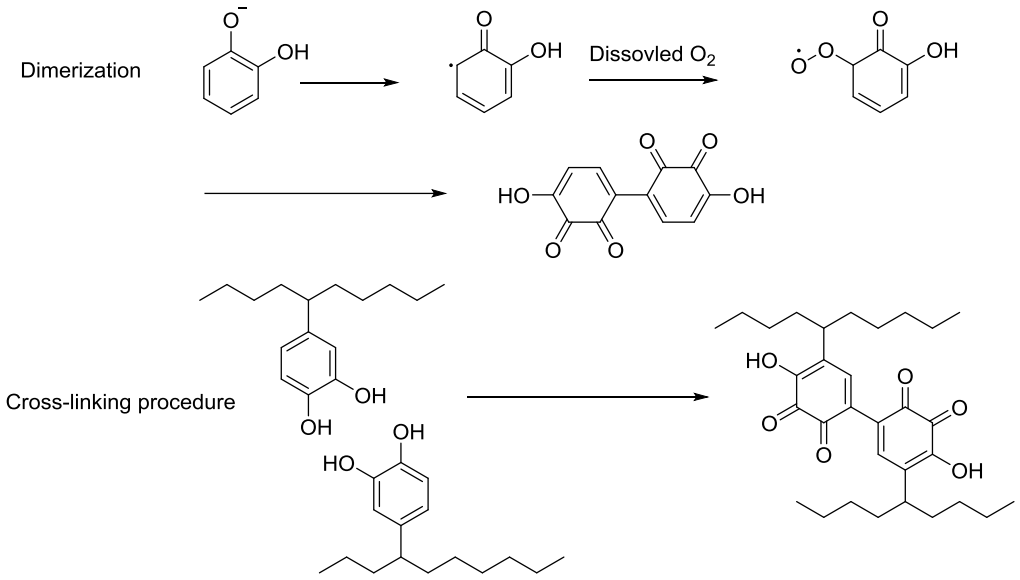

Figure 1.7. Dimerization and the cross-linking between catechol groups in different segments.[42]

1.4. Surface reorganization and crystallization

The interfacial structure of PC-contained amphiphilic surface modifier frequently reorganizes under hydrophobic/hydrophilic conditions, and shows a great impact on its surface properties.[21,22] PMPC-contained amphiphilic surface modifier with PC-segregated outmost surface in water results from the inherent strong hydrophilic interaction and hydration effect of PC groups. However, during the storage, the hydrophobic chain will move out and cover the outmost surface gradually since they possess much lower surface free energy than PC groups.[43] In another word, the surface of PMPC-contained amphiphilic polymeric films is switched between the hydrophobic part and hydrophilic PC under different conditions (Figure 1.8). In one research, the U937 macrophage cell was used to evaluate the surface PC density since this cell can adhere to PC surface selectively. There is an obvious reduction of the cell number which is adhering to coated films when changing the surface from fresh coated to the stored under normal ambient condition.

This research provides convincing evidence that the surface reorganization might induce the irreversible migration of the PC groups toward bulk state (Figure 1.8).[25]

Crystalline side chain has been utilized to address this phenomenon. Crystallization is a process that polymer chains fold together and form ordered regions.[44] Relatively strong intermolecular forces in crystalline polymer prevent softening even above the glass transition temperature, which indicated the mobility of polymer chain in the semi-crystalline polymer is low.[45] The predictable chain fold structure, relatively low mobility, and highly ordered orientation lead to a wide application in the surface orientated structure.[46, 47]

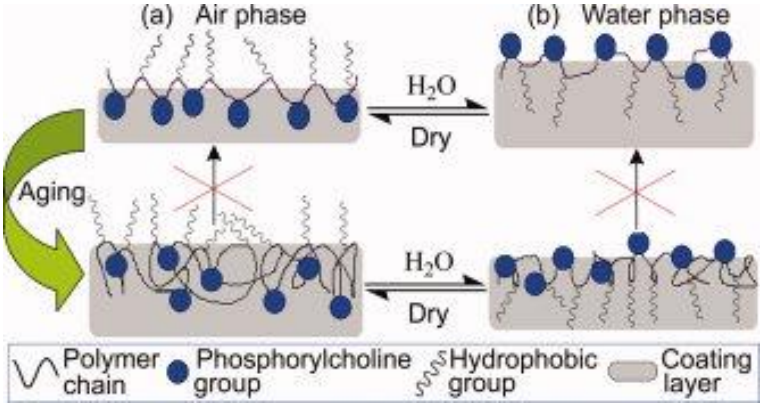

Figure 1.8. Surface reorganization in PC-based amphiphilic copolymers.[43]

1.5. Cardiovascular disease and drug-eluting stent

Cardiovascular disease which is also known as heart disease, influences life quality severely. This disease is not found relating to atherosclerosis in the blood vascular until 1856. Atherosclerosis is a condition that develops when plaque builds up in the walls of the arteries. Obviously, atherosclerosis makes blood more difficult to flow through. In the worst case, the heart attack and heart stroke take place with very high mortality.[48] During the last decades, percutaneous transluminal angioplasty (PTA) has emerged as an alternative treatment. This surgery uses a small, flexible plastic tube or catheter, with a "balloon" at the end of it. When the tube arrives at the lesion, it inflates to open the blood vessel, and normal blood flow is restored. This treatment

benefits from the minimally invasive property, immediate restoration of blood flow, and symptoms dissipation.[49]

Despite the success of coronary stenting surgery, in-stent restenosis continues to limit its long-term effectiveness.[50] In-stent restenosis refers to re-narrowing of a blood vessel after stent implantation.[13] The proliferation and migration of smooth muscle cells are considered as the main mechanisms of in-stent restenosis. To address this issues, the concept of using coronary stents for localized delivery of anti-proliferative drugs with programmed pharmacokinetics is an appealing solution.[51] Stent with localized drug delivery properties is also known as drug-eluting stents (DESs).[52] The DESs contain one special drug reservoir which ensures a programmed drug release. Since they contact with the coronary artery wall, anti-proliferation drugs can be directly delivered to the target site, resulting in a therapeutically effective drug concentration in the surrounding tissues. This approach minimizes the systemic drug concertation, which reduces the risk of systemic toxicity. Despite its relatively short history, DESs have already made significant impacts in the PTA treatment, whereby 8 kinds of different FDA-approved DESs are already clinically available, and more DESs are expected to be developed in the near future.[53]

The driving force of the drug-eluting contains diffusion, degradation/dissolution, and ion-exchange. The diffusion-controlled release uses a polymer layer functions as a barrier to reduce the diffusion of the drug and achieve a controlled release.[54-55] The drug release rate of diffusion-controlled drug release at steady state remains constant (zero-order release). While the drug releases from the matrix, the drug is away from the surface, resulting in non-zero-order release.[52] Although the non-degradable polymer is utilized in this approach, the use of degradable polymer can reduce the late adverse events and pathologic reactions.[56] Moreover, a thin polymer layer which is so-called rate-controlling membrane, can be prepared onto the surface of the

drug/polymer matrix. This layer can tailor the drug release kinetics.[57] The use of this layer reduces the initial burst release significantly and achieve the long-term drug release.[58] Dissolution/degradation-controlled release is based on dissolution or degradation of a polymer/drug matrix membrane.[59] Since the water-soluble polymer dissolved rather quickly, the hydrophobic biodegradable polyester or amphiphilic polymer is the most common material. The drug release of this mechanism is significantly influenced by the degradation rate or dissolution rate of polymer/drug matrix membrane.[58] Ion-exchange controlled release refers to the release of ionized drugs which are bonded to the polymer layer through the electrovalent bond in advance. After implantation, the surface ion exchange takes place between bonded drug and the ion in the blood (i.e. Na^+, K^+, and Cl^-). Although ion exchange is a promising approach for DNA-controlled release, the neutral drug is not available for this notion.[52]

1.6. Suggestion and content

In this thesis, a novel PCL-based drug eluting coating was developed, including the top PC-based rate-controlling membrane, middle drug-loading polymer layer, and bottom PC thin film (Figure 1.9). The top PC-based rate-controlling membrane can control the diffusivity of the drug loaded in the polymer film and improve the surface biocompatibility. The middle drug-loaded layer consists of PCL and dopamine-modified PCL to stabilize drugs. The bottom PC thin film endow stainless steel sheet with a good biocompatibility, after the drug-eluting layer is fully degraded. The preparation of dopamine and PC dual-functionalized PCL designed as PMPC-*block*-poly(α-dopamine-ε-caprolactone)-*block*-PCL-*block*-poly(α-dopamine-ε-caprolacton e)-*block*-PMPC [PCL-*b*-(PCL-DOPA-*b*-PMPC)$_2$] and (PCL-*co*-PCL-DOPA)-*b*-(PMPC)$_2$ was described in Chapter 2. Although they show similar structure, the crystallinity of PCL segments in PCL-*b*-(PCL-DOPA-*b*-PMPC)$_2$ and (PCL-*co*-PCL-DOPA)-*b*-(PMPC)$_2$ is different, which might have influence on the surface reorganization. The adsorption behavior of

PCL-*b*-(PCL-DOPA-*b*-PMPC)$_2$ was clarified using SUS as the template and described in Chapter 3. The interfacial structure changes under hydrophobic/hydrophilic condition was evaluated in Chapter 4. In Chapter 5, drug-loaded polymer films were prepared, and the role of catechol-modified PCL and PCL-*b*-(PCL-DOPA-*b*-PMPC)$_2$ rate-controlling membranes were verified by *in vitro* drug release experiment.

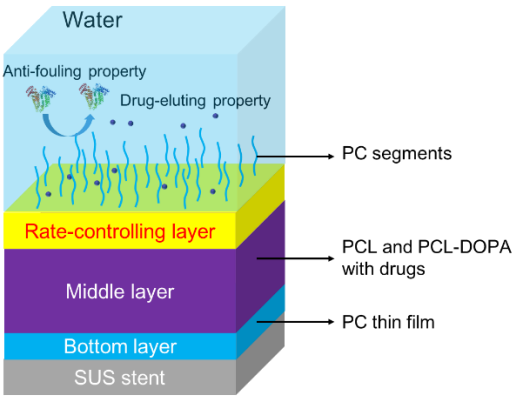

Figure 1.9. Design of tri-layer drug-eluting coating

1.7. Reference

1. van Natta, F. J.; Hill, J. W.; Carothers, W. H. Studies of Polymerization and Ring Formation. XXIII.[1] ε-Caprolactone and its Polymers. *Journal of the American Chemical Society* **1934,** *56*, 455-457.

2. Jagur-Grodzinski, J. Polymers for Tissue Engineering, Medical Devices, and Regenerative Medicine. Concise General Review of Recent Studies. *Polymers for Advanced Technologies* **2006,** *17* (6), 395-418.

3. Grant, R.; Hay, D.; Callanan, A. A Novel Drug Induced Hybrid Electrospun PCL-Cell Derived ECM Scaffold for Liver Tissue Engineering. *Tissue Engineering Part A* **2017,** *23* (13-14), 650-662.

4. Gilmartin, D. J.; Soon, A.; Thrasivoulou, C.; Phillips, A. R.; Jayasinghe, S. N.; Becker, D. L. Sustained Release of Cx43 Antisense Oligodeoxynucleotides from Coated Collagen Scaffolds Promotes Wound Healing. *Advanced Healthcare Materials* **2016,** *5* (14), 1786-1799.

5. Du, J.; Armes, S. P. Preparation of Biocompatible Zwitterionic Block Copolymer Vesicles by Direct Dissolution in Water and Subsequent Silicification within Their Membranes. *Langmuir* **2009,** *25* (16), 9564-9570.

6. McFadden, E. P.; Stabile, E.; Regar, E.; Cheneau, E.; Ong, A. T. L.; Kinnaird, T.; Suddath, W. O.; Weissman, N. J.; Torguson, R.; Kent, K. M.; Pichard, A. D.; Satler, L. F.; Waksman, R.; Serruys, P. W. Late Thrombosis in Drug-Eluting Coronary Stents after Discontinuation of Antiplatelet Therapy. *The Lancet* **2004,** *364* (9444), 1519-1521.

7. Riva, R.; Lenoir, S.; Jérôme, R.; Lecomte, P. Functionalization of Poly(ε-Caprolactone) by Pendant Hydroxyl, Carboxylic Acid and Epoxide Groups by Atom Transfer Radical Addition. *Polymer* **2005,** *46* (19), 8511-8518.

8. Zeininger, L.; Portilla, L.; Halik, M.; Hirsch, A. Quantitative Determination and Comparison of the Surface Binding of Phosphonic Acid, Carboxylic Acid, and Catechol Ligands on TiO_2 Nanoparticles. *Chemistry* **2016,** *22* (38), 13506-13512.

9. Nguyen, J. D.; Tucker, J. W.; Konieczynska, M. D.; Stephenson, C. R. Intermolecular Atom Transfer Radical Addition to Olefins Mediated by Oxidative Quenching of Photoredox Catalysts. *Journal of the American Chemical Society* **2011,** *133* (12), 4160-4163.

10. O'Brien, B.; Carroll, W. The Evolution of Cardiovascular Stent Materials and Surfaces in Response to Clinical Drivers: A Review. *Acta Biomaterialia* **2009,** *5* (4), 945-958.

11. Liu, Z.; Dong, K.; Liu, J.; Han, X.; Ren, J.; Qu, X. Anti-Biofouling Polymer-Decorated Lutetium-Based Nanoparticulate Contrast Agents for *In Vivo* High-Resolution Trimodal Imaging. *Small* **2014,** *10* (12), 2429-2438.

12. Spasojevic, M.; Paredes-Juarez, G. A.; Vorenkamp, J.; de Haan, B. J.; Schouten, A. J.; de Vos, P. Reduction of the Inflammatory Responses against Alginate-Poly-L-Lysine Microcapsules by Anti-Biofouling Surfaces of PEG-b-PLL Diblock Copolymers. *PloS one* **2014,** *9* (10), e109837 (1-11).

13. Pechook, S.; Sudakov, K.; Polishchuk, I.; Ostrov, I.; Zakin, V.; Pokroy, B.; Shemesh, M. Bioinspired Passive Anti-Biofouling Surfaces Preventing Biofilm Formation. *Journal of Materials Chemistry B* **2015,** *3* (7), 1371-1378.

14. Mohamed, A. M. A.; Abdullah, A. M.; Younan, N. A. Corrosion Behavior of Superhydrophobic Surfaces: A Review. *Arabian Journal of Chemistry* **2015,** *8* (6), 749-765.

15. Yin, H.; Akasaki, T.; Sun, T. L.; Nakajima, T.; Kurokawa, T.; Nonoyama, T.; Taira, T.; Saruwatari, Y.; Gong, J. P. Double Network Hydrogels from Polyzwitterions: High Mechanical Strength and Excellent Anti-Biofouling Properties. *Journal of Materials Chemistry B* **2013,** *1* (30), 3685-3693.

16. Liu, P.; Chen, Q.; Li, L.; Lin, S.; Shen, J. Anti-biofouling ability and cytocompatibility of the zwitterionic brushes-modified cellulose membrane. *Journal of Materials Chemistry B* **2014,** *2* (41), 7222-7231.

17. Elshaarawy, R. F. M.; Mustafa, F. H. A.; van Geelen, L.; Abou-Taleb, A. E. A.; Tadros, H. R. Z.; Kalscheuer, R.; Janiak, C. Mining Marine Shell Wastes for Polyelectrolyte Chitosan

Anti-Biofoulants: Fabrication of High-Performance Economic and Ecofriendly Anti-Biofouling Coatings. *Carbohydrate Polymers* **2017,** *172*, 352-364.

18. Credi, C.; De Marco, C.; Molena, E.; Pla Roca, M.; Samitier Marti, J.; Marques, J.; Fernandez-Busquets, X.; Levi, M.; Turri, S. Heparin Micropatterning onto Fouling-Release Perfluoropolyether-Based Polymers via Photobiotin Activation. *Colloids and surfaces. B, Biointerfaces* **2016,** *146*, 250-259.

19. Pan, C. J.; Tang, J. J.; Weng, Y. J.; Wang, J.; Huang, N. Preparation, Characterization and Anticoagulation of Curcumin-Eluting Controlled Biodegradable Coating Stents. *Journal of Controlled Release* **2006,** *116* (1), 42-49.

20. Liberio, M. S.; Sadowski, M. C.; Soekmadji, C.; Davis, R. A.; Nelson, C. C. Differential Effects of Tissue Culture Coating Substrates on Prostate Cancer Cell Adherence, Morphology and Behavior. *PloS one* **2014,** *9* (11), e112122 (1-13).

21. Matsuura, R.; Tawa, K.; Kitayama, Y.; Takeuchi, T. A Plasmonic Chip-Based Bio/chemical Hybrid Sensing System for the Highly Sensitive Detection of C-reactive Protein. *Chemical Communications* **2016,** *52* (20), 3883-3886.

22. Zwall, F. A. R.; Hemker, C. H. Blood Cell Menbranes and Haemostasis. *Haemostasis* **1982,** *11*, 12-39.

23. Whelan, D. M.; Van der Giessen, W. J.; Krabbendam, S. C.; Van Vliet, E. A.; Verdouw, P. D.; Serruys, P. W.; Van Beusekom, H. M. M. Biocompatibility of Phosphorylcholine Coated Stents in Normal Porcine Coronary Arteries. *Heart* **2000,** *83* (3), 338-345.

24. Ishihara, K.; Mu, M.; Konno, T.; Inoue, Y.; Fukazawa, K. The Unique Hydration State of Poly(2-Methacryloyloxyethyl Phosphorylcholine). *Journal of Biomaterials Science. Polymer Edition* **2017**, 1-16.

25. Feng, W.; Brash, J. L.; Zhu, S. Non-Biofouling Materials Prepared by Atom Transfer Radical Polymerization Grafting of 2-Methacryloloxyethyl Phosphorylcholine: Separate Effects of Graft Density and Chain Length on Protein Repulsion. *Biomaterials* **2006,** *27* (6), 847-855.

26. Krishnan, S.; Weinman, C. J.; Ober, C. K. Advances in Polymers for Anti-Biofouling Surfaces. *Journal of Materials Chemistry* **2008,** *18* (29), 3405-3413.

27. Seetho, K.; Zhang, S.; Pollack, K. A.; Zou, J.; Raymond, J. E.; Martinez, E.; Wooley, K. L. Facile Synthesis of a Phosphorylcholine-Based Zwitterionic Amphiphilic Copolymer for Anti-Biofouling Coatings. *ACS Macro Letters* **2015,** *4* (5), 505-510.

28. Murakami, D.; Kobayashi, M.; Moriwaki, T.; Ikemoto, Y.; Jinnai, H.; Takahara, A. Spreading and Structuring of Water on Superhydrophilic Polyelectrolyte Brush Surfaces. *Langmuir* **2013,** *29* (4), 1148-1151.

29. Kobayashi, M.; Terayama, Y.; Kikuchi, M.; Takahara, A. Chain Dimensions and Surface Characterization of Superhydrophilic Polymer Brushes with Zwitterion Side Groups. *Soft Matter* **2013,** *9* (21), 5138-5148.

30. Higaki, Y.; Nishida, J.; Takenaka, A.; Yoshimatsu, R.; Kobayashi, M.; Takahara, A. Versatile Inhibition of Marine Organism Settlement by Zwitterionic Polymer Brushes. *Polymer Journal* **2015,** *47* (12), 811-818.

31. Haar, S.; Ciesielski, A.; Clough, J.; Yang, H.; Mazzaro, R.; Richard, F.; Conti, S.; Merstorf, N.; Cecchini, M.; Morandi, V.; Casiraghi, C.; Samori, P. A Supramolecular Strategy to Leverage the Liquid-Phase Exfoliation of Graphene in the Presence of Surfactants: Unraveling the Role of the Length of Fatty Acids. *Small* **2015,** *11* (14), 1691-1702.

32. Hajdari, Z.; Ćurković, H. O.; Čadež, V.; Šegota, S. Corrosion Protection of Cupronickel Alloy by Self-Assembled Films of Fatty Acids. *Journal of The Electrochemical Society* **2016,** *163* (5), C145-C155.

33. Kämäräinen, T.; Arcot, L. R.; Johansson, L. S.; Campbell, J.; Tammelin, T.; Franssila, S.; Laine, J.; Rojas, O. J. UV-Ozone Patterning of Micro-Nano Fibrillated Cellulose (MNFC) with alkylsilane self-assembled monolayers. *Cellulose* **2016,** *23* (3), 1847-1857.

34. Castillo, J. M.; Klos, M.; Jacobs, K.; Horsch, M.; Hasse, H. Characterization of Alkylsilane Self-Assembled Monolayers by Molecular Simulation. *Langmuir* **2015,** *31* (9), 2630-2638.

35. Mazloum-Ardakani, M.; Dehghani-Firouzabadi, A.; Sheikh-Mohseni, M. A.; Benvidi, A.; Mirjalili, B. B. F.; Zare, R. A Self-Assembled Monolayer on Gold Nanoparticles Modified Electrode for simultaneous determination of isoproterenol and uric acid. *Measurement* **2015,** *62*, 88-96.

36. Metoki, N.; Liu, L.; Beilis, E.; Eliaz, N.; Mandler, D. Preparation and Characterization of Alkylphosphonic Acid Self-Assembled Monolayers on Titanium Alloy by Chemisorption and Electrochemical Deposition. *Langmuir* **2014,** *30* (23), 6791-6799.

37. Cheng, H.; Huai, J.; Cao, L.; Li, Z. Novel Self-Assembled Phosphonic Acids Monolayers Applied in N-Channel Perylene Diimide (PDI) Organic Field Effect Transistors. *Applied Surface Science* **2016,** *378*, 545-551.

38. Jeon, I.; Ogumi, K.; Nakagawa, T.; Matsuo, Y. Enhancement of Fill Factor in Air-Processed Inverted Organic Solar Cells Using Self-Assembled Monolayer of Fullerene Catechol. *Japanese Journal of Applied Physics* **2016,** *55* (8), 082301.

39. Waite, J. H. Nature's Underwater Adhesive Specialist. *International Journal of Adhesion and Adhesives* **1987,** *7* (1), 9-14.

40. Lee, B. P.; Messersmith, P. B.; Israelachvili, J. N.; Waite, J. H. Mussel-Inspired Adhesives and Coatings. *Annual review of materials research* **2011,** *41*, 99-132.

41. Nicklisch, S. C.; Waite, J. H. Mini-Review: the Role of Redox in Dopa-Mediated Marine Adhesion. *Biofouling* **2012,** *28* (8), 865-877.

42. Moulay, S. Dopa/Catechol-Tethered Polymers: Bioadhesives and Biomimetic Adhesive Materials. *Polymer Reviews* **2014,** *54* (3), 436-513.

43. Yang, S.; Zhang, S. P.; Winnik, F. M.; Mwale, F.; Gong, Y. K. Group Reorientation and Migration of Amphiphilic Polymer Bearing Phosphorylcholine Functionalities on Surface of Cellular Membrane Mimicking Coating. *Journal of biomedical materials research. Part A* **2008,** *84* (3), 837-841.

44. Bittiger, H.; Marchessault, R. H. Crystal Structure of Poly-Caprolactone. *Acta Crystallographica* **1970,** *B26* 1923-1927.

45. Muller, A. J.; Balsamo, V.; Arnal, M. L.; Jakob, T.; Schmalz, H.; Abetz, V. Homogeneous Nucleation and Fractionated Crystallization in Block Copolymers. *Macromolecules* **2002,** *35*, 3048-3058.

46. Woodruff, M. A.; Hutmacher, D. W. The Return of A Forgotten Polymer—Polycaprolactone in the 21st Century. *Progress in Polymer Science* **2010,** *35* (10), 1217-1256.

47. Ho, R.-M. Crystallization-Induced Orientation for Microstructures of Poly(L-lactide)-*b*-poly(ε-caprolactone) Diblock Copolymers. *Macromolecules* **2003,** *36*, 9085-9092.

48. Kaplan, G. A.; Keil, J. E. Socioeconomic Factors and Cardiovascular Disease: A Review of the Literature. *Circulation* **1993,** *88* (4), 1973-1998.

49. Knutsson, A.; Boggild, H. Shiftwork and Cardiovascular Disease: Review of Disease Mechanisms. *Reviews On Environmental Health* **2000,** *15* (4), 359-372.

50. Eberhart, R. C.; Su, S.-H.; Nguyen, K. T.; Zilberman, M.; Tang, L.; Nelson, K. D.; Frenkel, P. Review: Bioresorbable Polymeric Stents: Current Status and Future Promise. *Journal of Biomaterials Science, Polymer Edition* **2003,** *14* (4), 299-312.

51. Tung, R.; Kaul, S.; Diamond, G. A.; Shah, P. K. Narrative Review: Drug-Eluting Stents for the Management of Restenosis: A Critical Appraisal of the Evidence. *Annals of Internal Medicine* **2006,** *144* (12), 913-919.

52. Acharya, G.; Park, K. Mechanisms of Controlled Drug Release From Drug-Eluting Stents. *Advanced drug delivery reviews* **2006,** *58* (3), 387-401.

53. Pires, N. M.; van der Hoeven, B. L.; de Vries, M. R.; Havekes, L. M.; van Vlijmen, B. J.; Hennink, W. E.; Quax, P. H.; Jukema, J. W. Local Perivascular Delivery of Anti-Restenotic Agents from a Drug-Eluting Poly(epsilon-caprolactone) Stent Cuff. *Biomaterials* **2005,** *26* (26), 5386-5394.

54. Siepmann, J.; Lecomte, F.; Bodmeier, R. Diffusion-Controlled Drug Delivery Systems: Calculation of the Required Composition to Achieve Desired Release Profiles. *Journal of Controlled Release* **1999,** *60*, 379–389.

55. Peng, T.; Gibula, P.; Yao, K.-D.; Goosen, M. F. A. Role of polymers in improving the results of stenting in coronary arteries. *Biomotetiols* **1996,** *17*, 685-694.

56. Alhadad, A.; Ahle, M.; Ivancev, K.; Gottsater, A.; Lindblad, B. Percutaneous Transluminal Renal Angioplasty (PTRA) and Surgical Revascularisation in Renovascular Diseasea Retrospective Comparison of Results, Complications, and Mortality. *European Journal of Vascular and Endovascular Surgery : the Official Journal of the European Society for Vascular Surgery* **2004,** *27* (2), 151-156.

57. Bertrand, O. F.; Sipehia, R.; Mongrain, R.; Rodés, J.; Tardif, J.-C.; Bilodeau, L.; Côté, G.; Bourassa, M. G. Biocompatibility Aspects of New Stent Technology. *Journal of the American College of Cardiology* **1998,** *32* (3), 562-571.

58. Kaliaa, Y. N.; Guya, R. H. Modeling Transdermal Drug Release. *Advanced drug delivery reviews* **2001,** *48*, 159–172.

59. Rao, R.-P.; Ramakrishna, S.; Diwan, P. V. Drug Release Kinetics from Polymeric Films Containing Propranolol Hydrochloride for Transdermal Use. *Pharmaceutical Development and Technology* **2000,** *5* (4), 465–472.

Chapter 2

Synthesis of Dual-Functionalized Polycaprolactone

2.1. Introduction

Poly(ε-caprolactone) (PCL) is a kind of aliphatic polyester which composes of hexanoate repeat units.[1] Due to its good biocompatibility, drug capacity, and degradability, it has been used for different applications such as tissue engineering, long-term drug delivery systems, microelectronics, adhesives, and packaging.[2-4] However, some drawbacks including fouling, lack of the functional groups, and slow degradation rate have restricted its application.[5] The contemporary PCL modifications focus on the end-functionalization and graft-modification.[6-7] The end-functionalization is easy to achieve by the acylation and further polymerization.[8] However, graft-modification with high conversion rate and non-degradation still remains a challenge.[9] To our knowledge, both "click" reaction and atom transfer radical addition (ATRA) with drawbacks affected their performance in the functionalization of PCL.[10-11]

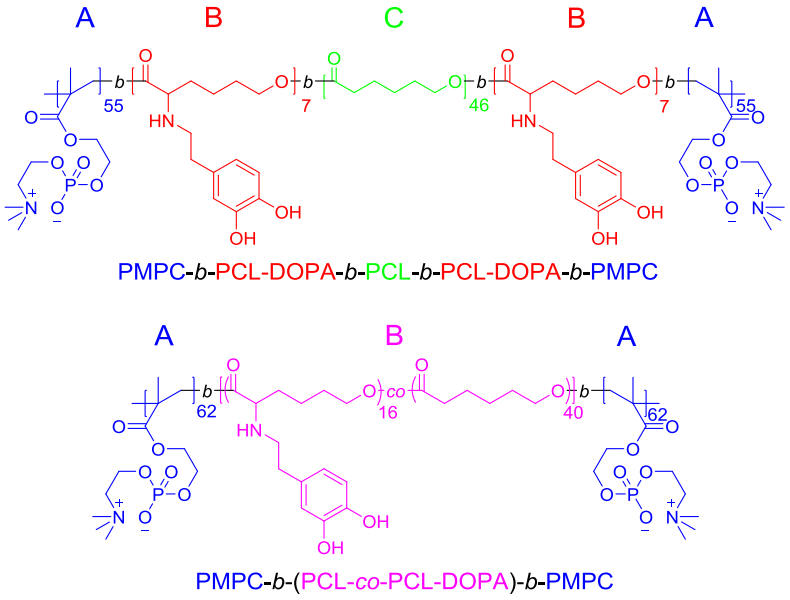

Figure 2.1. Design of two kinds of dual-functionalized block copolymer

In this chapter, the end-functionalization and graft-modification were performed to prepare dual-functionalized PCL. The end-functionalization of MPC was performed using ATRP method.[12] And the graft-modification of dopamine was carried out by a nucleophilic substitution reaction.

Before the graft-modification, chloride units are introduced to PCL on the basis of ring opening polymerization using α-chloride-ε-caprolactone (α-Cl-ε-CL).[11] Resultant polymers were designated as poly(α-chloride-ε-caprolactone)-*block*-poly(ε-caprolactone)-*block*-poly(α-chloride -ε-caprolactone) [PCL-*b*-(PCL-Cl)$_2$] and PCL-*co*-PCL-Cl. The further graft-modification were performed on the basis of nucleophilic substitution. The reaction condition is investigated carefully to achieve an acceptable conversion rate and avoid the degradation of PCL main chain. At last, the end-functionalization was performed to obtain final target which is shown in Figure 2.1.

2.2. Experiment

2.2.1. Materials

Potassium bicarbonate, potassium iodide (KI), 2-(methacryloyloxy)ethyl-2-(trimethylammonio) ethyl phosphate (MPC), tris[2-(dimethylamino)ethyl]amine (Me_6Tren), 3-chloroperoxybenzoic acid, sodium sulfite, imidazole, dopamine hydrochloride, tetrabutylammonium fluoride (TBAF) tetrahydrofuran solution (1mol/mL), *tert*-butyldimethylsilyl chloride (TBDMS-Cl), and *N*,*N*-ethyldiisopropylamine (DIPEA) were purchased from Tokyo Chemical Inc. (TCI), Japan, and used as received. CuBr(I), stannous octoate (Sn(OCT)$_2$), 2-bromine butyryl bromine, 2,2'-bipyridine (Bpy), α-chloride-cyclohexanone, 1,4-butanediol and ε-caprolactone (ε-CL) were obtained from TCI (Japan) and dried over $MgSO_4$ (Sigma-Aldrich, Japan) for 48 h at room temperature, distilled under reduced pressure before use. Anhydrous toluene and dichloromethane (DCM) were obtained by the ultimate solvent system (Nikko Hansen Corporation, Japan). Methanol, dimethyl formamide (DMF), acetonitrile, and tetrahydrofuran (THF) were purchased from Wako Pure Chemicals Co. (Japan) and directly used without any further purification.

Anhydrous triethylamine (TEA, Sigma-Aldrich, Japan) was prepared by refluxing over CaH_2 (Sigma-Aldrich, Japan) and distilled under a nitrogen atmosphere.

2.2.2. Synthesis of PCL-*b*-(PCL-DOPA-*b*-PMPC)$_2$

The synthesis strategy is presented in Figure 2.2. Copolymer designated PCL-*b*-(PCL-Cl)$_2$ was synthesized via 2-steps ring-opening polymerization (ROP). Sn(OCT)$_2$-mediated polymerization of ε-CL (27 g, 0.24 mol) was carried out using 1,4-butanediol (0.45 g, 4.5 mmol) as an initiator in toluene (15 mL) at 75 ℃ for 24 h to obtain PCL. PCL was purified by reprecipitation method using methanol and dried under vacuum oven, resulting in 25 g polymer (yield: 92 %). M_n was 4,500 and polydispersity index (PDI) was 1.3. ^{1}H NMR (400 MHz, $CDCl_3$-d_1, δ): 1.15-1.35 (m, -CO-CH_2-CH_2-CH_2), 1.75-1.61 (m, -CO-CH_2-CH_2, -O-CH_2-CH_2), 2.32 (t, O-C-CH_2), 3.66 (t, HO-CH_2), 4.08 (t, CO-O-CH_2).

α-Chloride-ε-caprolactone (α-Cl-ε-CL) was obtained through the oxidization of α-chloride-cyclohexanone (7.5 g, 0.056 mol) in DCM (25 mL) at room temperature via Baeyer-Villiger oxidation using 3-chloroperoxybenzoic acid (16 g, 0.061 mol).[12] After 24 h, the mixture was quenched by sodium sulfite solution and neutralized by bicarbonate solution. Subsequently, chloroform was used to extract product. The colorless α-Cl-ε-CL was obtained by distilling under vacuum condition with 74% yield.[7] Sn(OCT)$_2$-mediated ROP for α-Cl-ε-CL (5.8 g, 0.038 mol) was carried out using PCL (4.9 g, 0.82 mmol) as a macroinitiator in toluene at 75 ℃ for 24 h. The reaction mixture was poured into methanol to obtain PCL-*b*-(PCL-Cl)$_2$ triblock copolymer, and resultant sample was dried in a vacuum oven, resulting in 7.3 g. Yield: 65%. M_n(SEC) was 8,100 and PDI was 1.6. ^{1}H NMR (400 MHz, $CDCl_3$-d_1, δ): 1.15-1.35 (m, -CO-CH_2-CH_2-CH_2-), 1.75-1.61 (m, -CO-CH_2-CH_2-, -O-CH_2-CH_2-), 2.02 (m, Cl-CH_2-CH_2-,

Cl-CH_2-CH_2-CH_2-), 2.32 (m, O-CH_2-CH_2-), 3.66 (m, OH-CH_2-), 4.08 (m, CO-O-CH_2-), 4.27 (m, Cl-CH-CO-O-CH_2-), 4.32 (m, Cl-C*H*-).

The dopamine functionalization was performed via substitution reaction. To avoid the oxidation of catechol groups, TBDMS-Cl (15.5 g, 0.1 mol) anhydrous DCM solution with imidazole (8.84 g, 0.13 mol) was slowly added to dopamine hydrochloride solution (7.5 g, 0.040 mol, in 10 mL anhydrous DCM) to obtain TBDMS protected-dopamine. The reaction was performed at room temperature for 6 h and subsequently quenched by saturated potassium bicarbonate solution. After being extracted by chloroform, products were further purified by column chromatography using 3:2 hexane and ethyl acetate mixture as an eluent. A white solid (TBDMS protected dopamine) was obtained in 92% yield.

Subsequently, PCL-*b*-(PCL-Cl)$_2$ (3.0 g, 0.4 mmol), TBDMS-protected dopamine (4.9 g, 12.8 mmol), DIPEA (2.6 g, 20.1 mmol), KI (0.12 g, 0.7 mmol), and acetonitrile (7 mL) were added into a glass reactor. The mixture was stirred at 80 ℃ under nitrogen environment for 48 h and subsequently poured into MeOH. The product was further purified by column chromatography using chloroform as an eluent. A yellow solid (PCL-*b*-(PCL-DOPA$_{TBDMS}$)$_2$) was obtained in 75% yield. M_n(SEC) of 11,000 and polydispersity (M_w/M_n) of 1.6. ^{1}H NMR (400 MHz, $CDCl_3$-d_1, δ): 0.19 (s, -Si-CH_3), 0.99 (s, -Si-C-CH_3), 1.15-1.35 (m, -CO-CH_2-CH_2-CH_2-), 1.75-1.61 (m, -CO-CH_2-CH_2-, -O-CH_2-CH_2-), 2.32 (t, -O-CH_2-CH_2-), 2.63 (m, -NH-CH_2-CH_2-), 2.78 (m, -NH-CH_2-), 3.22 (m, -NH-C*H*-), 3.66 (t, OH-CH_2-), 4.08 (t, -CO-O-CH_2-), 6.79-6.59 (m, Ar-*H*).

The PMPC modification was performed using atom transfer radical polymerization (ATRP). Firstly, PCL-*b*-(PCL-DOPA$_{TBDMS}$)$_2$ (1.2 g, 0.071 mmol), 2-bromine butyryl bromine (0.016 g, 0.085 mmol) and anhydrous trimethylamine (0.01 g, 0.10 mmol) in anhydrous DCM were stirred

at 45 ℃ for 24 h to obtain block-macroinitiator. The reaction was quenched with water and extracted using chloroform several times. The obtained block-macroinitiator was purified by reprecipitation in methanol. Yield: 85%. ^{1}H NMR (400 MHz, $CDCl_3$-d_1, δ): 0.19 (s, -Si-CH_3), 0.99 (s, -Si-C-CH_3), 1.15-1.35 (m, -CO-CH_2-CH_2-CH_2-), 1.75-1.61 (m, -CO-CH_2-CH_2, -O-CH_2-CH_2-), 1.91 (s, Br-CH_2-CH_3), 2.32 (t, -O-CH_2-CH_2-), 2.63(s, -NH-CH_2-CH_2-), 2.78(s, -NH-CH_2-), 3.15 (q, -NH-C*H*-), 4.08 (t, -CO-O-CH_2-), 6.79-6.59 (m, Ar-*H*).

A mixture of block-macroinitiator (1.2 g, 0.07 mmol), MPC (2.95 g, 0.01 mol), Me_6Tren (0.046 g, 0.20 mmol), toluene (5 mL), and methanol (3 mL) was deoxygenated by freeze-thaw for 3 cycles, then backfilled with nitrogen. CuBr (0.028 g, 0.20 mmol) was subsequently added to the reaction mixture and kept in oil bath thermostat at 40 ℃ for 18 h to promote ATRP. The mixture was poured into diethyl ether and purified by dialysis against deionized water, and resultant sample was freeze-dried (Yield: 83%). ^{1}H NMR (400 MHz, 1:1 $CDCl_3$-d_1 and methonal-d_4, δ): 0.12 (s, -Si-CH_3), 0.99 (s, -Si-C-CH_3), 1.15-1.35 (m, -CO-CH_2-CH_2-CH_2-), 1.75-1.61 (m, -CO-CH_2-CH_2-, -O-CH_2-CH_2-), 1,91 (s, Br-C-CH_3), 2.32 (t, O-CH_2-CH_3), 2.78 (m, -NH-CH_2-, -NH-CH_2-CH_2-), 3.71 (s, -N-CH_2-), 4.08 (m, -CO-O-CH_2-), 4.23 (m, -P-O-CH_2-CH_2-O-CO-), 4.33 (s, -P-O-CH_2-), 6.67 (m, Ar-*H*).

The dopamine units in PCL-*b*-(PCL-$DOPA_{TBDMS}$-*b*-PMPC)$_2$ were deprotected using 1 mol/L TBAF THF solution for 6 h. The mixture was reprecipitated in diethyl ether for 3 times and dried in the vacuum oven at room temperature overnight to obtain PCL-*b*-(PCL-DOPA-*b*-PMPC)$_2$. ^{1}H NMR (400 MHz, 1:1 $CDCl_3$-d_1 and methanol-d_4, δ): 1.15-1.35 (m, -CO-CH_2-CH_2-CH_2-), 1.75-1.61 (m, -CO-CH_2-CH_2-, -O-CH_2-CH_2-), 1,91 (s, Br-C-CH_3), 2.32 (t, O-CH_2-CH_3), 2.78 (m, -NH-CH_2-, -NH-CH_2-CH_2-), 3.71 (s, -N-CH_2-), 4.08 (m, -CO-O-CH_2-), 4.23 (m, -P-O-CH_2-CH_2-O-CO-), 4.33 (s, -P-O-CH_2-), 6.67 (m, Ar-*H*).

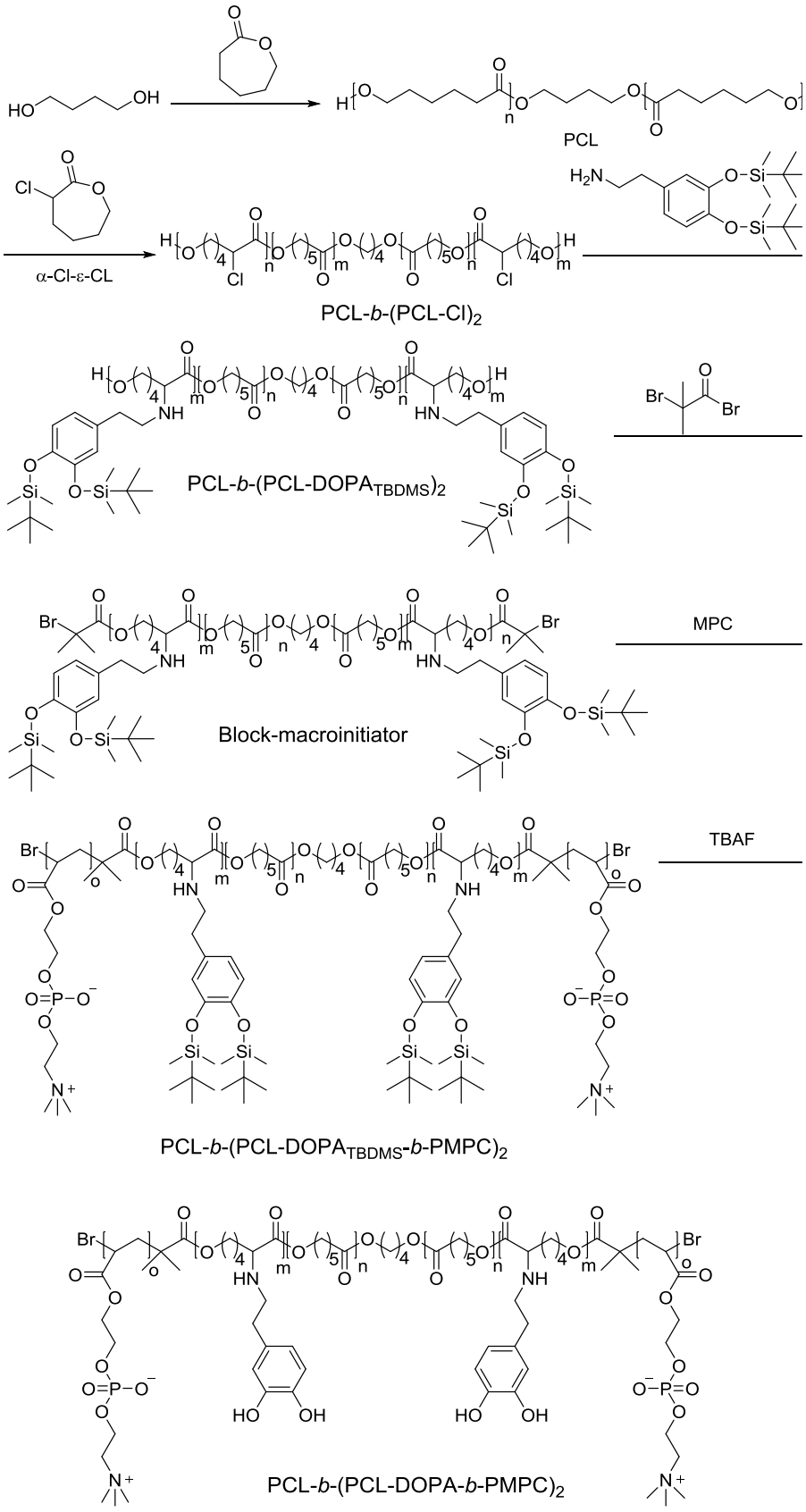

Figure 2.2. Synthesis strategy of PCL-*b*-(PCL-DOPA-*b*-PMPC)$_2$.

2.2.3. Synthesis of (PCL-*co*-PCL-DOPA)-*b*-$(PMPC)_2$

The synthesis strategy of (PCL-*co*-PCL-DOPA)-*b*-$(PMPC)_2$ was shown in Figure 2.3. Copolymer designated PCL-*co*-PCL-Cl was synthesized on the basis of one-step ROP. The $Sn(OCT)_2$-mediated polymerization of ε-CL (13.5 g, 0.12 mol) and α-Cl-ε-CL (14.7 g, 0.12 mol) was carried out using 1,4-butanediol (0.45 g, 4.5 mmol) as an initiator in toluene (15 mL) at 75 ℃ for 24 h to obtain PCL-*co*-PCL-Cl. PCL-*co*-PCL-Cl was purified by reprecipitation method using methanol and dried under vacuum oven, resulting in 25 g polymer (yield: 92 %). M_n was 8,720 and polydispersity (M_w/M_n) was 1.3. ^{1}H NMR (400 MHz, $CDCl_3$-d_1, δ): 1.15-1.35 (m, -CO-CH_2-CH_2-CH_2), 1.75-1.61 (m, -CO-CH_2-CH_2, -O-CH_2-CH_2), 2.32 (t, O-C-CH_2), 3.66 (t, HO-CH_2), 4.08 (t, CO-O-CH_2).

Subsequently, PCL-*co*-PCL-Cl (3.0 g, 0.4 mmol), TBDMS protected dopamine (4.9 g, 12.8 mmol), DIPEA (2.6 g, 20.1 mmol), KI (0.12 g, 0.7 mmol), and acetonitrile (7 mL) were added into a glass reactor. The mixture was stirred at 80 ℃ under nitrogen environment for 48 h and subsequently poured into MeOH. The product was further purified by column chromatography using chloroform as an eluent, resulted in yellow solid with 79% yield. M_n is 11,200 and polydispersity (M_w/M_n) is 1.3. ^{1}H NMR (400 MHz, $CDCl_3$-d_1, δ): 0.19 (s, -Si-CH_3), 0.99 (s, -Si-C-CH_3), 1.15-1.35 (m, -CO-CH_2-CH_2-CH_2-), 1.75-1.61 (m, -CO-CH_2-CH_2-, -O-CH_2-CH_2-), 2.32 (t, -O-CH_2-CH_2-), 2.63 (m, -NH-CH_2-CH_2-), 2.78 (m, -NH-CH_2-), 3.22 (m, -NH-C*H*-), 3.66 (t, OH-CH_2-), 4.08 (t, -CO-O-CH_2-), 6.79-6.59 (m, Ar-*H*).

The PMPC modification was performed using ATRP. Firstly, PCL-*co*-PCL-$DOPA_{TBDMS}$ (1.2 g, 0.071 mmol), 2-bromine butyryl bromine (0.016 g, 0.085 mmol) and anhydrous trimethylamine (0.01 g, 0.10 mmol) in anhydrous DCM was stirred at 45 ℃ for 24 h to obtain random-macroinitiator. The reaction was quenched with water and extracted using chloroform

several times. The obtained random-macroinitiator was purified by reprecipitation in methanol. Yield 92%. ^{1}H NMR (400 MHz, $CDCl_3$-d_1, δ): 0.19 (s, -Si-CH_3), 0.99 (s, -Si-C-CH_3), 1.15-1.35 (m, -CO-CH_2-CH_2-CH_2-), 1.75-1.61 (m, -CO-CH_2-CH_2, -O-CH_2-CH_2-), 1.91 (s, Br-CH_2-CH_3), 2.32 (t, -O-CH_2-CH_2-), 2.63(s, -NH-CH_2-CH_2-), 2.78(s, -NH-CH_2-), 3.15 (q, -NH-C*H*-), 4.08 (t, -CO-O-CH_2-), 6.79-6.59 (m, Ar-*H*).

A mixture of random-macroinitiator (1.2 g, 0.07 mmol), MPC (2.95 g, 0.01 mol), Me_6Tren (0.046 g, 0.20 mmol), toluene (5 mL), and methanol (3 mL) was deoxygenated by freeze-thaw for 3 cycles, then backfilled with nitrogen. CuBr (0.028 g, 0.20 mmol) was subsequently added to the reaction mixture and kept in oil bath thermostat at 40 ℃ for 18 h to promote ATRP. The mixture was poured into diethyl ether and purified by dialysis against deionized water, and the resultant solution was freeze-dried (Yield: 79%). ^{1}H NMR (400 MHz, 1:1 $CDCl_3$-d_1 and methonal-d_4, δ): 0.12 (s, -Si-CH_3), 0.99 (s, -Si-C-CH_3), 1.15-1.35 (m, -CO-CH_2-CH_2-CH_2-), 1.75-1.61 (m, -CO-CH_2-CH_2-, -O-CH_2-CH_2-), 1,91 (s, Br-C-CH_3), 2.32 (t, O-CH_2-CH_3), 2.78 (m, -NH-CH_2-, -NH-CH_2-CH_2-), 3.71 (s, -N-CH_2-), 4.08 (m, -CO-O-CH_2-), 4.23 (m, -P-O-CH_2-CH_2-O-CO-), 4.33 (s, -P-O-CH_2-), 6.67 (m, Ar-*H*).

The dopamine units in (PCL-*co*-PCL-$DOPA_{TBDMS}$)-*b*-$(PMPC)_2$ were deprotected using 1 mol/L TBAF THF solution for 6 h. The mixture was reprecipitated in diethyl ether for 3 times and dried in the vacuum oven at room temperature overnight to obtain (PCL-*co*-PCL-DOPA)-*b*-$(PMPC)_2$. ^{1}H NMR (400 MHz, 1:1 $CDCl_3$-d_1 and methanol-d_4, δ): 1.15-1.35 (m, -CO-CH_2-CH_2-CH_2-), 1.75-1.61 (m, -CO-CH_2-CH_2-, -O-CH_2-CH_2-), 1,91 (s, Br-C-CH_3), 2.32 (t, O-CH_2-CH_3), 2.78 (m, -NH-CH_2-, -NH-CH_2-CH_2-), 3.71 (s, -N-CH_2-), 4.08 (m, -CO-O-CH_2-), 4.23 (m, -P-O-CH_2-CH_2-O-CO-), 4.33 (s, -P-O-CH_2-), 6.67 (m, Ar-*H*).

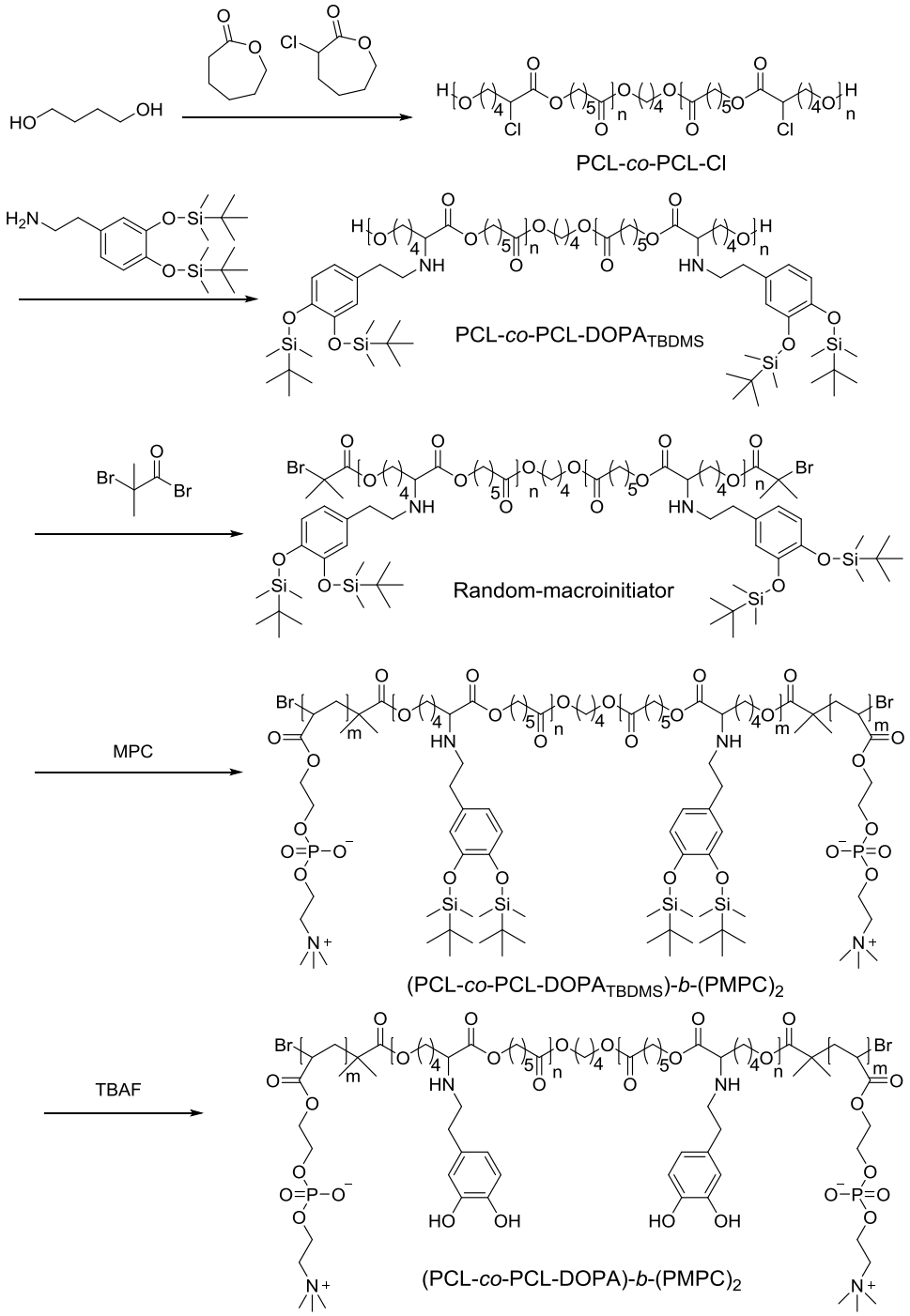

Figure 2.3. Synthesis strategy of (PCL-*co*-PCL-DOPA)-*b*-(PMPC)$_2$.

2.2.4. Exploration of dopamine modification

Since the nucleophilic substitution is the first time applied for the dopamine modification, the reaction condition was investigated carefully. Generally, the equilibrium constant of nucleophilic substitution reaction relates to the nucleophile, substrate, solvent and leaving groups. In the dopamine graft-modification, the nucleophile (dopamine) and substrate (PCL-*b*-(PCL-Cl)$_2$ or

PCL-*co*-PCL-Cl) are determined. We didn't discuss these factors here. Polar protic solvents are not preferred, because nucleophile might hydrogen bonded with the solvent, hindering it from the attacking to carbon. A polar aprotic solvent with low dielectric constant or a hindered dipole end is favored. Furthermore, the conjugate base stability of the leaving group showed a significant effect on the reaction. Since the chloride is not as good leaving group as other halogen units such as iodine or bromine, the halogen exchange reaction was introduced in to achieve better conversion rate. In addition, the base is important for the reaction to absorb the produced hydrochloric during the reaction, and improve the nucleophilicity of amino group in dopamine. However, the use of strong base may influence the polyester main chain due to the hydrolysis of the ester group. The high temperature is able to accurate the reaction rate but induces the degradation of polymer main chain. Because of this, both of conversion rate and degradation were evaluated. Conversion rate was calculated by the ^{1}H NMR and the degradation was evaluated by the combination of molecular weight changes and conversion rate.

2.2.5. Degradation test of PCL-*b*-(PCL-DOPA-*b*-PMPC)$_2$

The degradation tests of PCL, PCL-*b*-(PCL-DOPA)$_2$, and PCL-*b*-(PCL-DOPA-*b*-PMPC)$_2$ under enzyme condition were evaluated on the basis of quartz crystal microbalance (QCM, AFFINIX QN, ULVAC, Inc. Japan) measurement. The initial frequency (F0) of different QCM sensors (QCM27C-SUS, AFFINIX QN, ULVAC, Inc. Japan, the quartz crystal resonator with SUS film) was measured in the open air. The QCM sensors were coated by PCL (80 μL 50 mg/mL), PCL-*b*-(PCL-DOPA)$_2$ (80 μL, 50 mg/mL) and PCL-*b*-(PCL-DOPA-*b*-PMPC)$_2$ (80 μL 25 mg/mL) using spin-coating method (900 rpm, 30 s). Though PCL and PCL-*b*-(PCL-DOPA)$_2$ are not soluble in water, the unattached PCL-*b*-(PCL-DOPA-*b*-PMPC)$_2$ could dissolve in water. To remove those polymers, the obtained sensors were immersed in phosphate buffer saline (PBS, pH= 7.0) for 24 h and washed with pure water sufficiently. After being fully dried under vacuum state, the frequency

of coated QCM sensors (F_1) was measured for the calculation of coating mass (1 Hz frequency shift implies 30 pg polymer on QCM sensor). Then, polymer-coated sensors were immersed in 1 mL of 0.2 mg/mL lipase (from Pseudomonas cepacia 30 U/mg) PBS solution with sodium azide (0.02%) at 37 ℃ for 12 h.[37,38] Subsequently, the sensors were washed by the deionized water and dried for 12 h under vacuum state. The frequency after degradation test (F_2) was measured to calculate the weight loss by Equation 2.1.

$$\mathrm{WL}(\%) = \frac{F_0 - F_1}{F_0 - F_2} \quad (2.1)$$

2.2.6. Characterizations

The primary structure of obtained polymers was characterized using nuclear magnetic resonance spectroscopy (NMR, AVANCE III 400, Bruker Corporation, Germany). The number-average molecular weight (M_n) and polydispersity index (PDI) were evaluated by size exclusion chromatography (SEC system, JASCO Corporation, Japan). SEC measurements were carried out at a rate of 0.5 ml/min at 313 K using DMF as an eluent. The degradation tests of PCL, PCL-*b*-(PCL-DOPA)$_2$, and PCL-*b*-(PCL-DOPA-*b*-PMPC)$_2$ under enzyme condition were evaluated on the basis of quartz crystal microbalance (QCM, AFFINIX QN, ULVAC, Inc. Japan) measurement.

2.3. Results and Discussion

2.3.1. Synthesis of PCL-*b*-(PCL-Cl)$_2$ and PCL-*co*-PCL-Cl

Sn(OCT)$_2$-mediated polymerization of ε-CL was performed to obtain PCL. The primary structure was evaluated on the basis of ^{1}H NMR spectrum (Figure 2.4). All signals are clearly assigned and they are in good accord with the previous report.[13] The number of PCL repeat unit ($n_{(CL)}$) is calculated by Equation 2.2

$$n_{(CL)} = \frac{I_{2.32} \times 2}{I_{3.66}} \quad (2.2)$$

where $I_{2.32}$ and $I_{3.66}$ are the integral intensity of the signals at 2.32 and 3.66 ppm, respectively, assigned to methylene protons beside the carbonyl group and methylene protons beside the PCL hydroxyl terminal groups. Furthermore, M_n can be calculated by the Equation 2.3

$$M_n(\text{PCL}) = 90 + 114 \times DP_{(CL)} \quad (2.3)$$

where the values of 90 and 114 are the formula weight of 1,4-butyl glycol, CL repeat units. The primary structure of polymers is summarized in Table 2.1.

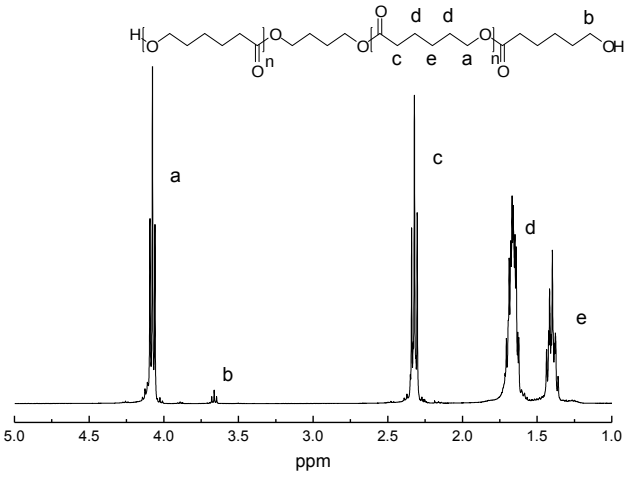

Figure 2.4. ^{1}H NMR spectrum of PCL.

To prepare PCL-*b*-(PCL-Cl)$_2$, Sn(OCT)$_2$-mediated ROP of *α*-Cl-*ε*-CL was performed using obtained PCL as a macroinitiator. The primary structure and chemical composition of PCL-*b*-(PCL-Cl)$_2$ were evaluated using ^{1}H NMR measurements (Figure 2.5.a). The number of PCL-Cl repeat unit ($n_{(CL\text{-}Cl)}$) are determined using Equation 2.4

$$n_{(CL-Cl)} = \frac{(I_{(4.35\sim3.97)} - I_{2.31}) \times 2}{I_{3.66} \times 3} \quad (2.4)$$

where $I_{(4.35\sim3.97)}$ and $I_{2.31}$ are the integral intensity of the signals at the range from 4.35 to 3.97 ppm and at 2.31 ppm. The signal at 4.31 ppm and 4.23 ppm are assigned to methenyl and methylene protons beside both sides of the ester groups in PCL-Cl segment. Meanwhile, the 4.03 and 2.31

ppm are assigned to two methylene protons beside both sides of ester groups in PCL segment. M_n can be calculated by the equation 2.5

$$M_n = M_n(\mathrm{PCL}) + 148 \times \mathrm{DP}_{(\mathrm{CL-Cl})} \quad (2.5)$$

where the value 148 is the formula weight of CL-Cl repeat unit.

Meanwhile, the ^{1}H NMR spectrum of PCL-*co*-PCL-Cl was shown in Figure 2.5.b, $n_{(CL)}$ and $n_{(CL\text{-}Cl)}$ are obtained using the ^{1}H NMR spectrum of PCL-*co*-PCL-Cl by Equation 2.2 and 2.4, and the M_n is calculated using Equation 2.5.

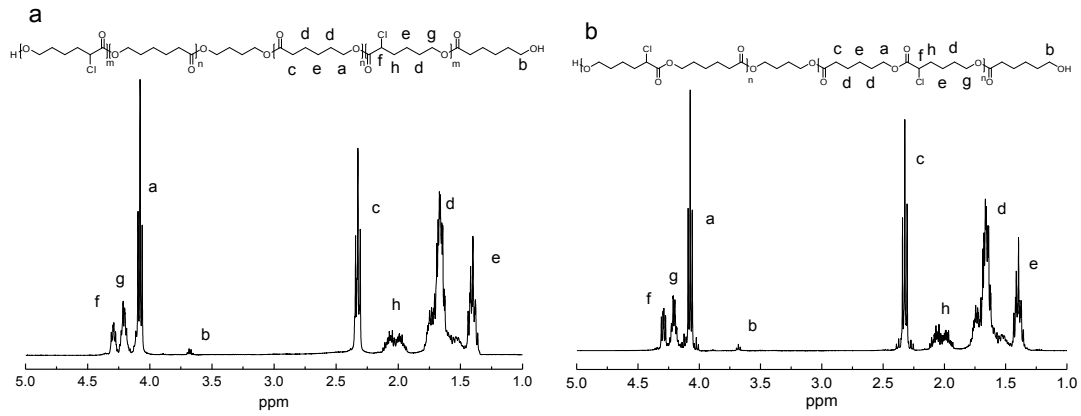

Figure 2.5. ^{1}H NMR spectrum of a) PCL-*b*-(PCL-Cl)$_2$ and b) PCL-*co*-PCL-Cl.

The results of dopamine functionalization were shown in Figure 2.6, the signal at 4.31 and 4.13 ppm was decreased obviously because the chloride groups were substituted by an amino group. Meanwhile, the very strong signals appeared at 0.12 and 0.99 ppm which are resulted in the TBDMS group. The number of dopamine-modified PCL can be calculated using Equation 2.6

$$n_{(\mathrm{CL-DOPA})} = \frac{I_{(6.86-6.48)} \times 2}{I_{3.63} \times 3} \quad (2.6)$$

where $I_{(6.86\sim6.84)}$ and $I_{3.66}$ are the integral intensity of the signals ranging from 6.86 to 6.84 and at 3.66 ppm, respectively, which are assigned to protons of phenyl groups and at methylene protons beside the PCL hydroxyl terminal groups. Furthermore, the conversion rate (R) was calculated from Equation 2.7.

$$R(\%) = \frac{n_{(CL-DOPA)}}{DP_{(CL-Cl)} + n_{(CL-DOPA)}} \times 100\% \quad (2.7)$$

where $DP_{(CL\text{-}CL)}$ is calculated by equation 2.3 using ^{1}H NMR spectrum of PCL-*b*-(PCL-Cl)$_2$ and $n_{(CL\text{-}DOPA)}$ is calculated by equation 2.5 using the same spectrum.

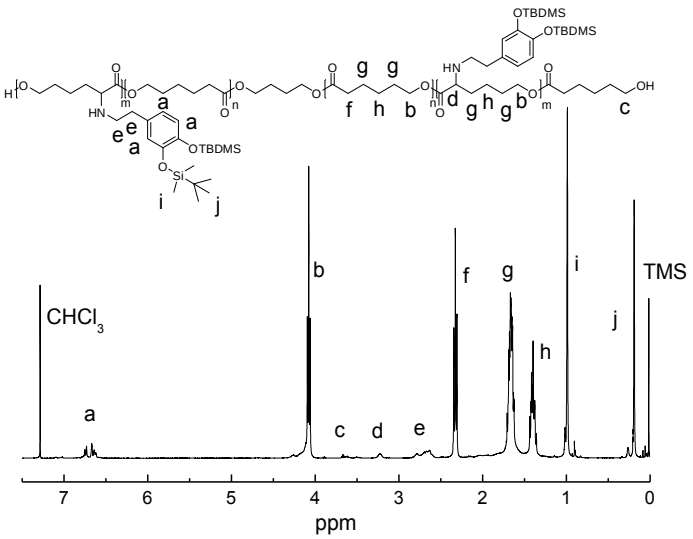

Figure 2.6. ^{1}H NMR spectrum of PCL-*b*-(PCL-DOPA$_{TBDMS}$)$_2$

The PCL-*co*-PCL-DOPA$_{TBDMS}$ was synthesized using the same condition and the information of chemical structure was also evaluated by the same method. As the result, no degradation was observed in this functionalization.

2.3.2. End-functionalization

PCL-*b*-(PCL-DOPA$_{TBDMS}$)$_2$ and PCL-*co*-PCL-DOPA$_{TBDMS}$ possess hydroxyl groups as the terminal groups. To demonstrate ATRP for MPC using this polymer as an initiator, the hydroxyl groups were modified by 2-bromine butyryl bromine. In the ^{1}H NMR spectrum of block-macroinitiator (Figure 2.7), the signal at 3.66 ppm which is assigned to the methylene protons beside the terminal hydroxyl group, was vanished and new proton signal for the methyl group beside bromide are observed at 1.90 ppm.

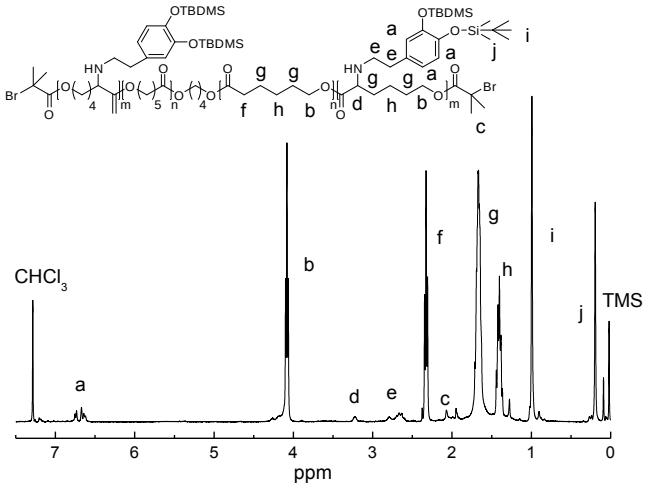

Figure 2.7. ^{1}H NMR spectrum of block-macroinitiator.

To obtain PCL-*b*-(PCL-DOPA$_{TBDMS}$-*b*-PMPC)$_2$, ATRP of MPC was performed using block-macroinitiator. We should note that obtained polymer possessing amphiphilicity, M_n cannot be evaluated by GPC measurements using a single solvent as an eluent. The primary structure of obtained PCL-*b*-(PCL-DOPA$_{TBDMS}$-*b*-PMPC)$_2$ and (PCL-*co*-PCL-DOPA$_{TBDMS}$)-*b*-(PMPC)$_2$ was clarified by ^{1}H NMR spectrum using mixture solvents of $CDCl_3$ and CD_3OD (Figure 2.8.a). All signals are clearly assigned, indicating target PCL-*b*-(PCL-DOPA$_{TBDMS}$-*b*-PMPC)$_2$ was successfully synthesized. The DP of PMPC segment was evaluated on the basis of ^{1}H NMR spectrum (Table 2.1 and 2.2). The M_n of PCL-*b*-(PCL-DOPA-*b*-PMPC)$_2$ was calculated by Equation 2.8

$$M_{\mathrm{n}} = 90 + 114 \times \mathrm{DP}_{(\mathrm{CL})} + (1 - \mathrm{R}) \times 148 \times \mathrm{DP}_{(\mathrm{CL-Cl})} + \mathrm{R} \times 267 \times \mathrm{DP}_{(\mathrm{CL-Cl})} + 419 \times \mathrm{DP}_{(\mathrm{MPC})} \quad (2.8)$$

where the values of 90, 114, 148, 267, 495, and 419 are the formula weight of 1,4-butyl glycol, PCL, PCL-Cl, PCL-DOPA, and PMPC repeat units, respectively. R is calculated from Equation 2.7. It is clear that PCL-*b*-(PCL-DOPA$_{TBDMS}$-*b*-PMPC)$_2$ with M_n of 58,500 was obtained. Meanwhile, the detail information of (PCL-*co*-PCL-DOPA$_{TBDMS}$)-*b*-(PMPC)$_2$ is prepared from

random-macroinitiator as an initiator using similar ATRP condition. A (PCL-*co*-PCL-DOPA$_{TBDMS}$)-*b*-(PMPC)$_2$ with 63,400 was obtained successfully.

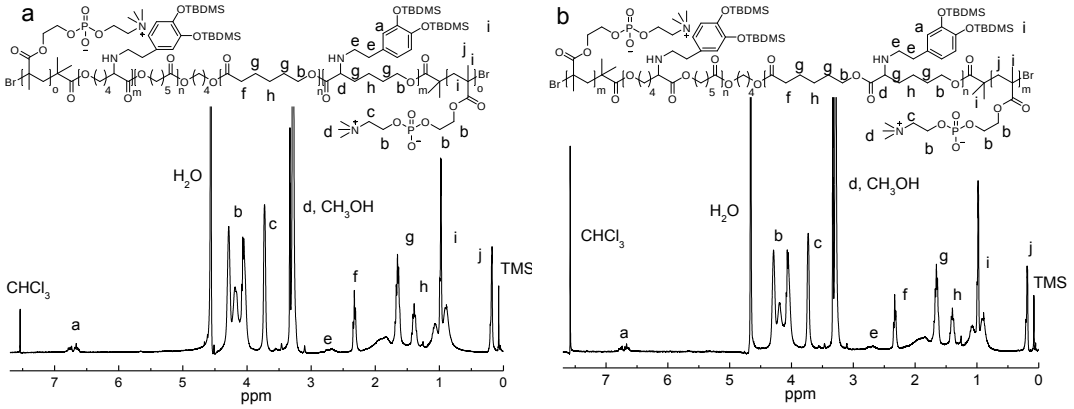

Figure 2.8. ^{1}H NMR spectrum of a) PCL-*b*-(PCL-DOPA$_{TBDMS}$-*b*-PMPC)$_2$ and b) (PCL-*co*-PCL-DOPA$_{TBDMS}$)-*b*-(PMPC)$_2$.

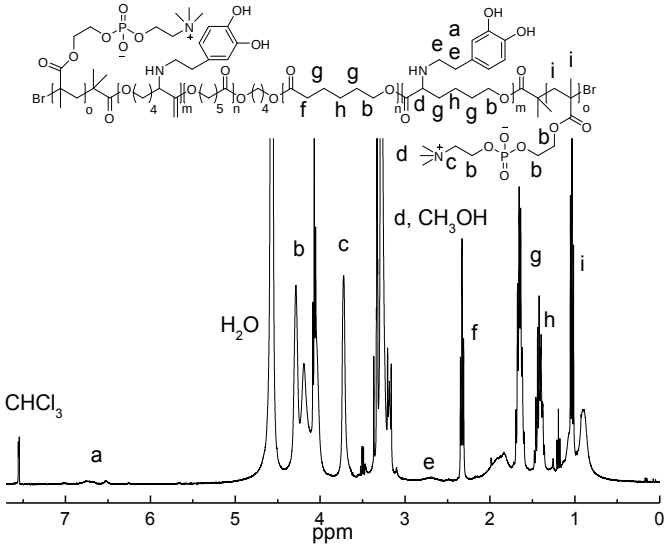

Figure 2.9. ^{1}H NMR spectrum of PCL-*b*-(PCL-DOPA-*b*-PMPC)$_2$.

After PCL-*b*-(PCL-DOPA$_{TBDMS}$-*b*-PMPC)$_2$ and (PCL-*co*-PCL-DOPA$_{TBDMS}$)-*b*-(PMPC)$_2$ were prepared, the deprotection of different polymers was performed to obtain PCL-*b*-(PCL-DOPA-*b*-PMPC)$_2$ and (PCL-*co*-PCL-DOPA)-*b*-(PMPC)$_2$ using TBAF in chloroform and methanol mixture. The reaction was evaluated on the basis of ^{1}H NMR spectrum (Figure 2.9 shows ^{1}H NMR of PCL-*b*-(PCL-DOPA-*b*-PMPC)$_2$ for representative). The disappearance of TBDMS signals indicates the complete deprotection.

Table 2.1. Molecular Weight and DP Information for PCL, PCL-*b*-(PCL-Cl)$_2$, PCL-*b*-(PCL-DOPA$_{TBDMS}$)$_2$, PCL-*b*-(PCL-DOPA-*b*-PMPC)$_2$

	PCL	PCL-*b*-(PCL-Cl)$_2$	PCL-*b*-(PCL-DOPA$_{TBDMS}$)$_2$	PCL-*b*-(PCL-DOPA-*b*-PMPC)$_2$
M_n (NMR)	4,990	7,270	10,800	58,500
M_n (SEC)	4,500	8,100	11,000	N/A
M_w (SEC)	5,100	13,000	17,000	N/A
PDI(SEC)	1.3	1.6	1.6	N/A
$DP_{(CL)}$	43	42	48	46
$n_{(CL\text{-}Cl)}$[b]	N/A	16	5	6
$n_{(CL\text{-}DOPA)}$[c]	N/A	N/A	13	14
$DP_{(MPC)}$[d]	N/A	N/A	N/A	109

[a]$n_{(CL\text{-}Cl)}$ is the number of PCL-Cl units in different copolymers calculated by ^{1}H NMR; [b]$n_{(CL\text{-}DOPA)}$ refers to the number of dopamine functionalized PCL in different copolymers.

Table 2.2. Molecular Weight and DP Information for PCL-*co*-PCL-Cl, PCL-*co*-PCL-DOPA$_{TBDMS}$ and (PCL-*co*-PCL-DOPA)-*b*-(PMPC)$_2$

	PCL-*co*-PCL-Cl	PCL-*co*-PCL-DOPA$_{TBDMS}$	(PCL-*co*-PCL-DOPA)-*b*-(PMPC)$_2$
M_n (NMR)	8,720	11,230	63,400
M_n (SEC)	9,200	10,030	N/A
M_w (SEC)	11,900	13,039	N/A
PDI(SEC)	1.3	1.3	N/A
$n_{(CL)}$[a]	40	40	40
$n_{(CL\text{-}Cl)}$[b]	18	5	5
$n_{(CL\text{-}DOPA)}$[c]	N/A	14	16
$DP_{(MPC)}$[d]	N/A	N/A	119

[a]$n_{(CL\text{-}Cl)}$ is the number of PCL-Cl units in different copolymers calculated by ^{1}H NMR; [b]$n_{(CL\text{-}DOPA)}$ refers to the number of dopamine functionalized PCL in different copolymers.

2.3.3. Exploration of dopamine modification

It is well known that PCL is degradable under both high temperature and strong alkaline condition. The determination of the degradation is difficult to evaluate by single size exclusion

chromatography (SEC) measurement. Here, we combined SEC and ^{1}H NMR results using following equation

$$\frac{M_{n(1)}}{M_{n(2)}} \times \frac{DP'_{(CL-Cl)}+DP'_{(CL-DOPA)}}{DP_{(CL-Cl)}} \leq 90\% \quad (2.9)$$

where the molecular weight of PCL-*co*-PCL-Cl ($M_{n(1)}$) and PCL-*b*-(PCL-DOPA$_{TBDMS}$)$_2$ ($M_{n(2)}$) was measured by SEC using DMF as eluent. The DP$_{(CL-Cl)}$ was calculated using Figure 2.6 from Equation 2.4, the DP'$_{(CL-Cl)}$ and DP'$_{(CL-DOPA)}$ were respectively calculated using Equation 2.4 and 2.6 by the ^{1}H NMR of block-macroinitiator. If any reaction result in nucleophilic substitution modification is in accord with Equation 2.9, this condition induced the degradation.

Table 2.3 shows the summarized results. The reaction progress was evaluated using ^{1}H NMR spectrum. To evaluate the solvent, chloroform, toluene, and acetonitrile with different boiling points and polarities were chosen.[14] The reaction was carried out in the presence of TEA and with or without KI (No. 1-6 in Table 2.3). The nucleophilic substitution reaction takes place in toluene with KI and in acetonitrile with and without KI. Polar solvents are accepted to promote nucleophilic substitution reactions since this solvent is able to enhance the nucleophilic of amino groups.[14] Meanwhile, the leaving groups in PCL-*b*-(PCL-CL)$_2$ which are chloride units, are stable leading to severer reaction conditions. The addition of KI is important to improve the conversion rate by the halogen exchange reaction (Figure 2.10).[15-16] More than one research indicates the addition of KI is able to replace the chloride units by iodine which is a better leaving group. To understand an effect of different bases on the reaction, TEA, KOH, Bpy, and DIEA were used (No. 6-11) in acetonitrile.[17] Though KOH, TEA and Bpy, the reaction did not progress, use of DIEA gave high conversation rate up to 69%. Moreover, in the case of KOH, the polymer main chain is degraded when the system is including water. As we mentioned above, it seems likely that

acetonitrile is a good solvent for this reaction. To understand further the effect of polar solvents on the reaction, DMF and DMSO were investigated (No. 12 and 13). The conversion of the reaction suppressed in DMF and DMSO. This is because of the solubility of PCL-*b*-$(PCL\text{-}Cl)_2$ in acetonitrile is better than others. We also investigated an effect of temperature on the reaction (No. 14-17). The conversion rate was increased with increasing reaction temperature, but polymer starts to degrade when the reaction was done at higher than 90 ℃. Finally, we focused on the ratio between the chloride units in PCL-*b*-$(PCL\text{-}Cl)_2$ and dopamine derivatives (No. 10 and 11). The reactions were carried out with two stoichiometric ratios of chloride units and dopamine derivatives (1:2 and 1:4). The conversion of nucleophilic substitution reaction for mixture ratio of 1:4 was higher than that of 1:2. This result indicates that excess amount of dopamine derivatives are needed for this reaction.

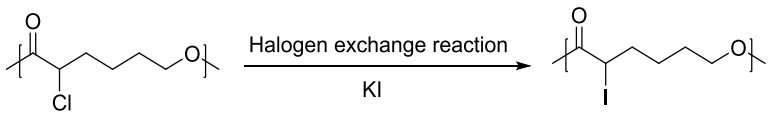

Figure 2.10. Mechanism of chloride units replaced by iodine through halogen exchange reaction.

Table 2.3. Exploration of Dopamine Functionalization via Nucleophilic Substitution

No.	Temperature	Solvent	Cl:DOPA[a]	Time (h)	Salt	Base	R[b]	Degrad[c]
1	40 ℃	Chloroform	1:2	24	——	TEA	0%	No
2	40 ℃	Chloroform	1:4	48	KI	TEA	0%	No
3	75 ℃	Toluene	1:2	24	——	TEA	0%	No
4	75 ℃	Toluene	1:4	48	KI	TEA	5%	No
5	80 ℃	Acetonitrile	1:2	24	——	TEA	<5%	No
6	80 ℃	Acetonitrile	1:2	48	KI	TEA	11%	No
7	80 ℃	Acetonitrile	1:2	48	KI	KOH	0%	No
8	80 ℃	Acetonitrile/H_2O	1:2	48	KI	KOH	0%	YES
9	80 ℃	Acetonitrile	1:2	48	KI	Bpy	0%	No
10	80 ℃	Acetonitrile	1:2	48	KI	DIEA	49%	No
11	80 ℃	Acetonitrile	1:4	48	KI	DIEA	69%	No
12	80 ℃	DMF	1:4	48	KI	DIEA	32%	No
13	80 ℃	DMSO	1:2	48	KI	DIEA	40%	No
14	60 ℃	DMF	1:2	24	KI	DIEA	0%	No
15	70 ℃	DMF	1:2	24	KI	DIEA	<5%	No
16	80 ℃	DMF	1:2	24	KI	DIEA	12%	No
17	90 ℃	DMF	1:2	24	KI	DIEA	27%	YES

[a]Cl:DOPA is the molar ratio of the chloride units in copolymer PCL-*b*-$(PCL\text{-}Cl)_2$ and protected dopamine; [b]R refers to the conversion rate of chloride unit in PCL-*b*-$(PCL\text{-}Cl)_2$ which is calculated using the ^{1}H NMR spectrum; [c]Degrad is the degradation of PCL main chain which is evaluated by combining the SEC and ^{1}H NMR using Equation 2.

2.3.4. Degradation test of PCL-*b*-$(PCL\text{-}DOPA\text{-}b\text{-}PMPC)_2$

The results of degradation test are summarized in Table 2.4. Though PCL and Polymer 2 are fully degraded within 12 h, the WL of PCL-*b*-$(PCL\text{-}DOPA\text{-}b\text{-}PMPC)_2$ is 56 %. This phenomenon

might be attributed to the PMPC modification, whereby the long PMPC segments hinder the interaction between lipase and PCL segments at the outermost surface.

Table 2.4. Degradation of PCL, PCL-*b*-(PCL-DOPA$_{TBDMS}$)$_2$ and PCL-*b*-(PCL-DOPA-*b*-PMPC)$_2$

	Total mass (μg)	Weight loss (μg)	Weight loss (%)
PCL	237.64	237.03	99.74
PCL-*b*-(PCL-DOPA$_{TBDMS}$)$_2$	238.57	237.58	99.58
PCL-*b*-(PCL-DOPA-*b*-PMPC)$_2$	181.50	101.25	55.79

2.4. Conclusion

The dual-functionalization of PCL was achieved on the basis of nucleophilic substitution reaction and ATRP. The nucleophilic substitution reaction condition was comprehensively evaluated for solvent, temperature, reaction time, base and the addition of inorganic salt. The resultant polymer showed high conversion rate (69%) which is close to that in ATRA. During the reaction, no obvious side reaction, degradation and cross-linking can be observed. Furthermore, the end-functionalization of PCL using MPC was realized by the ATRP. ^{1}H NMR of resultant polymer showed the reaction is succeeded. The enzyme degradability was proved by QCM measurement.

2.5. Reference

1. van Natta, F. J.; Hill, J. W.; Carothers, W. H. Studies of Polymerization and Ring Formation. ε-Caprolactone and its Polymers. *Journal of the American Chemical Society* **1934,** *56,* 455-457.

2. Du, J.; Armes, S. P. Preparation of Biocompatible Zwitterionic Block Copolymer Vesicles by Direct Dissolution in Water and Subsequent Silicification within Their Membranes. *Langmuir* **2009,** *25* (16), 9564-9570.

3. Pires, N. M.; van der Hoeven, B. L.; de Vries, M. R.; Havekes, L. M.; van Vlijmen, B. J.; Hennink, W. E.; Quax, P. H.; Jukema, J. W. Local Perivascular Delivery of Anti-Restenotic Agents from a Drug-eluting Poly(epsilon-caprolactone) Stent Cuff. *Biomaterials* **2005,** *26* (26), 5386-5394.

4. Woodruff, M. A.; Hutmacher, D. W. The Return of a Forgotten Polymer—Polycaprolactone in the 21st Century. *Progress in Polymer Science* **2010,** *35* (10), 1217-1256.

5. Lu, F.; Lei, L.; Shen, Y.-Y.; Hou, J.-W.; Chen, W.-L.; Li, Y.-G.; Guo, S.-R. Effects of Amphiphilic PCL–PEG–PCL Copolymer Addition on 5-fluorouracil Release from Biodegradable PCL Films for Stent Application. *International Journal of Pharmaceutics* **2011,** *419* (1-2), 77-84.

6. Childs, M. A.; Matlock, D. D.; Dorgan, J. R. Surface Morphology of Poly(caprolactone)-b-poly(dimethylsiloxane)-b-poly(caprolactone) Copolymers: Effects on Protein Adsorption. *Biomacromolecules* **2001,** *2*, 526-537.

7. Lecomte, P.; Riva, R.; Schmeits, S.; Rieger, J.; Van Butsele, K.; Jérôme, C.; Jérôme, R. New Prospects for the Grafting of Functional Groups onto Aliphatic Polyesters. Ring-Opening Polymerization of α- or γ- Substituted ε-Caprolactone Followed by Chemical Derivatization of the Substituents. *Macromolecular Symposia* **2006,** *240* (1), 157-165.

8. Li, S.; Cai, Y.; Cao, J.; Cai, M.; Chen, Y.; Luo, X. Phosphorylcholine micelles decorated by hyaluronic acid for enhancing antitumor efficiency. *Polymer Chemistry* **2017,** *8* (16), 2472-2483.

9. Labet, M.; Thielemans, W. Synthesis of Polycaprolactone: a Review. *Chemical Society reviews* **2009,** *38* (12), 3484-504.

10. He, X.; Liang, L.; Xie, M.; Zhang, Y.; Lin, S.; Yan, D. Synthesis of Novel Linear PEO-*b*-PS-*b*-PCL Triblock Copolymers by the Combination of ATRP, ROP, and a Click Reaction. *Macromolecular Chemistry and Physics* **2007,** *208* (16), 1797-1802.

11. Riva, R.; Lenoir, S.; Jérôme, R.; Lecomte, P. Functionalization of Poly(ε-caprolactone) by Pendant Hydroxyl, Carboxylic Acid and Epoxide Groups by Atom Transfer Radical Addition. *Polymer* **2005,** *46* (19), 8511-8518.

12. Riva, R.; Schmeits, S.; Stoffelbach, F.; Jerome, C.; Jerome, R.; Lecomte, P. Combination of Ring-opening Polymerization and "Click" Chemistry Towards Functionalization of Aliphatic Polyesters. *Chemical communications* **2005,** 42, 5334-5336.

13. Zhou, S.; Deng, X.; Yang, H. Biodegradable Poly(ε-caprolactone)-poly(ethylene glycol) Block Copolymers: Characterization and Their Use as Drug Carriers for a Controlled Delivery System. *Biomaterials* **2003,** *24* (20), 3563-3570.

14. Martí-Centelles, V.; Burguete, M. I.; Luis, S. V. Template Effects in S_N2 Displacements for the Preparation of Pseudopeptidic Macrocycles. *Chemistry - A European Journal* **2012,** *18* (8), 2409-2422.

15. McBee, E. T.; Christman, D. L.; Johnson Jr, R. W.; Roberts, C. W. Rates of Reaction of Some Halogen-containing Esters with Potassium Iodide in Dry Acetone 1, 2. *Journal of the American Chemical Society* **1956,** *78* (18), 4595-4596.

16. Massari, L.; Panelli, L.; Hughes, M.; Stazi, F.; Maton, W.; Westerduin, P.; Scaravelli, F.; Bacchi, S. A Mechanistic Insight into a Simple C−N Bond Formation via SN2 Displacement: A Synergistic Kinetics and Design of Experiment Approach. *Organic Process Research & Development* **2010,** *14* (6), 1364-1372.

17. Kumar, S. R.; Gallazzi, F. A.; Quinn, T. P.; Deutscher, S. L. 64Cu-Labeled Peptide for PET of Breast Carcinomas Expressing the Thomsen-Friedenreich Carbohydrate Antigen. *Journal of Nuclear Medicine* **2011,** *52* (11), 1819-1826.

Chapter 3

Adsorption Behavior of Dual-Functionalized Polycaprolactone

3.1. Introduction

Stainless steel (SUS) with high impact strength, wear resistance, ductility and toughness is widely used as scaffolding materials in biomedical fields.[1] Contemporary SUS materials contain different kinds of metals, for example, 316L SUS contains nickel (12 wt%), chromium (17 wt%), and molybdenum (2.5 wt%).[2-3] After implantation into human bodies, those metal ions release during the continuous contact with blood, which triggers the local immune responses and inflammatory reactions.[4-5] To address these problems, polymer coating have been introduced onto SUS surface, which is able to isolate the materials from blood.[6-7] The "graft-to" method is well-suitable for the materials with various shapes. Catechol groups in PCL-*b*-(PCL-DOPA-*b*-PMPC)$_2$ endow this material with strong adhesion properties.[8-9] This surface modifier is able to form a PC layer on the surface of the surface which reduces the protein adsorption and improves the biocompatibility.[10-11]

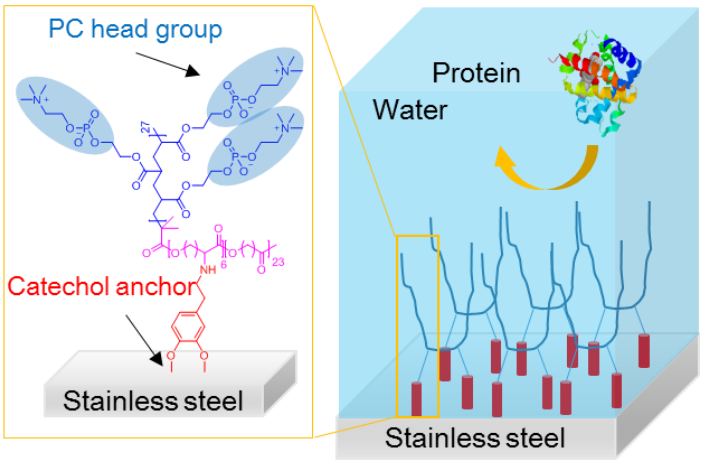

Figure 3.1. Formation of PCL-*b*-(PCL-DOPA-*b*-PMPC)$_2$ thin film on SUS surface, reducing the fouling properties on the SUS substrate in water.

In this chapter, we try to prepare the polymer thin film onto the stainless steel surface via "graft-to" technique (Figure 3.1). The PCL-*b*-(PCL-DOPA-*b*-PMPC)$_2$ was utilized as the template to evaluate the adhesion properties of dopamine-modified PCL-*b*-PMPC on SUS. The impact of

polymeric film formation was evaluated using X-ray photoelectron spectroscopy (XPS) and contact angle measurements. The coating stability was tested to show the strong adhesion between surface and dopamine functionalized PCL-*b*-PMPC. The further anti-fouling property was clarified by the fluorescence-labeled bovine serum albumin (BSA) and fibrinogen (Fg).

3.2. Experiment

3.2.1. Materials

Dodecylphosphonic acid, fluorescein isothiocyanate (FITC), tetramethylrhodamine (TRITC), bovine serum albumin (BSA), and fibrinogen (Fg) were purchased from Sigma-Aldrich, Japan and used without further purification. Methanol, dimethyl formamide (DMF), dimethylsulfoxide (DMSO), acetonitrile, and tetrahydrofuran (THF) were purchased from Wako Pure Chemicals Co. (Japan). All solvents mentioned above were used without any further purification. Anhydrous toluene and dichloromethane (DCM) were obtained by the ultimate solvent system (Nikko Hansen Corporation, Japan). Anhydrous triethylamine (TEA), purchased from Sigma-Aldrich (Japan) was dehydrated by refluxing using CaH_2 (Sigma-Aldrich, Japan) and collected by distillation under a nitrogen atmosphere.

3.2.2. Adsorption behavior of PCL-*b*-(PCL-DOPA-*b*-PMPC)$_2$ on SUS

The adsorption behavior of PCL-*b*-(PCL-DOPA-*b*-PMPC)$_2$ was evaluated by immersing stainless steel sheets in polymer solutions with different concentrations in a mixed solvent of chloroform and methanol (v:v = 1:1). Stainless steel sheets (1 cm × 1 cm) were cleaned by sonication in hexane, acetone, and water sequentially (in triplicate, 15 min for each replicate). The substrates were exposed twice to vacuum ultraviolet (VUV) radiation for 15 min (each exposure). After that, the cleaned stainless steel sheets were immersed in the polymer solutions for 18 h to promote film formation of PCL-*b*-(PCL-DOPA-*b*-PMPC)$_2$ onto the substrates. Deprotected

copolymer solution in four concentrations (i.e., 15, 25, 50, and 75 mg/mL), the protected copolymer (50 mg/mL) solution, and a chloroform:methanol (v:v = 1:1) solution were used for the investigation. The corresponding samples have been labeled as SUS-PC-15, SUS-PC-25, SUS-PC-50, SUS-PC-75, SUS-Protect-50, and SUS-Solvent, respectively. For the polymer with a concentration of 75 mg/mL, the high viscosity and opaque of the solution indicate that the polymer is not able to be well-dissolved. Thus, concentrations higher than 75 mg/mL was not explored. After 18 h of immersion, the samples were rinsed for several times with a chloroform: methanol (v:v= 1:1) solution. The formation of the polymer thin film on the SUS samples at various conditions was evaluated by X-ray photoelectron spectroscopy (XPS) and contact angle measurements.

3.2.3. Durability of PCL-*b*-(PCL-DOPA-*b*-PMPC)$_2$ film on SUS

The durability of the PCL-*b*-(PCL-DOPA-*b*-PMPC)$_2$ thin film on SUS in water was tested. Samples were immersed in a phosphate-buffered saline (PBS) buffer solutions for 45 days at 25 ℃. Subsequently, the samples were dried in a vacuum oven and the integrity of the thin film surfaces was characterized using attenuated total reflectance Fourier transform infrared (ATR-FTIR) spectroscopy and XPS.

3.2.4. Evaluation of protein adsorption

Two types of protein (i.e., BSA and Fg) were chosen as probes to evaluate the anti-fouling properties of the copolymer-coated SUS samples. BSA is the most common protein in blood, and Fg plays an important role in the formation of blood clots. Before the tests, the BSA and Fg were labeled with different fluorescence probes to visualize the adsorbed protein on the sample surfaces. BSA was labeled with FITC, which fluoresces green (λ_{Ex} = 497 nm, λ_{Em} = 524 nm), whereas Fg was labeled by TRITC, which fluoresces red (λ_{Ex} = 547 nm, λ_{Em} = 572 nm). With stirring at 0 ℃,

a specific amount of protein, with a fixed concentration of 20 mg/mL, was dissolved in normal saline (NS) and a Na_2CO_3/$NaHCO_3$ buffer solution (pH = 9.0) (v:v = 1:10). Concomitantly, FITC or TRITC solution dissolved in a mixture of water/DMSO (v:v = 2:1), was dripped into the protein solution, and the solution was kept at 0 ℃ for 12 h. Note that the amount of fluorescence probe was 1% (wt%) relative to the amount of protein. After the reaction, any free probe and salt was removed using pre-packaged disposable PD-10 columns (GE Healthcare, Japan), and the TRITC- and FTIC-labeled protein was obtained by freeze-drying.[12-13]

The protein solutions were prepared by dissolving BSA-FITC (31 mg) and Fg-TRITC (22 mg) into 10 mL PBS (pH= 7.4), respectively. The initial protein concentrations (C_o) were determined by the fluorescence intensity of the prepared protein solutions. To evaluate the anti-fouling property of the SUS samples coated with different treatments, 4 samples of PCL-*b*-(PCL-DOPA-*b*-PMPC)$_2$-coated surface (SUS-PC-50), dodecylphosphonic acid self-assembled SUS (Control), PCL spin-coated (PCL), and bare SUS (SUS) were prepared. Subsequently, all samples were immersed in the 0.7 mL BSA-FITC solutions and 0.7 mL Fg-TRITC solutions for 5 h. The samples were then rinsed with 3 mL PBS (pH= 7.4) to remove any unabsorbed protein. The solutions used in the adsorption test and wash procedure were collected and diluted in a 5 mL volumetric flask using PBS. The concentration of protein solution after protein adsorption test (C_1) can be determined by fluorescence spectrometer and the amount of adsorbed protein (M) is calculated using Equation 3.1.

$$M = C_0 \times 0.7 - C_1 \times 5 \quad (3.1)$$

3.2.5. Characterizations

The X-ray photoelectron spectroscopy (XPS) analysis was performed by ULVAC-PHI XPS instrument (ULVAC-PHI, Inc. Japan) at room temperature under 2×10^{-9} torr, and the take-off angle

was set at 45 °. Atomic force microscope (AFM) observation was performed using an Asylum Cypher scanning probe microscope (SPA400, Cypher Corporation, Japan) in tapping mode with silicon cantilevers (f=324 kHz, spring constant=36 N/m, Si-DF40, SII Instruments Corporation, Japan) coated with aluminum. Before the AFM observation, all samples were dried under high vacuum for 12 h. Contact angle measurements were performed using a Theta T200 Auto3 contact angle instrument (Altech Corporation, Japan), where 2 μL water droplet and 2 μL air bubbles were used for in-air and in-water contact angle measurement, respectively. Attenuated total reflectance Fourier transform infrared (ATR-FTIR) spectroscopy was performed by Spectrum One FTIR spectrometer (PerkinElmer, USA) equipped with an ATR accessory (Ge crystal, 45 °). Each FT-IR spectrum was obtained with 4 cm^{-1} resolution and 1024 scans in the range of 4000-650 cm^{-1}. A Nikon Eclipse E400 biological microscope system with a super-high pressure fluorescent mercury lamp was used to collect fluorescent images after protein adsorption test. For the fluorescence spectroscopy was conducted by a spectrofluorometer (FP-8300, Jasco). The BSA-FTIC samples were measured at λ_{Ex} = 497 nm and λ_{Em} = 524 nm; Fg-TRITC samples were measured at λ_{Ex} =547 nm and λ_{Em} = 572 nm. Each sample was done in triplicate and the average value obtained was reported.

3.3. Results and Discussion

3.3.1. Adsorption behavior of PCL-b-(PCL-DOPA-b-PMPC)$_2$ on SUS

In order to understand the adsorption of PCL-*b*-(PCL-DOPA-*b*-PMPC)$_2$ on the SUS substrate, AFM observations were made. Figure 3.2 shows AFM phase-contrast (Figures 3.2.a1–d1) and topographic images (Figures 3.2.a2–f2) of a) SUS-Solvent, b) SUS-Protect-50, c) SUS-PC-15, d) SUS-PC-25, e) SUS-PC-50, and f) SUS-PC-75. The SUS substrate was not always completely flat and smooth, whereby linear flaws can be observed. For the samples grafted with the copolymers,

the less linear flaws of the SUS substrates can be observed when the higher concentrations of the copolymer solutions were used to form modification layers on SUS substrates (Figure 3.2 (c-f)), implying the successful formation of the copolymer coatings on the surfaces. Considering the roughness of the surfaces of the SUS substrates, however, the samples prepared using higher concentrations (eg. SUS-PC-75, Figure 3.2(f)) are much easier to form aggregate structures and increase the surface roughness than those using moderate (relatively lower) concentrations (eg. SUS-PC-50, Figure 3.2(e)), which might be caused by stronger inter- and intra-molecular interactions of the samples prepared using copolymer solutions with higher concentrations.

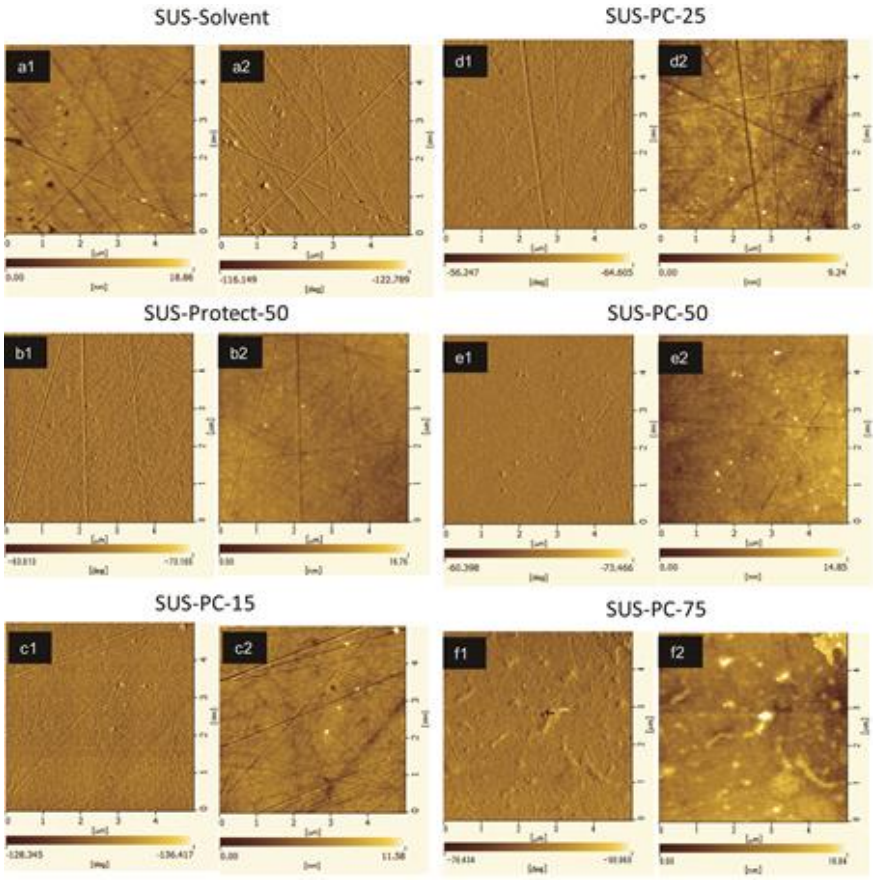

Figure 3.2. AFM phase images (a1–f1) and height images (a2–f2). a) SUS-solvent, b) SUS-Protect-50, c) SUS-PC-15, d) SUS-PC-25, e) SUS-PC-50, and f) SUS-PC-75.

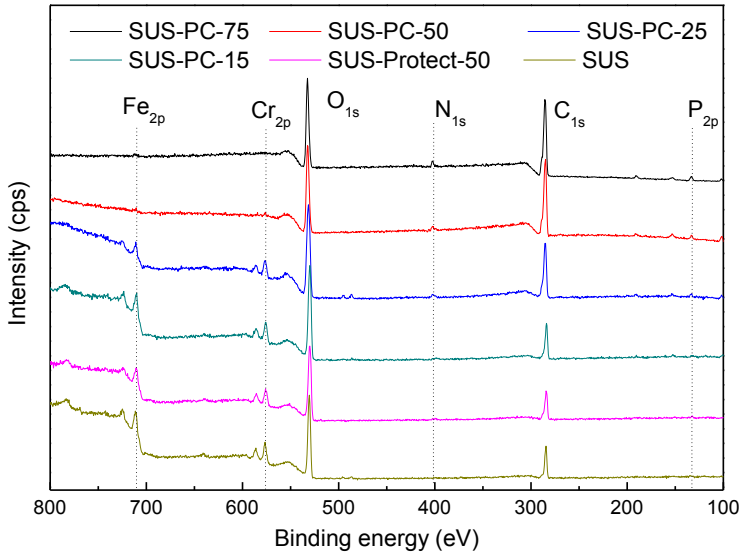

Figure 3.3. XPS spectrum of SUS, SUS-Protect-50, SUS-PC-15, SUS-PC-25, SUS-PC-50, and SUS-PC-75.

Table 3.1 Elemental Ratio Obtained from Survey Scans of the Polymer Thin Films

Ratio (%)	C_{1s}	N_{1s}	O_{1s}	P_{2s}	Fe_{2p}
SUS-Solvent	43.52	2.2	48.9	<0.1	5.37
SUS-Protect-50	43.33	<0.1	51.03	<0.1	5.61
SUS-PC-15	47.72	0.33	46.92	0.43	4.6
SUS-PC-25	56.71	1.42	39.02	1.77	1.08
SUS-PC-50	66.72	1.36	29.05	2.49	<0.1
SUS-PC-75	68.22	2.94	27.32	1.48	<0.1

The surface chemical compositions of functionalized SUS samples were characterized by XPS. The corresponding spectra are shown in Figure 3.3 and their elemental ratios are summarized in Table 3.1. The SUS-Protect-50 and SUS samples showed a comparable ratio of Fe_{2p}, indicating the protected dopamine units do not adsorb strongly on the SUS surface. After rinsing with a chloroform: methanol (v:v = 1:1) solution, most of the polymer detached from the surface. The Fe_{2p} ratio decreased for the substrate immersed in the PCL-*b*-(PCL-DOPA-*b*-PMPC)$_2$ solution as the ratios of C_{1s}, N_{1s}, and P_{2s} increased, indicating that PCL-*b*-(PCL-DOPA-*b*-PMPC)$_2$ possesses strong polymer-substrate interactions and can resist detachment during the rinsing procedure.

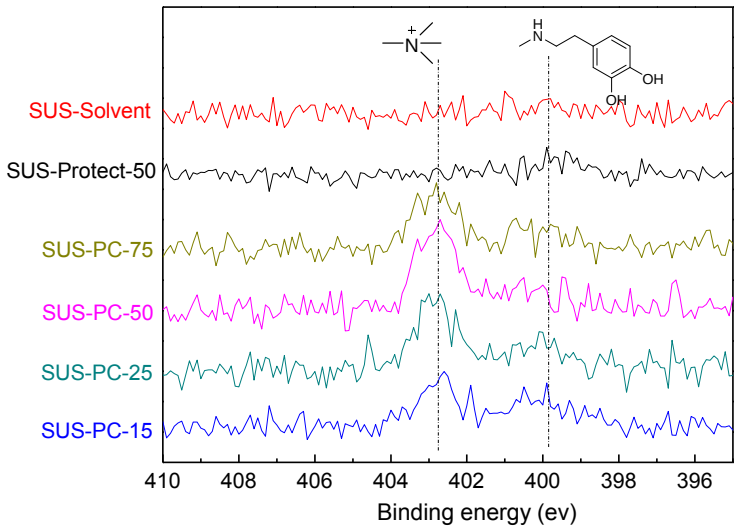

Figure 3.4. High-resolution scan of N_{1s} on SUS, SUS-Protect-50, SUS-PC-15, SUS-PC-25, SUS-PC-50, SUS-PC-75.

Figure 3.4 shows the XPS high-resolution scan of N_{1s} for PCL-*b*-(PCL-DOPA-*b*-PMPC)$_2$. Two kinds of N_{1s} peaks which are attributed to PC (402.4 eV) and dopamine groups (400.2 eV), could be observed. The integral intensity of the peak at 402.4 eV was increased relative to the peak at 400.2 eV in SUS-PC-15, SUS-PC-25, and SUS-PC-50. These results indicate that the density of PMPC segments at the outermost surface was increased in the order of SUS-PC-15, SUS-PC-25, and SUS-PC-50. On the other hand, SUS-PC-75 showed the different trend. The aggregate structures in SUS-PC-75 caused the surface reorganization, resulting in the reduction of the peak at 402.4 eV relative to the peak at 400.2 eV. Generally, surface reorganization takes place to minimize surface free energy when the samples were placed in hydrophilic or hydrophobic conditions. XPS measurements were performed at high vacuum condition, leading to the migration of PCL segments toward the outermost surface. SUS-PC-15, SUS-PC-25 and SUS-PC-50 films are consisting of flat and the dopamine groups are interacting with the substrate.

This interaction could control the surface reorganization. However, SUS-PC-75 is consisting of aggregate structures, and this interaction is regulated, leading to the surface reorganization.

Taking the results of AFM observation and XPS data into account, the formation of polymer thin film is proposed in Figure 3.5. At a low concentration, the polymer density is low and only a small amount of the polymer adsorbed onto the SUS surface. This phenomenon is why the SUS-PC-15 sample showed a high Fe_{2p} ratio but low P_{2s} and N_{1s} ratios. For the SUS-PC-50 film, the Fe_{2p} ratio decreased significantly to below 0.1 %, indicating that the film became more uniform as the solution concentration increases. When the concentration was above 50 mg/mL, the polymer formed aggregate structures due to strong polymer-polymer interactions, which led to a thicker film on the SUS surface. During the drying procedure, the hydrophobic segments of PCL-*b*-(PCL-DOPA)$_2$ migrated to the outermost surface to reduce the surface free energy. Hence, PCL segments covered the outermost surface, causing the week P_{2s} ratio.

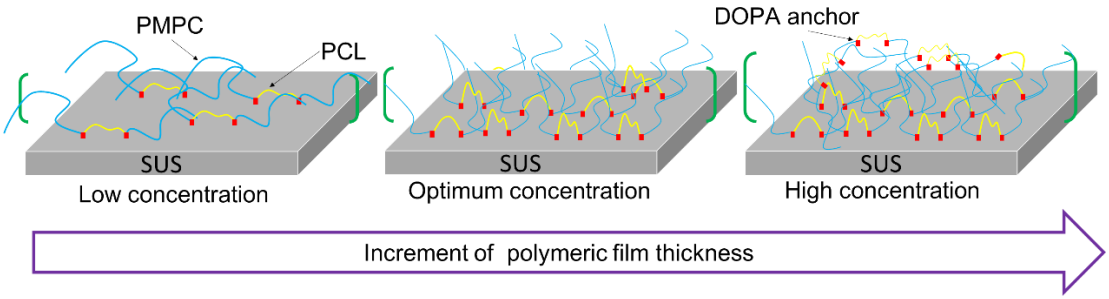

Figure 3.5. Adsorption behavior of PCL-*b*-(PCL-DOPA-*b*-PMPC)$_2$.

The surface wettability of the samples was investigated by contact angle measurements using air bubbles and water droplets as probes. The contact angle values are summarized in Table 3.2 and the side-view images of a water droplet in open air and air bubbles in water for samples are shown in Figures 3.6 and 3.7, respectively. Similar values were obtained for the SUS and SUS-Protect-50 samples, suggesting that PCL-*b*-(PCL-DOPA$_{TBDMS}$-*b*-PMPC)$_2$ does not adsorb onto the SUS substrate. The contact angle of the water droplet in the open air decreased for the

PCL-*b*-(PCL-DOPA-*b*-PMPC)$_2$ systems. As described above, the polymer film thickened with the increase of polymer concentration. This behavior induced a decrease of the contact angle from SUS-PC-15 to SUS-PC-50. The higher contact angle observed for SUS-PC-75 suggests that hydrophobic moieties cover the outermost surface. Further, the air bubble contact angle in water implies an insufficient adsorption of SUS-PC-15, as evidenced by the 137.6 ° value measured using air bubbles as the probe. Since super-hydrophilic surfaces were present for the SUS-PC-25, SUS-PC-50, and SUS-PC-75 samples, it is clear that the polymer thin film can provide a super-hydrophilic surface for SUS in water.

Table 3.2. Contact Angle Data of Different Surface Coated Stainless Steel Samples

Contact angle (°)	In-air[a]	In-water[b]
SUS-Solvent	90.7±0.4	124.5±1.8
SUS-Protect-50	90.2±0.7	129.1±0.4
SUS-PC-15	58.3±0.6	137.6±0.8
SUS-PC-25	52.6±1.3	N/A[c]
SUS-PC-50	44.7±0.3	N/A[c]
SUS-PC-75	52.9±1.0	N/A[c]

[a]Contact angle was measured in the open air with a 2 μL water droplet; [b]Contact angle was measured in water condition with a 2 μL air bubble; [c]Air-bubble contact angle in the water, polymer thin film showed super-hydrophilicity; the air bubble cannot attach onto the surface.

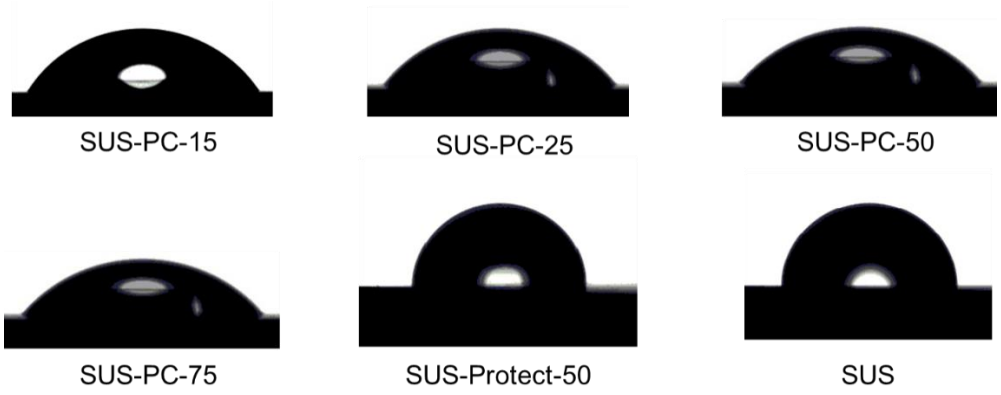

Figure 3.6. Photographs (side-view) of water droplets in the open air on the surfaces of SUS-PC-15, SUS-PC-25, SUS-PC-50, SUS-PC-75, SUS-Protect-50, and SUS using 2 μL water drop as the probe at room temperature.

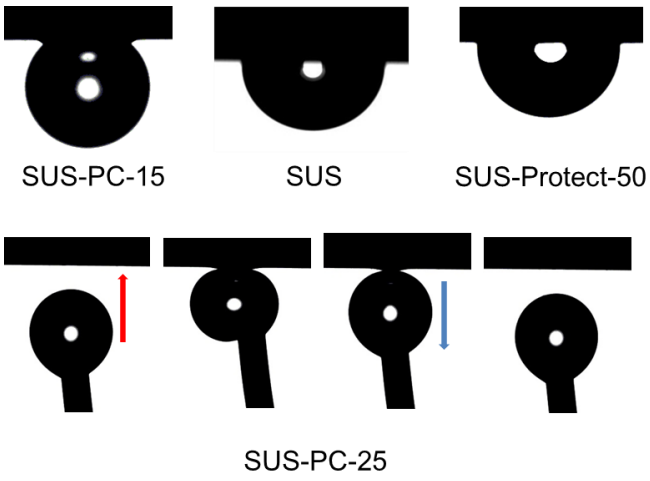

Figure 3.7. Photographs (side view) of air bubbles in water on the surfaces of SUS-PC-15, SUS-PC-25, SUS-Protect-50, and SUS samples using 2 μL air bubbles as the probe at room temperature for the samples.

3.3.2. Durability of PCL-*b*-(PCL-DOPA-*b*-PMPC)$_2$ film on SUS

The durability of PCL-*b*-(PCL-DOPA-*b*-PMPC)$_2$-adsorbed SUS under aqueous conditions was evaluated by ATR-FITR spectroscopy. Figure 3.8 shows the ATR-FITR spectra of SUS-PC-50 before water immersion and after water immersion for 45 days. As seen, these two spectra are almost identical. The characteristic peaks of O=P-O stretching (1090, 1069 and 1044 cm^{-1}) and –$N^+(CH3)_3$ stretching (960 cm^{-1}) in PMPC unit, and C=O stretching (1725 cm-1) in both PCL and PMPC blocks present in the spectra of both two samples, demonstrating a good durability of PCL-*b*-(PCL-DOPA-b-PMPC)$_2$ thin film in the PBS buffer solution.

Furthermore, the change of surface chemical composition after 45-days immersion was also characterized using XPS measurements. If the decomposition takes place, it is anticipated that the atomic ratio of C_{1s}/P_{2s} should increase. The atomic ratio of C_{1s}/P_{2s} was calculated to show the surface changes (Figure 3.9). The values of the initial stage and after 45-day immersion were similar, implying the polymer film remains stable in PBS solution under room temperature for a very long period of time.

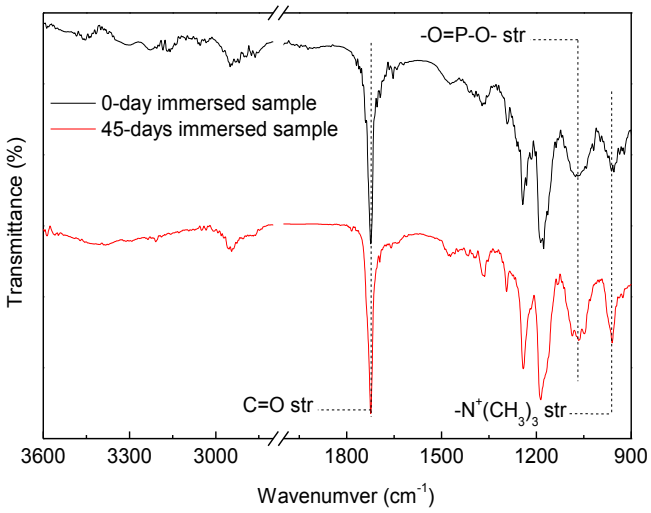

Figure 3.8. ATR-FTIR spectra of SUS-PC-50 sample before/after 45-days immersion in water.

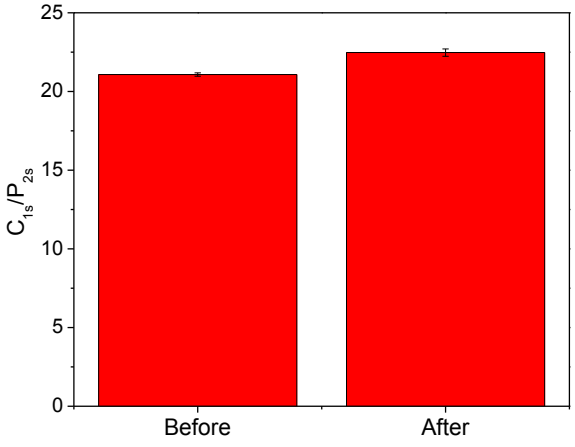

Figure 3.9. XPS atomic ratio of C_{1s}/P_{2s} before (left) and after (right) 45-days immersion.

3.3.3.Evaluation of protein adsorption

In the protein adsorption test, 4 samples including SUS-PC-50, bare stainless steel (SUS), PCL coated stainless steel (PCL), and dodecylphosphonic acid modified stainless steel (control) were prepared to examine their anti-fouling properties. The amount of protein adsorption on these substrates was evaluated by fluorescence spectrophotometry. Here, the fluorescence intensity of the protein solution before and after substrate immersion was converted to the amount of absorbed protein on the substrate (Figure 3.10). It is widely accepted that PCL and dodecylphosphonic acid modified surfaces do not demonstrate anti-fouling because of a favorable protein/hydrophobic surface affinities.[14] The dodecylphosphonic acid and PCL-modified SUS absorbed a higher amount of protein than that of bare stainless steel. However, the amount of protein adsorption on SUS-PC-50 was approximately one-half of that on the bare stainless steel sample.

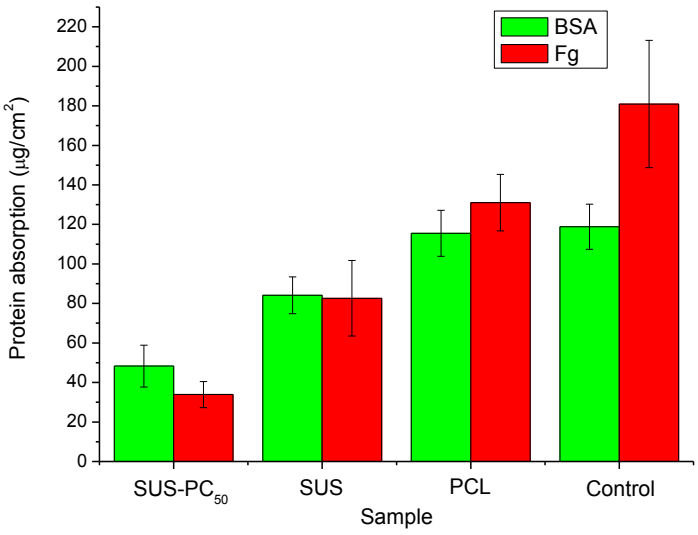

Figure 3.10. BSA and Fg adsorption on SUS-PC-50, SUS, PCL, and control samples.

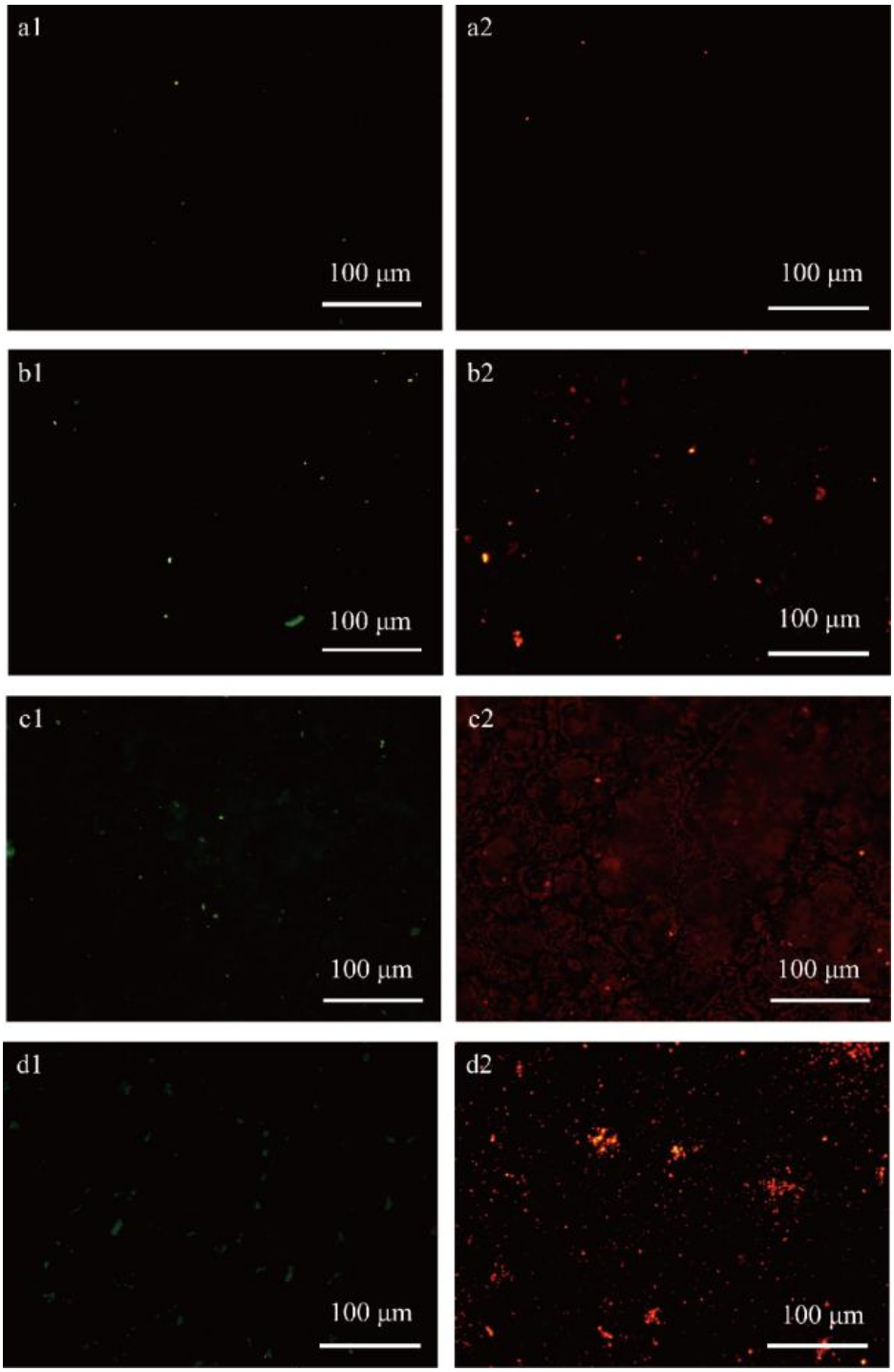

Figure 3.11. Fluorescence microscopy images of BSA adsorption (1) and Fg adsorption (2) on a) SUS-PC-50, b) Bare SUS, c) PCL spin-coated SUS, and d) dodecylphosphonic acid-modified SUS.

In order to directly evaluate protein adsorption, fluorescence microscopy was performed (Figure 3.11). Figures 3.11.a1–d1 show samples immersed in BSA-FITC, whereas Figures 3.11.a2–d2 show samples immersed in Fg-TRITC. It is clear that the fluorescence brightness of

SUS-PC-50 is much less than the other samples. Figures 3.11.b1, d1, b2, c2, and d2 show non-uniform adsorption that originates from protein aggregation. This surface-induced aggregation may cause secondary or tertiary structural changes that induce the formation of protein aggregates with undesirable characteristics, leading to reduced biocompatibility.[15] However, this type of aggregation was not observed in SUS-PC-50, indicating that surface modification using PCL-*b*-(PCL-DOPA-*b*-PMPC)$_2$ has significant potential as a surface modifier for stent materials.

3.4. Conclusion

The "graft-to" method is applied to modify SUS surface using PCL-*b*-(PCL-DOPA-*b*-PMPC)$_2$. The thickness of PCL-*b*-(PCL-DOPA-*b*-PMPC)$_2$ thin film is highly dependent on the concentrations of the used polymer solutions. The thickness of polymer thin film increases with the increment of concentration used. However, the excessive polymer concentration (> 50 mg/mL) may result in aggregate structures of adsorbing polymers because of the stronger interaction resulted in aggregate adsorption. The wettability and anti-fouling properties of the SUS substrates are significantly improved by this polymeric film. The chemical compositions of the PCL-*b*-(PCL-DOPA-b-PMPC)$_2$-coated SUS surface does not change after a 45-days water immersion, demonstrating the stability and durability of the polymer layer. Since polymers containing dopamine groups which possess excellent adhesion properties can be well adsorbed on various metal substrates, the functionalization using PCL-*b*-(PCL-DOPA-*b*-PMPC)$_2$ is possible to have a wide application scope for modification of metal materials.[16-17]

3.5. Reference

1. Sos, T. A.; Sniderman, K. W. Percutaneous Transluminal Angioplasty. *Seminars in Roenrgenology* **1981,** *16* (1), 26-41.

2. Cutlip, D. E.; Baim, D. S.; Ho, K. K. L.; Popma, J. J.; Lansky, A. J.; Cohen, D. J.; Carrozza, J. P.; Chauhan, M. S.; Rodriguez, O.; Kuntz, R. E. Stent Thrombosis in the Modern Era A Pooled Analysis of Multicenter Coronary Stent Clinical Trials. *Circulation* **2001,** *103*, 1967-1971.

3. Bertrand, O. F.; Sipehia, R.; Mongrain, R.; Rodés, J.; Tardif, J.-C.; Bilodeau, L.; Côté, G.; Bourassa, M. G. Biocompatibility aspects of new stent technology. *Journal of the American College of Cardiology* **1998,** *32* (3), 562-571.

4. Moravej, M.; Mantovani, D. Biodegradable metals for cardiovascular stent application: interests and new opportunities. *International Journal of Molecular Sciences* **2011,** *12* (7), 4250-4270.

5. Waterhouse, A.; Yin, Y.; Wise, S. G.; Bax, D. V.; McKenzie, D. R.; Bilek, M. M.; Weiss, A. S.; Ng, M. K. The Immobilization of Recombinant Human Tropoelastin on Metals Using a Plasma-activated Coating to Improve the Biocompatibility of Coronary Stents. *Biomaterials* **2010,** *31* (32), 8332-8340.

6. Dalsin, J. L.; Tosatti, S.; Voros, J.; Textor, M.; Messersmith, P. B. Protein Resistance of Titanium Oxide Surfaces Modified by Biologically Inspired mPEG-DOPA. *Langmuir* **2005,** *21*, 640-646.

7. Acharya, G.; Park, K. Mechanisms of Controlled Drug Release from Drug-eluting Stents. *Advanced drug delivery reviews* **2006,** *58* (3), 387-401.

8. Nicklisch, S. C.; Waite, J. H. Mini-review: the Role of Redox in Dopa-mediated Marine Adhesion. *Biofouling* **2012,** *28* (8), 865-877.

9. Moulay, S. Dopa/Catechol-tethered Polymers: Bioadhesives and Biomimetic Adhesive Materials. *Polymer Reviews* **2014,** *54* (3), 436-513.

10. Goda, T.; Matsuno, R.; Konno, T.; Takai, M.; Ishihara, K. Photografting of 2-Methacryloyloxyethyl Phosphorylcholine from Polydimethylsiloxane: Tunable protein Repellency and Lubrication property. *Colloids and surfaces. B, Biointerfaces* **2008,** *63* (1), 64-72.

11. Ishihara, K.; Mu, M.; Konno, T.; Inoue, Y.; Fukazawa, K. The Unique Hydration State of Poly(2-methacryloyloxyethyl phosphorylcholine). *Journal of biomaterials science. Polymer edition* **2017**, 1-16.

12. Benesch, J.; Hungerford, G.; Suhling, K.; Tregidgo, C.; Mano, J. F.; Reis, R. L. Fluorescence Probe Techniques to Monitor Protein Adsorption-Induced Conformation Changes on Biodegradable Polymers. *Journal of Colloid and Interface Science* **2007,** *312* (2), 193-200.

13. Lok, B. K.; Cheng, Y.-L.; Robertson, C. R. Protein Adsorption on Crosslinked Polydimethylsiloxane Using Total Internal Reflection Fluorescence. *Journal of colloid and interface science* **1983,** *91* (1), 104-116.

14. Yah, W. O.; Xu, H.; Soejima, H.; Ma, W.; Lvov, Y.; Takahara, A. Biomimetic Dopamine Derivative for Selective Polymer Modification of Halloysite Nanotube Lumen. *Journal of the American Chemical Society* **2012,** *134* (29), 12134-12137.

15. Wang, W.; Nema, S.; Teagarden, D. Protein Aggregation-Pathways and Influencing Factors. *International Journal of Pharmaceutics* **2010,** *390* (2), 89-99.

16. Guardingo, M.; Bellido, E.; Miralles-Llumà, R.; Faraudo, J.; Sedó, J.; Tatay, S.; Verdaguer, A.; Busqué, F.; Ruiz-Molina, D. Bioinspired Catechol-Terminated Self-Assembled Monolayers with Enhanced Adhesion Properties. *Small* **2014,** *10* (8), 1594-1602.

17. Jeon, I.; Ogumi, K.; Nakagawa, T.; Matsuo, Y. Enhancement of Fill Factor in Air-processed Inverted Organic Solar Cells Using Self-assembled Monolayer of Fullerene Catechol. *Japanese Journal of Applied Physics* **2016,** *55* (8), 082301 (1-4).

Chapter 4

Crystallization-Induced Suppression of Surface Reorganization

4.1. Introduction

Although PC-based amphiphilic surface modifier possesses good biocompatibility, excellent anti-fouling properties, and non-toxic, the interfacial structures may undergo surface reorganization.[1-3] This phenomenon certainly causes the reduction of functionalities of resultant materials.[4] To address this problem, some research introduced crystalline structure to the polymer chain. Crystallization is a phenomenon whereby atoms or molecules are highly organized in a structure.[5] In a crystalline polymer, the polymer chains fold together and form ordered regions.[6] This indicates the surface reorganization of PC-based surface modifier could be reduced by introducing crystalline hydrophobic segments.[7] PCL-*b*-(PCL-DOPA-*b*-PMPC)$_2$ processing block-polymerized hydrophobic segment, poly(α-dopamine-ε-caprolactone)-*block*-poly(ε-caprolactone)-*block*-poly(α-dopamine-ε-caprolactone) [(PCL-*b*-(PCL-DOPA)$_2$)], is able to form the PCL crystal.[8] However, (PCL-*co*-PCL-DOPA)-*b*-(PMPC)$_2$ with a random-copolymerized hydrophobic segment, PCL-*co*-PCL-DOPA, is amorphous. In this chapter, the surface reorganization tests were performed on PCL-*b*-(PCL-DOPA-*b*-PMPC)$_2$ and (PCL-*co*-PCL-DOPA)-*b*-(PMPC)$_2$. The crystallization properties of different polymer were clarified by wide-angle X-ray diffraction (WAXD) measurement and thin film WAXD. Furthermore, the polymer films of PCL-*b*-(PCL-DOPA-*b*-PMPC)$_2$ and (PCL-*co*-PCL-DOPA)-*b*-(PMPC)$_2$ were prepared via spin-coating method, the surface roughness and morphology were analyzed using AFM observation. The surface reorganization was evaluated with contact angle and XPS measurements.

4.2. Experiment

4.2.1. Analysis of crystallization state

The crystallinity of bulk polymer and polymer films were measured using WAXD measurement and thin film WAXD measurement, respectively. The WAXD measurements of the bulk polymer were performed at two temperatures, namely 25 and 65 ℃. 65 ℃ is beyond the melting point of PCL. To evaluate the molecular aggregation structure in the film state, thin film WAXD measurements were performed on polymer films with a thickness of ~200 nm on stainless steel plates. Both in-plane and out-of-plane scans were carried out to analyze the crystalline state of the polymer films.

4.2.2. Preparation of polymer films

The polymer films were prepared by the spin-coating. Both PCL-*b*-(PCL-DOPA-*b*-PMPC)$_2$ and (PCL-*co*-PCL-DOPA)-*b*-(PMPC)$_2$ were dissolved in DCM/methanol (v:v= 1:1) mixed solvent at 50 mg/mL. The spin-coating was performed at 1500 rpm under normal pressure at room temperature. Resultant samples were dried in vacuum oven.

4.2.3. Evaluation of surface reorganization

The PCL-*b*-(PCL-DOPA-*b*-PMPC)$_2$, (PCL-*co*-PCL-DOPA)-*b*-(PMPC)$_2$, and PCL polymer films were exposed to five sets of conditions, as shown in Figure 4.1.a. The polymer films with 200 nm thickness, which were prepared by spin-coating onto stainless steel substrate, were immersed in water for 24 h and denoted as sample 1. This sample 1 was then dried under high vacuum at 25 ℃ (sample 2) and 60 ℃ (sample 3) for 24 h. Sample 5 and sample 4 were prepared by immersing sample 2 and sample 3 in water. The surface reorganization was evaluated according to contact angle measurements using either water droplet or air bubbles as a probe. The contact angles of sample 1, sample 4, and sample 5, which were immersed in water, were measured using an air bubble in water, while sample 2 and sample 3 were evaluated using a water droplet in the open air.

4.2.4. Characterizations

The wide angle X-ray diffraction (WAXD) measurements were performed on bulk polymer samples at two temperatures, namely 25 ℃ and 65 ℃. Before the measurements, 7 mg of PCL, PCL-*b*-(PCL-DOPA-*b*-PMPC)$_2$, and (PCL-*co*-PCL-DOPA)-*b*-(PMPC)$_2$, were placed in the alumina plate on a heating stage. After heating at 65 ℃ for 10 min, samples were annealed at 45 ℃ for 12 h under nitrogen atmosphere. The X-ray photoelectron spectroscopy (XPS) analysis was performed with ULVAC-PHI XPS instrument (ULVAC-PHI, Inc. Japan) at room temperature under 2×10^{-9} torr, and the take-off angle was set at 15°. Contact angle measurements were performed on a Theta T200 Auto3 contact angle instrument (Altech Corporation, Japan) using either 2 μL water droplet or 8 μL air bubbles as a probe. The thin film WAXD were performed on polymer films, including in-plan and out-of-plane scans. The samples were measured at a rate of 1°/min from 5° to 45° at room temperature. The in-plane scan was carried out at 1° as the incident X-ray angle and scanned $2\theta\chi/\phi$ axis; the out-of-plane scan was performed at 1° as the incident X-ray angle and scanned $2\theta/\omega$ axis.

4.3. Results and Discussion

4.3.1. Analysis of crystallization state

The line profiles (Figure 4.1.a) are the WAXD results of different samples at 25 ℃. Generally, PCL exhibits characteristic diffraction peaks at 2θ of 15.5°, 21.3°, 21.9°, and 23.6°, which are assigned to the (102), (110), (111), and (200) planes, respectively, of the orthorhombic unit cell.[5] Although the line profile of PCL-*b*-(PCL-DOPA-*b*-PMPC)$_2$ is broad, the crystallization peaks at 2θ of 21.3° and 23.6° can be distinguished, which correspond to the (110) and (200) plane of PCL crystal lattice.[13] For (PCL-*co*-PCL-DOPA)-*b*-(PMPC)$_2$ samples, the amorphous PCL were revealed by the observation of amorphous halo in the WAXD measurements. After melting (Figure 4.1.b),

crystallization peaks in PCL-*b*-(PCL-Cl-*b*-PMPC)$_2$ and PCL line profiles vanished and were replaced by amorphous halos. These results proved that PCL-*b*-(PCL-DOPA-*b*-PMPC)$_2$ possesses crystalline PCL, the random-copolymerization hampered folding of the PCL segments resulting in the amorphous hydrophobic segments in (PCL-*co*-PCL-DOPA)-*b*-(PMPC)$_2$.

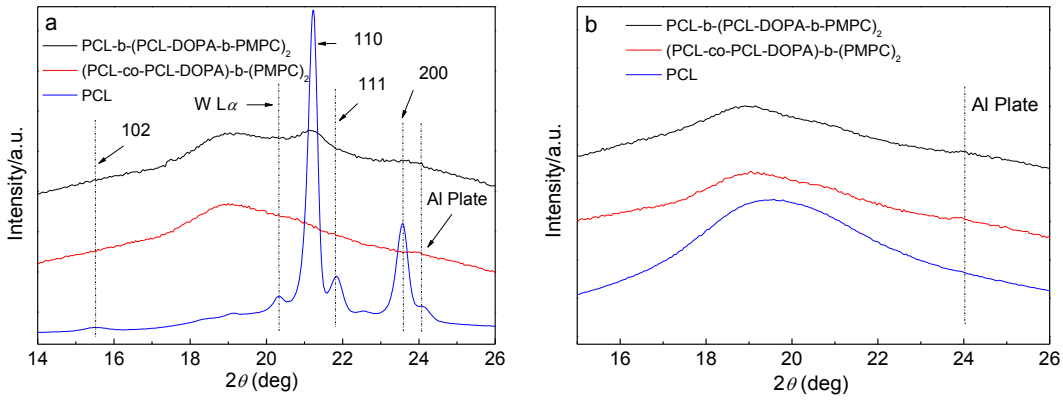

Figure 4.1. WAXD line profiles of PCL-*b*-(PCL-DOPA-*b*-PMPC)$_2$, (PCL-*co*-PCL-DOPA)-*b*-(PMPC)$_2$ and PCL in bulk state at 25 ℃ (a) and 65 ℃ (b).

Figure 4.2 a and b show the in-plane and out-of-plane scans of the thin film WAXD for the PCL-*b*-(PCL-DOPA-*b*-PMPC)$_2$, (PCL-*co*-PCL-DOPA)-*b*-(PMPC)$_2$, and PCL films. The specific diffractions that correspond to the (110) and (200) planes were observed from both in-plane and out-of-plane scans of the PCL film.[13] The (110) diffraction peak along the in-plane direction is more striking than that of the out-of-plane direction. In contrast, the integral intensity of the out-of-plane (200) diffraction peak is more suppressed than that of the in-plane scan. This WAXD result suggests that the (110) and (200) planes orient perpendicular and parallel to the substrate.[14] In the case of the PCL-*b*-(PCL-DOPA-*b*-PMPC)$_2$ film, the diffraction peak corresponding to the (110) plane was observed in the in-plane direction. This indicates that PCL segments in the PCL-*b*-(PCL-DOPA-*b*-PMPC)$_2$ film formed a crystalline structure to which the (110) plane orients perpendicularly. On the other hand, no such diffraction was observed in the

(PCL-*co*-PCL-DOPA)-*b*-(PMPC)$_2$, implying that the (PCL-*co*-PCL-DOPA)-*b*-(PMPC)$_2$ thin film was amorphous, as expected.

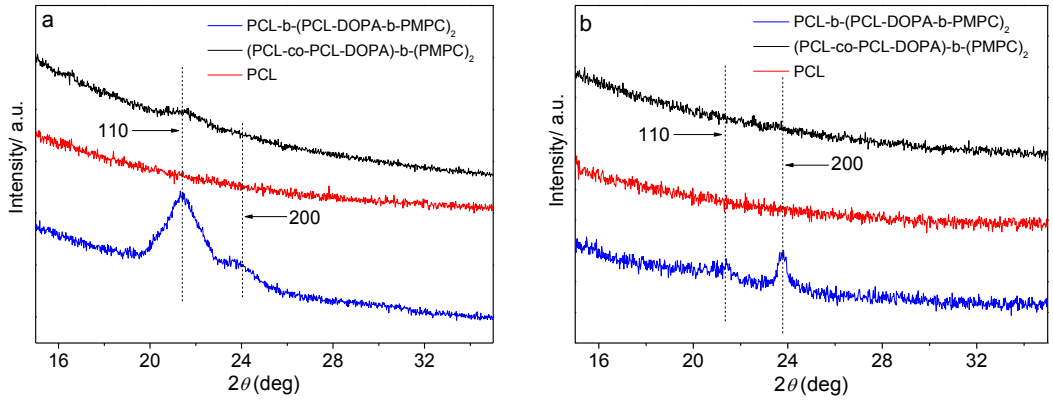

Figure 4.2. Thin film WAXD line profiles of PCL, PCL-*b*-(PCL-DOPA-*b*-PMPC)$_2$ and (PCL-*co*-PCL-DOPA)-*b*-(PMPC)$_2$ spin-coated surface. a. the in-plane scan, b. the out-of-plane scan.

4.3.2. Evaluation of surface reorganization

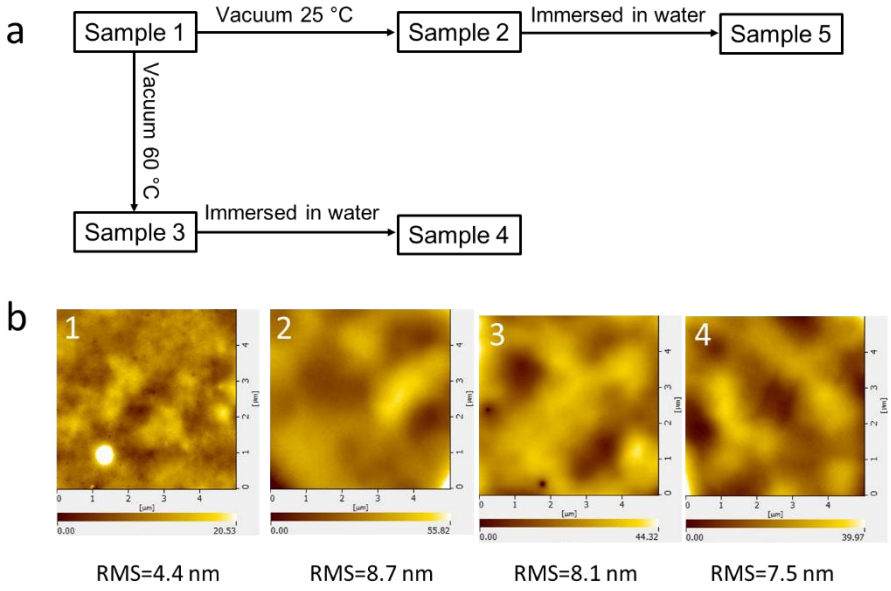

Figure 4.3. a. Different procedure designed for the evaluation of surface reorganization. b. Typical AFM height images. 1) PCL-*b*-(PCL-DOPA-*b*-PMPC)$_2$ (sample 2), 2) PCL-*b*-(PCL-DOPA-*b*-PMPC)$_2$ (sample 3), 3) (PCL-*co*-PCL-DOPA)-*b*-(PMPC)$_2$ (sample 2), and 4) (PCL-*co*-PCL-DOPA)-*b*-(PMPC)$_2$ (sample 3).

AFM observation was performed to show the surface morphology. The AFM images are presented in Figure 4.3 and detailed surface information are summarized in Table 4.1. Both the

RMS and AFM images indicate the spin-coating method is well-suited for PCL-*b*-(PCL-DOPA-*b*-PMPC)$_2$ and (PCL-*co*-PCL-DOPA)-*b*-(PMPC)$_2$ to form a smooth surface that reduces the influence of surface roughness on the contact angle measurements.

The results of the contact angle measurements are summarized in Table 4.1. The PCL-*b*-(PCL-DOPA-*b*-PMPC)$_2$ and (PCL-*co*-PCL-DOPA)-*b*-(PMPC)$_2$ exhibited higher contact angles than that of the PCL in sample 1. These results implied that the PMPC segments segregated at the surface of PCL-*b*-(PCL-DOPA-*b*-PMPC)$_2$ and (PCL-*co*-PCL-DOPA)-*b*-(PMPC)$_2$ films in sample 1. The contact angles of sample 2 increased in the order of PCL-*b*-(PCL-DOPA-*b*-PMPC)$_2$, PCL, and (PCL-*co*-PCL-DOPA)-*b*-(PMPC)$_2$. It has been widely accepted that the sum of the contact angles between air bubble (sample 1) and water droplet (sample 2) is close to 180 ° when the surface reorganization is controlled. In the case of PCL, the sum of the values was 180.6 °, implying that no surface reorganization occurred on the PCL surface. On the other hand, the sum of contact angle values for (PCL-*co*-PCL-DOPA)-*b*-(PMPC)$_2$ (253.2 °) was higher than that of PCL-*b*-(PCL-DOPA-*b*-PMPC)$_2$ copolymer (212.2 °), suggesting that the surface reorganization of PCL-*b*-(PCL-DOPA-*b*-PMPC)$_2$ was more suppressed than (PCL-*co*-PCL-DOPA)-*b*-(PMPC)$_2$. This phenomenon was not observed in sample 3. Although the (PCL-*co*-PCL-DOPA)-*b*-(PMPC)$_2$ and PCL showed similar contact angles, as observed in sample 2, PCL-*b*-(PCL-DOPA-*b*-PMPC)$_2$ copolymer presented a much higher value. This result suggests that the surface reorganization takes place in both (PCL-*co*-PCL-DOPA)-*b*-(PMPC)$_2$ and PCL-*b*-(PCL-DOPA-*b*-PMPC)$_2$ films in sample 3. The value of sample 5 showed a good accordance with that of sample 1. This also strongly suggests that surface reorganization of PCL-*b*-(PCL-DOPA-*b*-PMPC)$_2$ is restricted by the crystallization of PCL domains, while the surface reorganization does take place in (PCL-*co*-PCL-DOPA)-*b*-(PMPC)$_2$.

Table 4.1. Contact Angle Value of Different Samples

Procedure	Contact angle	PCL-*b*-(PCL-DOPA-*b*-PMPC)$_2$	(PCL-*co*-PCL-DOPA)-*b*-(PMPC)$_2$	PCL
Sample 1	Θ_w[b]	160.3 ±1.0 °	169.9 ±0.4 °	112.2 ±0.6 °
Sample 2	Θ_s[a]	51.9 ±1.3 °	83.3 ±0.9 °	74.8 ±1.3 °
	Θ_A	54.5 ±0.9 °	91.1 ±2.2 °	77.7 ±0.4 °
	Θ_R	8.1 ±0.6 °	8.8 ±0.5 °	45.4 ±0.5 °
	Θ_H	46.4 °	74.6 °	32.3 °
Sample 3	Θ_s[a]	79.48 ±2.8 °	85.4 ±1.3 °	76.8 ±1.7 °
	Θ_A	80.15 ±0.6 °	95.9 ±1.0 °	78.7 ±0.4 °
	Θ_R	8.27 ±0.5 °	8.4 ±0.5 °	44.4 ±0.5 °
	Θ_H	71.9 °	87.6 °	34.3 °
Sample 4	Θ_w[b]	137.3 ±3.1 °	164.7 ±0.3 °	110.0 ±0.9 °
Sample 5	Θ_w[b]	164.8 ±0.9 °	169.5 ±1.2 °	111.8 ±1.3 °

[a]Static contact angle using water droplet. [b]Static contact angle using air bubble as probe after immersing the samples in the water for 10min.

The dynamic contact angle measurements were performed using dynamic sessile drop method. Homogenous PCL showed low hysteresis. All samples presented similar and low receding angle. Those results indicated that PMPC segments led to high contact angle (i.e. sample 3), reduced the receding angle and increased hysteresis effect.

Further XPS measurements were performed to evaluate the migration of surface groups. As both PCL-*b*-(PCL-DOPA-*b*-PMPC)$_2$ and PCL-*co*-PCL-DOPA-*b*-PMPC copolymers consist of carbon, nitrogen, and oxygen, it was difficult to clarify the interfacial structure changes. To overcome this problem, dopamine units in the hydrophobic segments were protected using tert-butyldimethylsilyl chloride (TBDMS-Cl). Sample 2 and sample 3 was prepared using TBDMS-protected PCL-*b*-(PCL-DOPA-*b*-PMPC)$_2$ and (PCL-*co*-PCL-DOPA)-*b*-(PMPC)$_2$. Before XPS measurements, samples were kept under high vacuum state for 1 day to obtain fully dried samples. Since the introduction of silicon might reduce the surface free energy of resultant

hydrophobic polymer chain, sample 1, sample 2 and sample 3 were prepared using the protected polymer and the contact angle results are shown in Table 4.2.

Table 4.2. Contact Angle of PCL, PCL-*b*-(PCL-DOPA-*b*-PMPC)$_2$, and (PCL-*co*-PCL-DOPA)-*b*-(PMPC)$_2$ Films with/without Protection

	PCL-*b*-(PCL-DOPA-*b*-PMPC)$_2$/deg		(PCL-*co*-PCL-DOPA)-*b*-(PMPC)$_2$/deg	
	Deprotected	Protected	Deprotected	Protected
Sample 1[a]	160.3 ±1.0	164.3 ±1.4	169.9 ±0.4	167.8 ±1.0
Sample 2[b]	51.9 ±1.3	51.2 ±0.6	83.3 ±0.9	87.7 ±0.4
Sample 3[b]	79.5 ±1.4	80.9 ±0.9	85.4 ±1.3	87.6 ±0.3
Sample 4[a]	137.3 ±3.1	132.5 ±1.7	164.7 ±0.3	167.2 ±2.1

[a]Static contact angle in water using 8 μL air bubbles as a probe. [b]Static contact angle under air condition using 2 μL water droplet as a probe.

From Table 4.2, the difference in values of contact angle between films with and without modification is almost negligible. These results indicate the small amount of silicon modification will not influence the outcome of the surface reorganization. Subsequently, XPS measurements were performed and resultant spectra are shown in Figure 4.4.

The Si_{2p} and Si_{2s} peaks corresponding to TBDMS groups were observed in sample 2 of (PCL-*co*-PCL-DOPA)-*b*-(PMPC)$_2$ (Figure 4.4a, line 1). Since TBDMS groups only exist in PCL-DOPA segments, it is clear that the hydrophobic part segregates at the outermost surface. On the other hand, the silicon peaks vanished from sample 2 of the PCL-*b*-(PCL-DOPA-*b*-PMPC)$_2$ (Figure 4.4a, line 2), and the P_{2p} peak is assigned to PMPC, which was observed at the outermost surface. This suggests that the surface reorganization was suppressed in the sample with a PCL

domain. When the vacuum treatment was performed at a temperature higher than the melting point of PCL, all samples exhibited Si_{2p} and Si_{2s} signals. Since the PCL domain is in an amorphous state under these conditions, the surface reorganization took place in PCL-*b*-(PCL-DOPA-*b*-PMPC)$_2$.

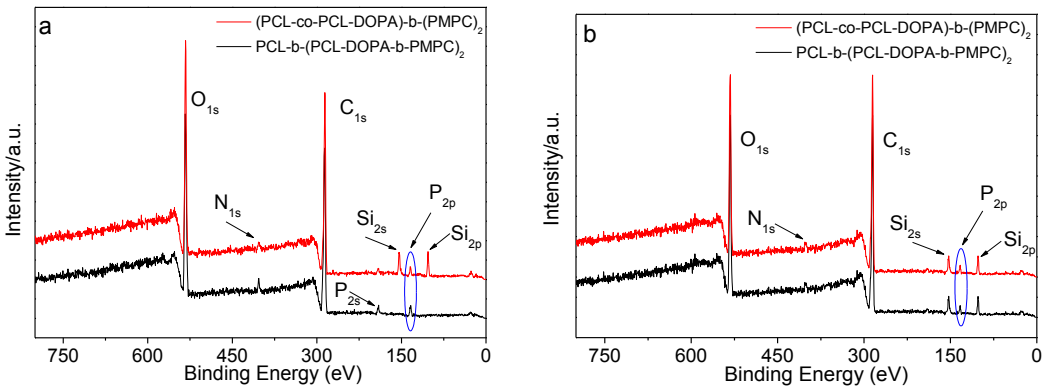

Figure 4.4. XPS spectra of TBDMS-protected PCL-*b*-(PCL-DOPA-*b*-PMPC)$_2$ and TBDMS-protected (PCL-*co*-PCL-DOPA)-*b*-(PMPC)$_2$ of a) sample 2 and b) sample 3.

4.3.3.Crystallization-induced suppression of surface reorganization

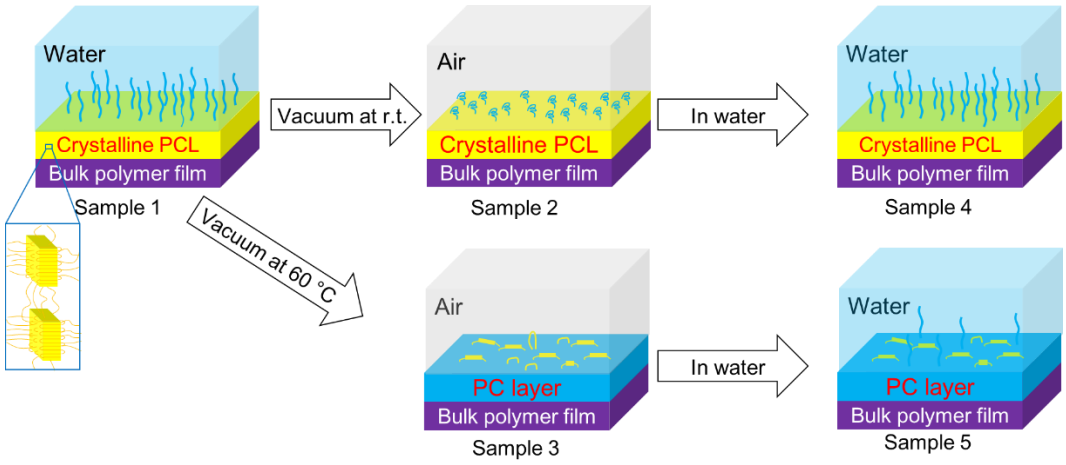

Figure 4.5. Surface reorganization of PCL-*b*-(PCL-DOPA-*b*-PMPC)$_2$ film.

The surface reorganization of PCL-*b*-(PCL-DOPA-*b*-PMPC)$_2$ films is described in Figure 4.5. Sample 1 shows the PC-segregated outmost surface with the crystalline PCL. When sample 1 was dried under vacuum state, the crystalline PCL segment suppressed the migration of PCL segments.

However, the vacuum treatment at 60 ℃ which is higher than the melting point of PCL, induced a complete surface reorganization. Since sample 2 has PC segments at its surface, the super-hydrophilic surface was formed after the water immersion. On the other hand, the crystalline PCL at the outmost surface of sample 3 that suppressed migration of PMPC segments, induced a more hydrophobic surface in sample 5.

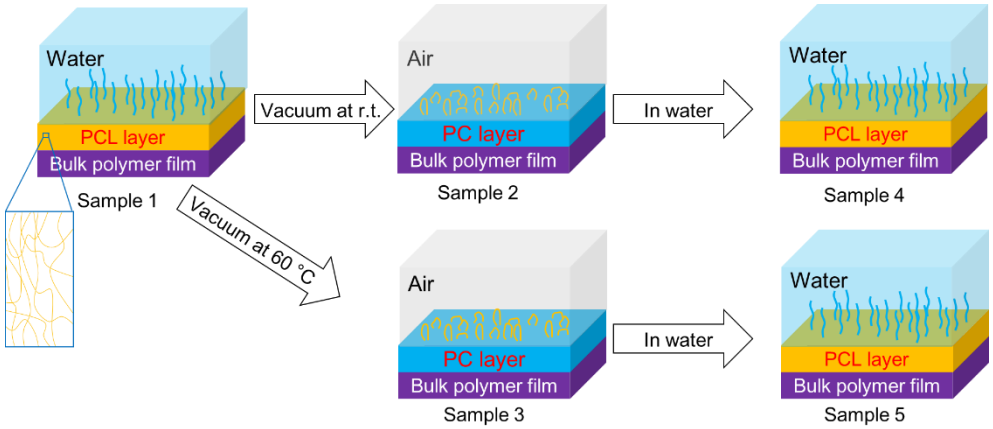

Figure 4.6. Surface reorganization of (PCL-*co*-PCL-DOPA)-*b*-$(PMPC)_2$.

For instance, (PCL-*co*-PCL-DOPA)-*b*-$(PMPC)_2$ without crystalline hydrophobic segments shows no suppression of surface reorganization (Figure 4.6). The generation of PCL with a lower surface free energy at the outmost surface is favored in the open air, whereas the strong hydration effect and hydrophilic interaction induced the PC-segregated surface in water.

4.4. Conclusion

In this chapter, we have proven that the crystalline main chain is a promising method for the suppression of surface reorganization. Although the PCL-*b*-(PCL-DOPA-*b*-$PMPC)_2$ and (PCL-*co*-PCL-DOPA)-*b*-$(PMPC)_2$ share similar structure between the hydrophobic parts and hydrophilic parts, the crystallinity of the PCL-*b*-$(PCL\text{-}DOPA)_2$ suppressed the surface reorganization in PCL-*b*-$(PCL\text{-}DOPA\text{-}b\text{-}PMPC)_2$ films. Meanwhile, the lack of crystallinity in (PCL-*co*-PCL-DOPA)-*b*-$(PMPC)_2$ induced the reorganization under vacuum and water conditions.

4.5. References

1. Seetho, K.; Zhang, S.; Pollack, K. A.; Zou, J.; Raymond, J. E.; Martinez, E.; Wooley, K. L. Facile Synthesis of a Phosphorylcholine-Based Zwitterionic Amphiphilic Copolymer for Anti-Biofouling Coatings. *ACS Macro Letters* **2015,** *4* (5), 505-510.

2. Krishnan, S.; Weinman, C. J.; Ober, C. K. Advances in Polymers for Anti-Biofouling Surfaces. *Journal of Materials Chemistry* **2008,** *18* (29), 3405-3413.

3. Gong, Y.-K.; Nakanishi, F.; Abe, K. Stability of a Photoreactive Polymer LB Film. *Molecular Crystals and Liquid Crystals Science and Technology. Section A. Molecular Crystals and Liquid Crystals* **1999,** *327* (1), 123-126.

4. Yang, S.; Zhang, S. P.; Winnik, F. M.; Mwale, F.; Gong, Y. K. Group Reorientation and Migration of Amphiphilic Polymer Bearing Phosphorylcholine Functionalities on Surface of Cellular Membrane Mimicking Coating. *Journal of biomedical materials research. Part A* **2008,** *84* (3), 837-841.

5. Bittiger, H.; Marchessault, R. H. Crystal Structure of Polyε-caprolactone. *Acta Crystallographica* **1970,** *B26*, 1923-1927.

6. Muller, A. J.; Balsamo, V.; Arnal, M. L.; Jakob, T.; Schmalz, H.; Abetz, V. Homogeneous Nucleation and Fractionated Crystallization in Block Copolymers. *Macromolecules* **2002,** *35*, 3048-3058.

7. Ho, R.-M. Crystallization-Induced Orientation for Microstructures of Poly(L-lactide)-*b*-poly(ε-caprolactone) Diblock Copolymers. *Macromolecules* **2003,** *36*, 9085-9092.

8. Darensbourg, D. J.; Karroonnirun, O. Ring-Opening Polymerization of l-Lactide and ε-Caprolactone Utilizing Biocompatible Zinc Catalysts. Random Copolymerization of l-Lactide and ε-Caprolactone. *Macromolecules* **2010,** *43* (21), 8880-8886.

9. Kanduc, M.; Schlaich, A.; Schneck, E.; Netz, R. R. Water-Mediated Interactions between Hydrophilic and Hydrophobic Surfaces. *Langmuir* **2016,** *32* (35), 8767-8782.

10. Lyakhova, K. S.; Horvat, A.; Zvelindovsky, A. V.; Sevink, G. J. A. Dynamics of Terrace Formation in a Nanostructured Thin Block Copolymer Film. *Langmuir* **2006,** *22* (13), 5848-5855.

11. Auton, M.; Ferreon, A. C.; Bolen, D. W. Metrics that differentiate the origins of osmolyte effects on protein stability: a test of the surface tension proposal. *Journal of molecular biology* **2006,** *361* (5), 983-992.

12. Inoue, Y.; Watanabe, J.; Ishihara, K. Dynamic motion of phosphorylcholine groups at the surface of poly(2-methacryloyloxyethyl phosphorylcholine-random-2,2,2-trifluoroethyl methacrylate). *Journal of colloid and interface science* **2004,** *274* (2), 465-471.

13. Beekmans, L. G. M.; Vancso, G. J. Real-time crystallization study of poly(e-caprolactone) by hot-stage atomic force microscopy. *Polymer* **2000,** *41*, 8975–8981.

14. Wang, Y.; Chan, C.-M.; Ng, K.-M. What Controls the Lamellar Orientation at the Surface of Polymer Films during Crystallization? *Macromolecules* **2008,** *41*, 2548-2553.

Chapter 5

Preparation of Drug-Loading Film and Its Release Properties

5.1. Introduction

Recently, the drug-eluting stent implantation has emerged as an excellent approach for the treatments of cardiovascular disease.[1-2] Drug-eluting stent is realized by a drug-loaded polymer film onto metal coronary artery stent.[3-4] This approach is able to release anti-proliferation drugs directly to the lesion since they contact with the blood vessel immediately.[4] Drug-eluting stent shows excellent performance on the inhibiting proliferation and migration of smooth muscle cells which are widely accepted as the principal mechanism underlying in-stent restenosis after stent implantation.[5-6] Contemporary drug-loading material employs hydrophobic interaction to stabilize drugs, which is weak, resulting in a less controlled release.[7-8] Some new methods were put forward to improve the drug capacity by introducing different functional groups with strong interaction.[9-11]

In this capture, we try to give a detailed evaluation of the drug release property. Firstly, the surface properties of different polymer films including PCL (M_n= 21,000), deprotected PCL-*b*-(PCL-DOPA)$_2$, and PCL-*b*-(PCL-DOPA-*b*-PMPC)$_2$, were tested. After that, the drug-loaded polymer film is prepared on the SUS substrate.[12-13] Based on our knowledge, there is no report on the effects of catechol group in drug-eluting coating using PCL-based film. It is well-known that catechol groups can form a cross-linked structure which is expected to reduce the drug release rate.[14-15] Therefore, the PCL/PCL-*b*-(PCL-DOPA)$_2$ with 5-FU-loaded film was prepared and the impact of the different ratios between PCL and PCL-*b*-(PCL-DOPA)$_2$ on controlled release was investigated.[16-17] The rate-controlling membrane was utilized to achieve a better release kinetics. The polymer film of PCL or PCL-*b*-(PCL-DOPA-*b*-PMPC)$_2$ was prepared onto the PCL/PCL-*b*-(PCL-DOPA)$_2$/drug matrix. The surface morphology and film thickness were

evaluated using SEM. The *in vitro* drug release was performed in PBS buffer solution (pH= 7.4) at 37.5 ℃.

5.2. Experiment

5.2.1. Materials

Stannous octoate ($Sn(OCT)_2$), *tetra*-Butylammonium fluoride (TBAF) tetrahydrofuran solution (1 mol/mL) were purchased from Tokyo Chemical Inc. (TCI) and used as received. 1,4-Butanediol and *ε*-caprolactone (*ε*-CL) were obtained from TCI (Japan), *ε*-CL was dried over $MgSO_4$ (Sigma-Aldrich, Japan) for 48 h at room temperature and distilled under reduced pressure before use. Fluorescein isothiocyanate (FITC), tetramethylrhodamine (TRITC), albumin bovine serum (BSA), and fibrinogen (Fg) were purchased from Sigma-Aldrich (Japan) and used without further purification. Anhydrous toluene and dichloromethane (DCM) were obtained by an ultimate solvent system (Nikko Hansen Corporation, Japan). Methanol, chloroform, and tetrahydrofuran (THF) were purchased from Wako Pure Chemicals Co. (Japan) and used directly without further purification.

5.2.2. Preparation of PCL and PCL-*b*-$(PCL\text{-}DOPA)_2$

The PCL was prepared via bulk ring-opening polymerization. $Sn(OCT)_2$-mediated polymerization of *ε*-CL (27 g, 0.24 mol) was carried out using 1,4-butanediol (0.45 g, 4.5 mmol) as an initiator at 125 ℃ for 4 h to obtain PCL. PCL was purified by reprecipitation method using methanol and dried under vacuum oven, resulting in 25 g polymer (yield: 92 %). M_n was 21,000 and polydispersity index (PDI) was 1.6. ^1H NMR (400 MHz, $CDCl_3$-d_1, δ): 1.15-1.35 (m, -CO-CH_2-CH_2-CH_2), 1.75-1.61 (m, -CO-CH_2-CH_2, -O-CH_2-CH_2), 2.32 (t, O-C-CH_2), 3.66 (t, HO-CH_2), 4.08 (t, CO-O-CH_2).

The PCL-*b*-(PCL-DOPA$_{TBDMS}$)$_2$ (1.0 g, 0.02 mmol) was deprotected by dripping 0.3 mL TBFA THF solution (0.3 mmol) (Figure 5.1). The resultant solution was poured into methanol and purified by precipitation in methanol and dried under vacuum resulting in PCL-*b*-(PCL-DOPA)$_2$ (yield: 92 %). ^{1}H NMR (400 MHz, $CDCl_3$-d_1, δ): 1.15-1.35 (m, -CO-CH$_2$-CH$_2$-C*H*$_2$-), 1.75-1.61 (m, -CO-CH$_2$-C*H*$_2$-, -O-CH$_2$-C*H*$_2$-), 2.32 (t, -O-CH$_2$-C*H*$_2$-), 2.63 (m, -NH-CH$_2$-C*H*$_2$-), 2.78 (m, -NH-C*H*$_2$-), 3.22 (m, -NH-C*H*-), 3.66 (t, OH-C*H*$_2$-), 4.08 (t, -CO-O-C*H*$_2$-), 6.79-6.59 (m, Ar-*H*).

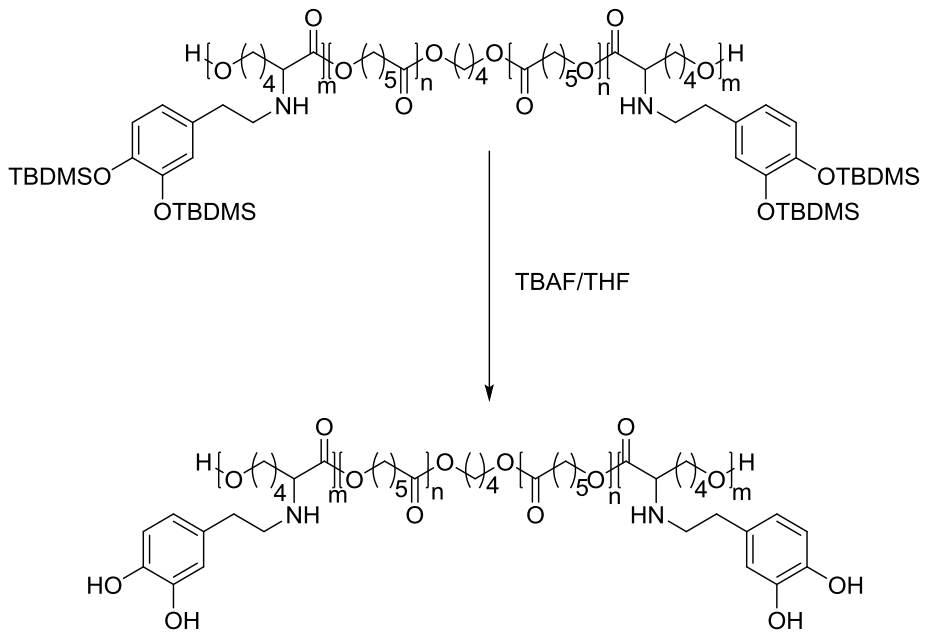

Figure 5.1. Synthesis of PCL-*b*-(PCL-DOPA)$_2$.

5.2.3.Surface properties of polymer films

PCL, PCL-*b*-(PCL-DOPA)$_2$, and PCL-*b*-(PCL-DOPA-*b*-PMPC)$_2$ films were prepared on the basis of the spin-coating method. Different polymers were dissolved in chloroform at 50 mg/mL, PCL-*b*-(PCL-DOPA-*b*-PMPC)$_2$ was dissolved in chloroform with 40 v% methanol. After that, 80 μL of the polymer solution was dropped onto the cleaned SUS surface which was put onto the spin-coater in advance. The spin-coating procedure was performed at 2000 rpm for 60 s. Wet films

were transferred to the vacuum oven and dried at 40 ℃. The polymer films of PCL-*b*-(PCL-DOPA-*b*-PMPC)$_2$, PCL, and PCL-*b*-(PCL-DOPA)$_2$ are prepared and designated as SUS-PC, SUS-PCL, and SUS-PCL-DOPA. The bare stainless steel sheet was used as negative control and labeled as SUS sample. The wettability of different surfaces was measured by the contact angle measurement.

5.2.4. Protein adsorption tests

To evaluate the anti-fouling properties of different surfaces. The Fg and BSA adsorption were tested on SUS-PC, SUS-PCL, SUS-PCL-DOPA and bare SUS surface. The BSA and Fg were labeled by FITC and TRITC, respectively. Different samples were immersed in 0.7 mL 1.2 mg/mL of BSA-FTIC solution and 0.7 mL 0.7 mg/mL of Fg-TRITC solution for 4 h and subsequently rinsed with pure water to remove the unabsorbed protein. The protein adsorption state was observed by fluorescence microscope, and the amount was converted from the fluorescence intensity of the protein solution before and after substrate immersion. All samples were done in triplicate and the average value obtained was reported.

5.2.5. Preparation of drug-loaded polymer films

The drug-loaded polymer films were prepared by the combination of drop-coating method and thermo-compression formation. The drug/polymer mixture was prepared by dissolving PCL, PCL-*b*-(PCL-DOPA)$_2$, and 5-FU into methanol/chloroform (v:v= 1:1). The mass of drug is fixed at 30 wt% of the polymer weight. Polymer solutions with different ratios between PCL and PCL-*b*-(PCL-DOPA)$_2$ including 2:1, 1:1, and 1:2 were prepared. Cleaned SUS substrate was put into a watch-glasses, and 80 μL drug-contained polymer solutions were dropped onto its surface carefully. After natural air drying, another 80 μL drug-contained polymer solutions were dripped onto it. This drip-and-drying procedure was repeated for 8 times to prepare a thick drop-coated

surface. After the drop-coating procedure, a further thermo-compression formation was performed to obtain smooth polymer layer. The thermo-compression formation is shown in Figure 5.2, the top hot plate was heated at 70 ℃. The samples were put into a cavhollow template with 220 μm thickness and pressed at 4 MPa for 10 min. To avoid the contaminating of drug-loading films, a "Teflon" thin film was used to separate the hot plant and samples. After 10 min press, the temperature was gradually reduced to 25 ℃. This heat-press-cool procedure was repeated for 3 times to obtain a smooth surface. Different samples were labelled as No.1 film (PCL with 5-FU-loaded film), No.2 film [PCL/ PCL-*b*-(PCL-DOPA)$_2$ (wt:wt= 2:1) with 5-FU-loaded film], No.3 film [PCL/ PCL-*b*-(PCL-DOPA)$_2$ (wt:wt= 1:1) with 5-FU-loaded film], and No.4 film [PCL/ PCL-*b*-(PCL-DOPA)$_2$ (wt:wt= 1:2) with 5-FU-loaded film] presented in Table 5.1.

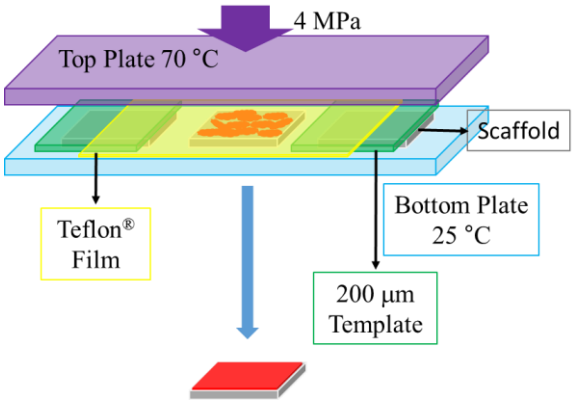

Figure 5.2. Thermo-compression formation of smooth drug-loading films.

The cover layer was prepared onto the drug-loaded polymer film by the spin-coating method. The resultant drug/polymer matrix was placed onto the spin-coater, subsequently, 80 μL 50 mg/mL PCL-*b*-(PCL-DOPA-*b*-PMPC)$_2$ or PCL solution was dropped onto the surface, and samples were fabricated at 2000 rpm for 2 min. Resultant samples were labeled as No.5 film [PCL-*b*-(PCL-DOPA-*b*-PMPC)$_2$-covered PCL/PCL-*b*-(PCL-DOPA)$_2$ (wt:wt= 1:1) with 5-FU-loaded film] and No.6 film [PCL-covered PCL/PCL-*b*-(PCL-DOPA)$_2$ (wt:wt= 1:1) with

5-FU-loaded film] shown in Table 5.1. Samples were stored under vacuum state at 25 ℃. The thin film WAXD measurements and SEM observations were performed to investigate drug-loaded state and surface morphology. The detail information of different samples is illustrated in Table 5.1. The thickness of different drug-loaded layers was determined by SEM.

Table 5.1. Preparation of Different Drug-loading Films

No.	Drug	Drug carrier	Rate-controlling membrane
No.1	30%	PCL	No
No.2	30%	PCL/PCL-*b*-(PCL-DOPA)$_2$ (2:1)[a]	No
No.3	30%	PCL/PCL-*b*-(PCL-DOPA)$_2$ (1:1) [b]	No
No.4	30%	PCL/PCL-*b*-(PCL-DOPA)$_2$ (1:2) [c]	No
No.5	30%	PCL/PCL-*b*-(PCL-DOPA)$_2$ (1:1) [a]	PCL-*b*-(PCL-DOPA-*b*-PMPC)$_2$
No.6	30%	PCL/PCL-*b*-(PCL-DOPA)$_2$ (1:1) [a]	PCL

[a]Weight ratio between PCL and PCL-*b*-(PCL-DOPA)$_2$ is 2:1; [b]Weight ratio between PCL and PCL-*b*-(PCL-DOPA)$_2$ is 1:1; [c]Weight ratio between PCL and PCL-*b*-(PCL-DOPA)$_2$ is 1:2.

5.2.6. *In vitro* drug release

In vitro drug release was performed to evaluate the release kinetics. Different samples were immersed in 5 mL PBS solution at 37 ℃ and shook at 100 rpm. At predetermined time intervals, 1 ml of PBS was taken by a micropipette and replaced with an equal volume of fresh PBS into the test tubes. The amount of released 5-FU in the supernatant solutions was measured by a UV–Vis spectrophotometer (UV-1601 PC, SHIMADZU) at a wavelength of 266 nm. The cumulative release percentage was calculated using following Equation

$$\mathrm{CRP} = C_n \times 3 + [(C_1 \times 0.5) + (C_2 \times 0.5) + \cdots + (C_{(n-1)} \times 0.5)] \quad (5.1)$$

where C_1-C_n refers to the concentration of 5-FU in different samples which are converted from UV absorption.

5.2.7. Characterizations

Atomic force microscopy (AFM) observations were performed using a scanning probe microscopy (SPA400, Hitachi High-Tech Science Corporation, Tokyo, Japan) in tapping mode with aluminum-coated silicon cantilevers (f = 324 kHz, spring constant = 36 N/m, Si-DF40, SII Instruments Corporation, Japan). Prior to the AFM observations, the substrates were dried under high vacuum for 12 h. Contact angle measurements were performed with a Theta T200 Auto3 contact angle instrument (Altech Corporation, Japan) using 2 μL water droplets and 2 μL air bubbles as the probes. A Nikon Eclipse E400 biological microscope system with super-high pressure fluorescent mercury lamp was used to collect fluorescent images after protein adsorption test. The fluorescence spectroscopy was collected by a spectrofluorometer (FP-8300, Jasco). The BSA-FTIC samples were measured at λ_{Ex} = 497 nm and λ_{Em} = 524 nm; Fg-TRITC samples were measured at λ_{Ex} =547 nm and λ_{Em} = 572 nm. Each sample was examined in triplicate and the average value obtained was reported. The UV absorption was measured by a UV–Vis-Nir spectrophotometer (UV-3600, SHIMADZU) at a wavelength of 266 nm. All the UV experiments were measured in triplicate and the average value obtained was reported.

5.3. Results and discussion

5.3.1. Preparation of polymer films

AFM observation was used to evaluate the surface morphology and surface roughness. The AFM images are shown in Figure 5.3, meanwhile, coating thickness and root mean square (RMS) are summarized in Table 5.2. A uniform surface is obtained by the spin-coating method. Although PCL-coated surface showed rough surface, a smooth surface is obtained in PCL-*b*-(PCL-DOPA)$_2$ and PCL-*b*-(PCL-DOPA-*b*-PMPC)$_2$.

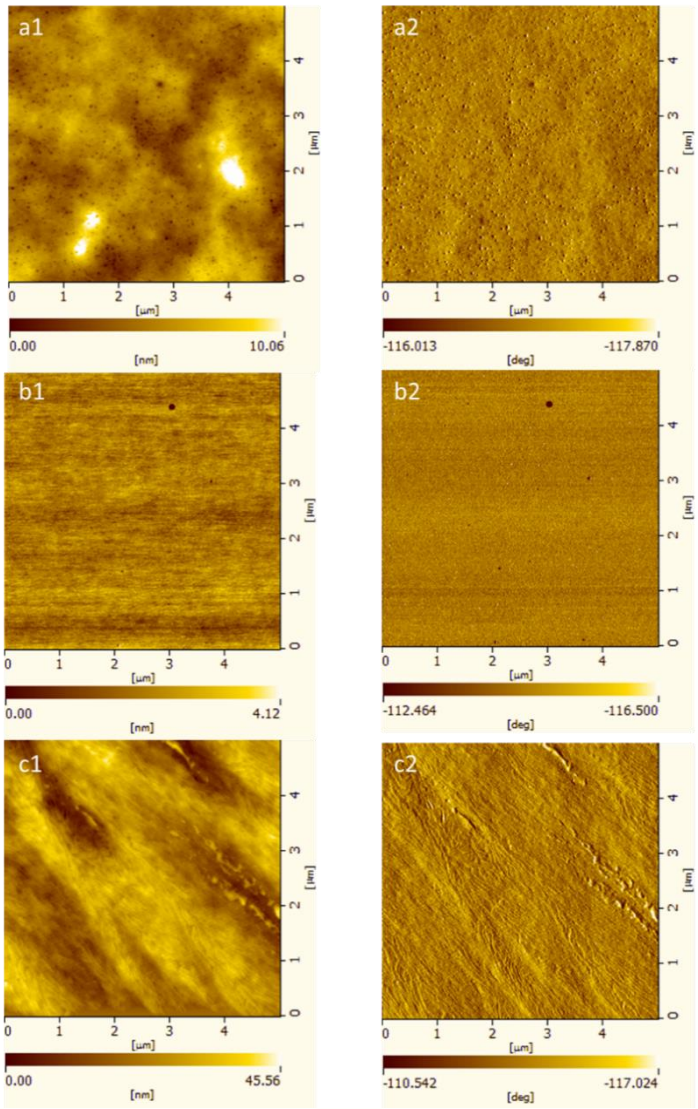

Figure 5.3. AFM images of PCL-*b*-(PCL-DOPA-*b*-PMPC)$_2$ film (a), PCL-*b*-(PCL-DOPA)$_2$ film (b) and PCL film (c) prepared by the spin-coating method, 1) height images, 2) phase images.

After that, contact angle measurements are performed to evaluate the surface wettability and summarized in Table 5.2. PCL possessing inherent hydrophobicity resulted in high contact angle (72.5 °). Catechol groups in PCL-*b*-(PCL-DOPA)$_2$ samples possessing hydroxyl groups are considered to improve the surface hydrophilicity of PCL-based polymer, however, the strong inter- and intra-molecular interactions induce aggregate structures which reduce the hydrophilicity of PCL-*b*-(PCL-DOPA)$_2$ samples (83.3 °). Meanwhile, high contact angle (81.6 °) observed from SUS-PC samples which indicated surface reorganization occurred on it during drying procedure.

The contact angle measurements in water using air bubble as the probe were performed. SUS-PCL samples showed lower contact angle (124.9 °) than SUS-PCL-DOPA samples (152.7 °). After immersion in water, SUS-PC samples showed super-hydrophilic surface.

Table 5.2. Coating Properties and Contact Angle of PCL-*b*-(PCL-DOPA-*b*-PMPC)$_2$, PCL-*b*-(PCL-DOPA)$_2$, and PCL Films

Concentration	RMS (nm)	Coating thickness (nm)	Contact angle (air)[a]	Contac angle (water)[b]
SUS-PCL	3.29	270 nm	124.9 ±2.0	75.2 ±1.7
SUS-PC	2.04	260 nm	N/A	81.6 ±1.3
SUS-DOPA	3.79	130 nm	152.7 ±1.6	83.3 ±0.9
SUS	1.35	N/A	124.5 ±1.8	90.7 ±0.4

[a]Contact angle was measured using air bubble as the probe in water. [b]Contact angle was measured using water droplet as a probe in the open air, [c]Surface showed super-hydrophilicity, whereby the air bubble cannot adhere to the surface.

5.3.2. Protein adsorption tests

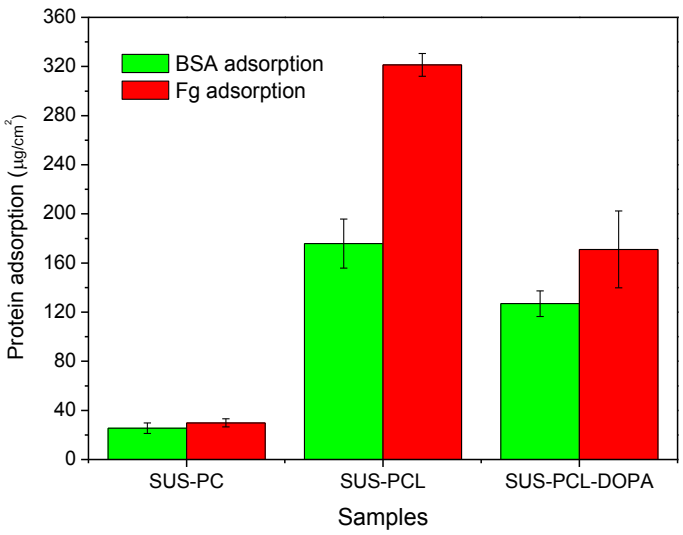

Figure 5.4. BSA and Fg adsorption on SUS-PC, SUS-PCL, and SUS-PCL-DOPA.

The protein adsorption using BSA and Fg were performed to evaluate the surface anti-fouling properties (Figure 5.4 and 5.5). The PCL-*b*-(PCL-DOPA)$_2$ surface adsorbed less protein than the

PCL surface. SUS-PC sample provides an excellent performance since only 25.5 ug and 29.8 ug were adsorbed onto its surface during the tests, respectively. Notably, this value is 5 times lower than SUS-PCL-DOPA samples.

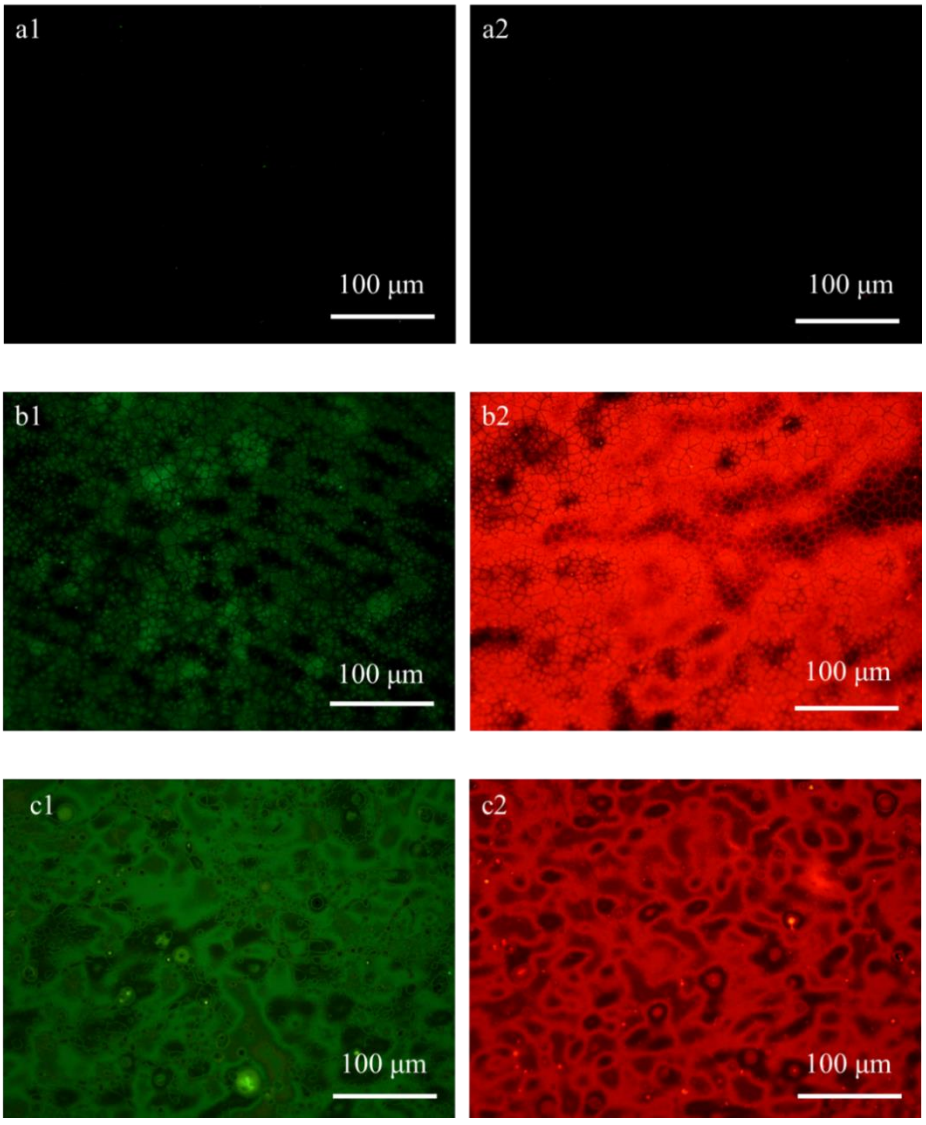

Figure 5.5. Protein adsorption state observed by fluorescence microscopy of PCL-*b*-(PCL-DOPA-*b*-PMPC)$_2$ film (a), bare stainless steel (b), PCL film (c), and PCL-*b*-(PCL-DOPA)$_2$ film (d), 1) is the BSA-FITC adsorption, 2) is Fg-TRITC adsorption.

Further fluorescence microscope observations were performed to evaluate the protein adsorption state. SUS-PC samples with very dark pictures imply its excellent anti-fouling properties. While, both SUS-PCL and SUS-PCL-DOPA surfaces showed very bright pictures, the

surface morphology is clearly seen in Figure 5.5.a2, a3, b2, b3. Both of the fluorescence microscope observation and fluorescence intensity suggested the good anti-fouling properties of SUS-PC surface.

5.3.3. Preparation of drug-loaded polymer films

The drug loading film was prepared via the combination of drop-coating method and thermo-compression formation. The thin film WAXD measurement and SEM observation were performed to evaluate the drug loading state and surface morphology. The WAXD line profiles are presented in Figure 5.6. Five samples including PCL/drug film, PCL/PCL-*b*-(PCL-DOPA)$_2$/drug (wt:wt= 1:1) film, PCL film, and free drug powder was measured. The peaks appeared at 2θ angles of 21.3 ° and 23.6 ° which correspond to the (110) and (200) reflections from the orthorhombic unit cell in PCL crystal. The peak appeared at 2θ angles of 28.6 °which correspond to 5-FU crystal. This result implies that the drug contains in the polymer films, however, the concertation of 5-FU is higher than its solubility in PCL. Rather than the 5-FU molecule in a polymer film, the 5-FU crystal exists in the polymer films.

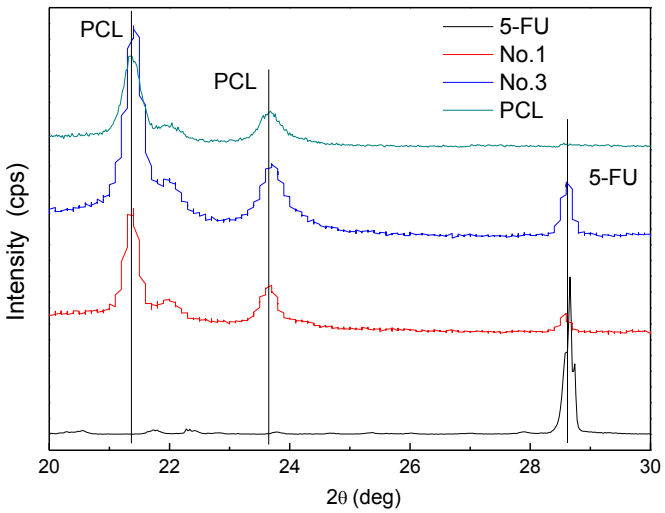

Figure 5.6. Thin film WAXD line profiles of 5-FU powder, PCL/PCL-*b*-(PCL-DOPA)$_2$ (wt:wt= 1:1) with 5-FU-loaded film, PCL with 5-FU-loaded films and PCL.

After that, the surface morphology and coating thickness were evaluated using SEM observation. The surface morphology of No.1, No.2, No.3 and No.4 samples were shown in Figure 5.7. Compared with PCL-*b*-$(PCL\text{-}DOPA)_2$-contained films, PCL/drug film presented an orientated surface, which is consisted of some small filamentous morphology. This morphology probably results in the "Teflon" films which are used in the thermo-compression formation to separate the hot plate and samples. Meanwhile, with the addition of PCL-*b*-$(PCL\text{-}DOPA)_2$, the surface morphology becomes rougher and irregular. The strong interaction between polymer/polymer and between polymer/drug is considered to be responsible for such morphologies.

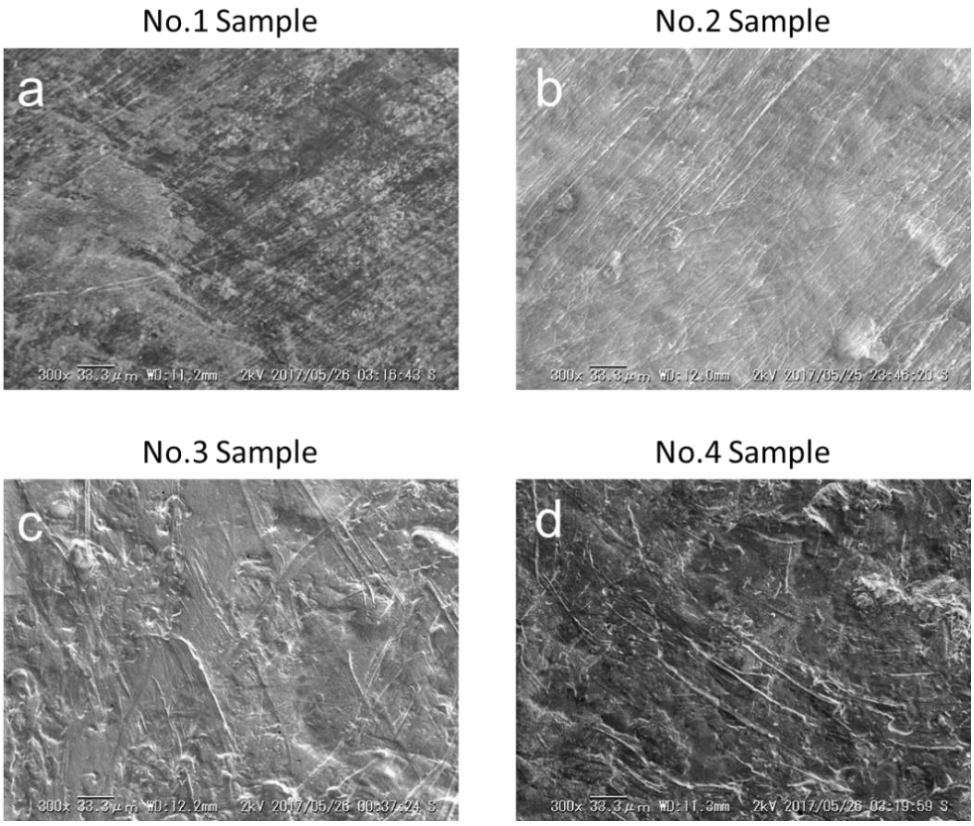

Figure 5.7. SEM images of drug-loading film including a) No.1 sample, b) No.2 sample, c) No.3, sample, and d) No.4 sample.

PCL/PCL-*b*-(PCL-DOPA)$_2$ (wt:wt= 1:1) with the 5-FU-loaded film was chosen as the template to prepare drug-loading film with a rate-controlling membrane. The SEM images were presented in Figure 5.8. The surface morphology changed astonishingly. The filamentous morphology was observed instead of a flat surface. Notable, very clear spherocrystal can be observed from the PCL-covered PCL/PCL-*b*-(PCL-DOPA)$_2$ surface indicated that the covers were formed onto the drug-loaded layer successfully.

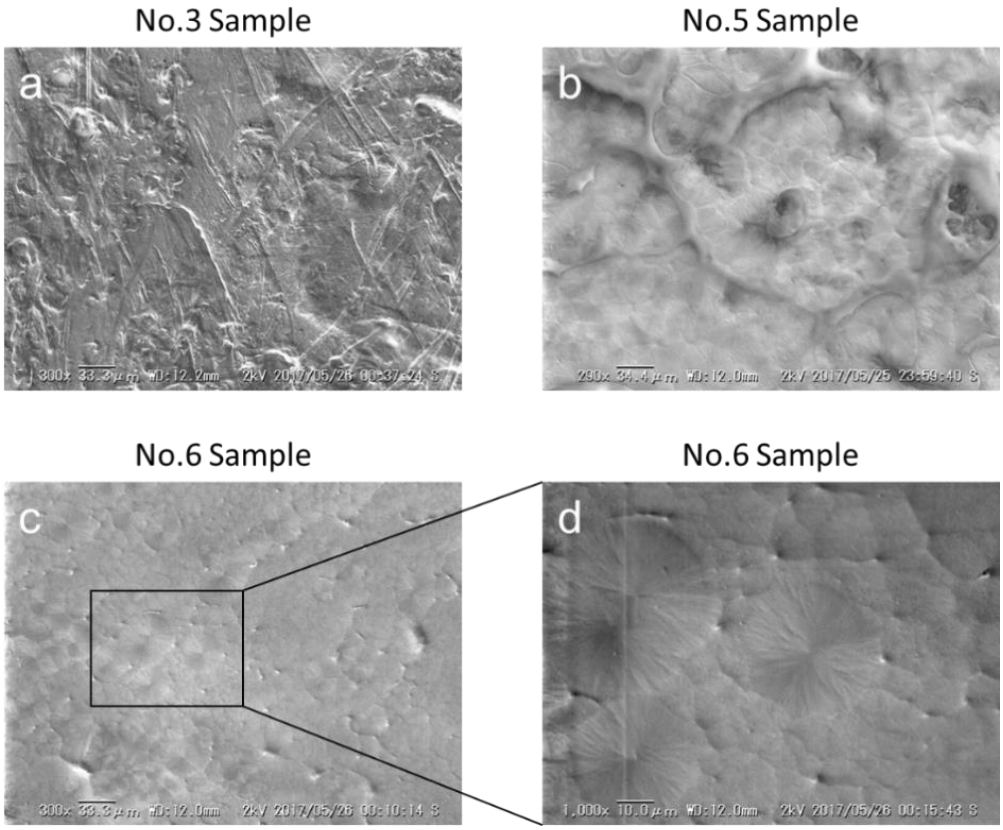

Figure 5.8. SEM images of drug-loading film including with/without rate-controlling membrane a) No.3 sample, b) No.5 sample, c) No.6 sample, and d) the spherocrystal observed on the surface of No.6 sample.

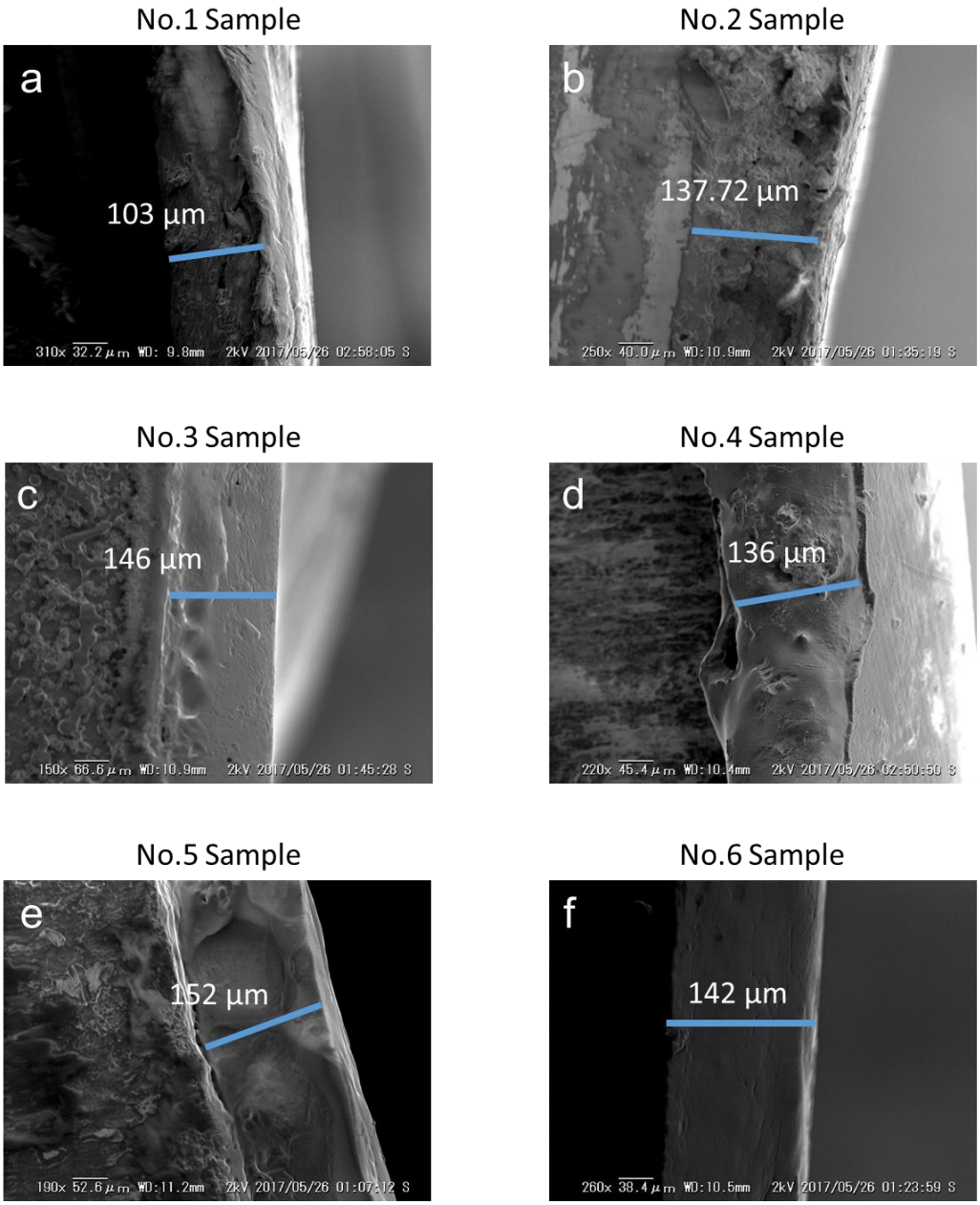

Figure 5.9. Coating thickness of drug-loaded films with/without rate-controlling membrane, including a) No.1 sample, b). No.2 sample, c) No.3 sample, d) No.4 sample, e) No.5 sample, and f) No.6 sample.

Furthermore, the thickness of different films was determined by SEM observation by placing sample vertically on the sample holder, and the images are presented in Figure 5.9. Despite PCL/drug film (the thickness is 103 µm), other samples showed similar thickness around 140 µm. Compared with No.2 samples, the PC- and PCL-covered drug loading film showed similar coating thickness. This result indicates that rate-controlling membranes on the polymer/drug matrix are

very thin and difficult to be observed by thickness changes. Moreover, the spin-coating method in the preparation of the rate-controlling membrane didn't lead to the loss of the drug/polymer matrix. Actually, the dopamine units in PCL-*b*-$(PCL\text{-}DOPA)_2$ induced a reduction of polymer solubility. Strong interaction makes dopamine-contained polymer is difficult to be dissolved in the solvent.

5.3.4. *In vitro* drug release

The *in vitro* drug release experiments were performed to analyze the influence of different dopamine concentrations. The results were shown in Figure 5.10. Notably, PCL with 5-FU-loaded film showed significant initial burst release: 18% drug was released within first 15 min. In the case of PCL-*b*-(PCL-DOPA)-contained film, the initial burst release was reduced to 11.04% [PCL/ PCL-*b*-$(PCL\text{-}DOPA)_2$ (wt:wt= 2:1) 5-FU-loaded film], 6.64% [PCL/ PCL-*b*-$(PCL\text{-}DOPA)_2$ (wt:wt= 1:1) with 5-FU-loaded film] and 9.35% [PCL/PCL-*b*-$(PCL\text{-}DOPA)_2$ (wt:wt= 1:2) with 5-FU-loaded film]. The burst release results from the 5-FU on the surface of the drug-loaded film which could diffuse rapidly into the PBS. However, the strong interaction between catechol groups and 5-FU suppressed initial burst release. Although low concentration PCL-*b*-$(PCL\text{-}DOPA)_2$ [No.2, PCL/ PCL-*b*-$(PCL\text{-}DOPA)_2$ (wt:wt= 1:2) with 5-FU-loaded film] reduced the initial burst release significantly, the drug release profile suggests its drug release rate is faster than that of No.1 sample (PCL with 5-FU-loaded film). As described above the PCL-*b*-$(PCL\text{-}DOPA)_2$ shows better hydrophilicity inside water, which accelerated the diffusion process. Low ratio of PCL-*b*-$(PCL\text{-}DOPA)_2$ induces week interaction between polymer and drug. As the result, high diffusion rate and week interaction accurate the drug release rate of low concentration samples. No.3 and No.4 samples showed a better-controlled release property. The increase of PCL-*b*-$(PCL\text{-}DOPA)_2$ induces the faster diffusion, which caused the faster release of No.4 sample at first 35 h.

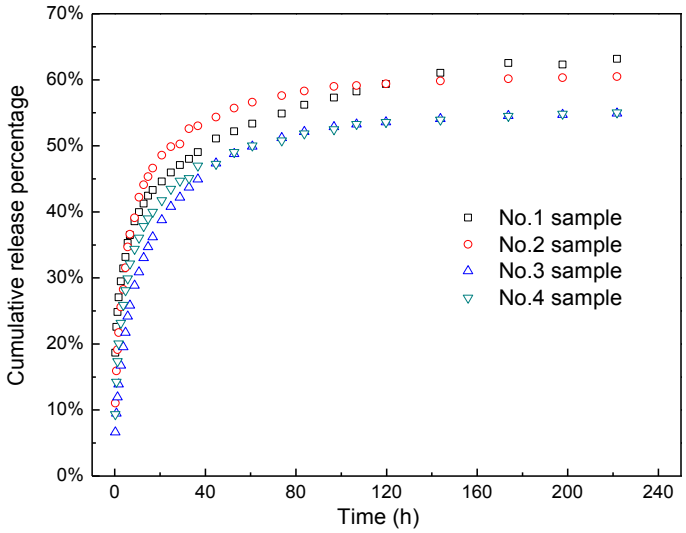

Figure 5.10. Cumulative release curve of drug-loaded films without rate-controlling membrane, including No.1 sample (square), No.2 sample (circle), No.3 sample (triangle), and No.4 sample (inverted triangle).

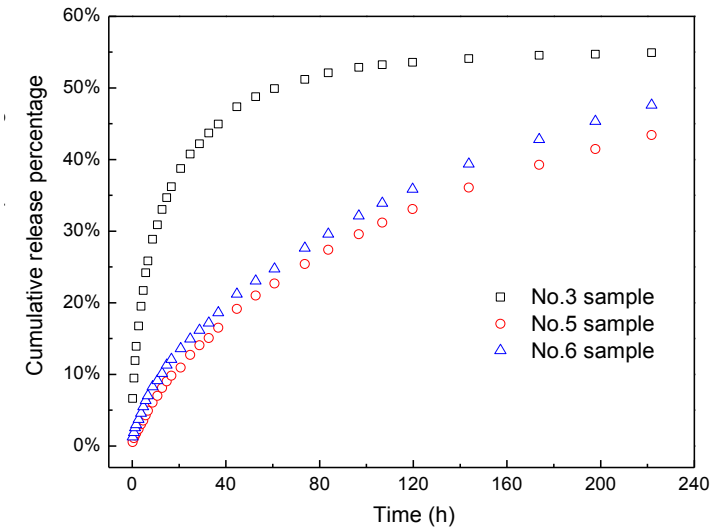

Figure 5.11. Cumulative release curve of drug-loaded films without/without rate-controlling membrane, including No.3 sample (without rate-controlling membrane, square), No.5 sample (with PCL-based rate-controlling membrane, circle), and No.6 sample (with PC-based rate-controlling membrane, triangle).

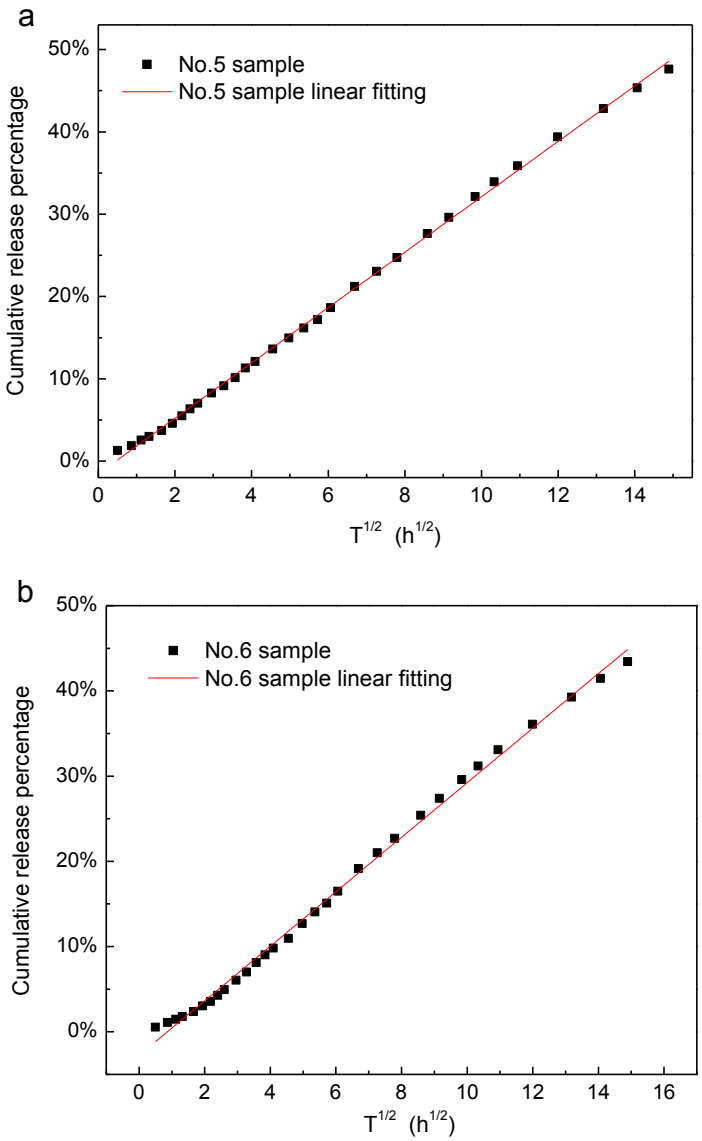

Figure 5.12. Fitting curve of No.5 sample and No.6 sample using Higuchi Model.

The *in vitro* drug release profiles of No.5 and No.6 were shown in Figure 5.11. The initial burst release was reduced to 0.54% (No.5) and 1.28% (No.6) indicated the covers isolate drug loading film away from the water and extended the diffusion time. Meanwhile, PC with better hydrophilicity and hydration effects induced higher initial burst release and faster releases profile.

Furthermore, the drug release was fitted using Higuchi Model, this model shown in Equation 5.2.

$$CRP\% = K_h t^{1/2} \quad (5.2)$$

where K_h is the drug release rate constants and W is the percent release of drugs at the different time. Recent research shows this model is very suitable to describe the kinetics of drug release from the membrane-matrix composites. The fitting curve and intercept are shown in Figure 5.12 and Table 5.3, respectively. Higuchi Model is based on the hypotheses that (1) drug concentration of drug-loading film is much higher than its solubility; (2) drug diffusion takes places only in one dimension; (3) drug particle is much smaller than system thickness; and (4) drug diffusivity is constant. Both No.5 and No.6 sample showed a well-fitted linear curve, implying that the drug release from covered polymer film is first order. In this system, (1) the thin film WAXD measurement implies that the drug concertation is higher than its solubility, whereby the 5-FU crystals exist in polymer films; (2) the polymer film was immobilized on a SUS substrate, and the drug release only occurs at top face (the superficial area of side face is much lower than that of top face, and the drug release at side face is neglectable); (3) the polymer film was prepared from the mixture, which ensured the very small size of 5-FU crystals. Since the Higuchi-type drug release is not observed in No.2, No.3, and No.4 sample, rate-controlling membrane might be able to control the drug diffusivity. Moreover, due to the stronger hydration effect and better hydrophilicity, PCL-*b*-(PCL-DOPA-*b*-PMPC)$_2$ membrane shows higher K_h, indicating a faster release rate

Table 5.3 Fitting Information of Rate-Controlling-Membrane-Contained Samples

Rate-controlling membrane	PCL-*b*-(PCL-DOPA-*b*-PMPC)$_2$	PCL
Intercept	1.52±0.07	2.76±0.15
K_h	3.36±0.02	3.20±0.02
R	0.999	0.997

5.4. Conclusion

In this chapter, we evaluated the surface properties of different polymer films including PCL-*b*-(PCL-DOPA-*b*-PMPC)$_2$, PCL-*b*-(PCL-DOPA)$_2$, and PCL. PCL-*b*-(PCL-DOPA-*b*-PMPC)$_2$ film is able to provide a super-hydrophilic and anti-fouling surface. The drug-loaded films were prepared with different ratios between PCL and PCL-*b*-(PCL-DOPA)$_2$. Lower PCL-*b*-(PCL-DOPA)$_2$ ratio induced lower initial burst release but faster release rate; with the increase of PCL-*b*-(PCL-DOPA)$_2$ ratio, an enhanced interaction can be achieved; excess PCL-*b*-(PCL-DOPA)$_2$ leads to faster diffusion rate and faster release rate. The rate-controlling membrane was prepared using PCL-*b*-(PCL-DOPA-*b*-PMPC)$_2$ or PCL via spin-coating method. Although the thickness of obtained drug loading layer didn't increase, the changes of surface morphology implied the successful formation of different polymer covers. Especially, some spherocrystal was observed on the outmost surface of PCL-covered PCL/PCL-*b*-(PCL-DOPA)$_2$ (wt:wt= 1:1) with the 5-FU-loaded film. Resultant samples showed Higuchi-type controlled release, implying the rate-controlling membrane could control the drug diffusivity.

5.5. References

1. Eisenberg, M. J.; Konnyu, K. J. Review of Randomized Clinical Trials of Drug-Eluting Stents for the Prevention of In-stent Restenosis. *American Journal of Cardiology* **2006,** *98* (3), 375-382.

2. Lamerton, A. Percutaneous Transluminal Angioplasty. *British Journal of Surgery* **1986,** *73* (2), 91-97.

3. Kaplan, G. A.; Keil, J. E. Socioeconomic Factors and Cardiovascular Disease: A Review of the Literature. *Circulation* **1993,** *88* (4), 1973-1998.

4. Rao, R. P.; Ramakrishna, S.; Diwan, P. V. Drug Release Kinetics from Polymeric Films Containing Propranolol Hydrochloride for Transdermal Use. *Pharmaceutical Development and Technology* **2000,** *5* (4), 465–472.

5. Franklin, S. M.; Faxon, D. P. Pharmacologic Prevent of Restenosis after Coronary Angioplasty: Review of the Random. *Coronary Artery Disease* **1993,** *4* (3), 232-242.

6. Andrés, V. Control of Vascular Smooth Muscle Cell Growth and its Implication in Atherosclerosis and Restenosis (Review). *International Journal of Molecular Medicine* **1998,** *2*, 81-89.

7. Zhou, B.; Hu, X.; Zhu, J.; Wang, Z.; Wang, X.; Wang, M. Release Properties of Tannic Acid from Hydrogen Bond Driven Antioxidative Cellulose Nanofibrous Films. *International Journal of Biological Macromolecules* **2016,** *91*, 68-74.

8. Burt, H. M.; Hunter, W. L. Drug-Eluting Stents: a Multidisciplinary Success Story. *Advanced Drug Delivery Reviews* **2006,** *58* (3), 350-357.

9. Kim, B.-S.; Park, S. W.; Hammond, P. T. Hydrogen-Bonding Layer-by-Layer-Assembled Biodegradable Polymeric Micelles as Drug Delivery Vehicles from Surfaces. *ACS Nano* **2008,** *2* (2), 386-392.

10. Kim, S. M.; Park, S. B.; Bedair, T. M.; Kim, M. H.; Park, B. J.; Joung, Y. K.; Han, D. K. The Effect of Solvents and Hydrophilic Additive on Stable Coating and Controllable Sirolimus Release

System for Drug-eluting Stent. *Materials Science & Engineering. C, Materials for Biological Applications* **2017,** *78*, 39-46.

11. Sousa, J. E.; Costa, M. A.; Abizaid, A.; Abizaid, A. S.; Feres, F.; Pinto, I. M. F.; Seixas, A. C.; Staico, R.; Mattos, L. A.; Sousa, A. G. M. R.; Falotico, R.; Jaeger, J.; Popma, J. J.; Serruys, P. W. Lack of Neointimal Proliferation After Implantation of Sirolimus-Coated Stents in Human Coronary Arteries A Quantitative Coronary Angiography and Three-dimensional Intravascular Ultrasound Study. *Circulation* **2001,** *103*, 192-195.

12. Lu, F.; Lei, L.; Shen, Y.-Y.; Hou, J.-W.; Chen, W.-L.; Li, Y.-G.; Guo, S.-R. Effects of Amphiphilic PCL–PEG–PCL Copolymer Addition on 5-Fluorouracil Release from Biodegradable PCL Films for Stent Application. *International Journal of Pharmaceutics* **2011,** *419* (1-2), 77-84.

13. Siepmann, J.; Lecomte, F.; Bodmeier, R. Diffusion-controlled Drug Delivery Systems: Calculation of the Required Composition to Achieve Desired Release Profiles. *Journal of Controlled Release* **1999,** *60*, 379–389.

14. Lin, W.; Ma, G.; Kampf, N.; Yuan, Z.; Chen, S. Development of Long-Circulating Zwitterionic Cross-Linked Micelles for Active-Targeted Drug Delivery. *Biomacromolecules* **2016,** *17* (6), 2010-2018.

15. Moulay, S. Dopa/Catechol-Tethered Polymers: Bioadhesives and Biomimetic Adhesive Materials. *Polymer Reviews* **2014,** *54* (3), 436-513.

16. Tian, Y.; Grishkewich, N.; Bromberg, L.; Hatton, T. A.; Tam, K. C. Cross-linked Pluronic-g-polyacrylic Acid Microgel System for the Controlled Release of Doxorubicin in Pharmaceutical Formulations. *European journal of pharmaceutics and biopharmaceutics : official journal of Arbeitsgemeinschaft fur Pharmazeutische Verfahrenstechnik e.V* **2017,** *114*, 230-238.

17. Wu, Q.; Tang, X.; Liu, X.; Hou, Y.; Li, H.; Yang, C.; Yi, J.; Song, X.; Zhang, G. Thermo/pH Dual Responsive Mixed-Shell Polymeric Micelles Based on the Complementary Multiple Hydrogen Bonds for Drug Delivery. *Chemistry, an Asian Journal* **2016,** *11* (1), 112-119.

Chapter 6

Conclusion and Perspective

6.1. Additional ideas and application

Despite the good performance of dual-functionalized poly(ε-caprolactone) (PCL) in surface modification, this material is also able to be utilized as a carrier for different hydrophobic drugs.[1] Nowadays, cancer becomes an increasing threaten. Contemporary medical treatment engaged anti-cancer drug with high toxicity to the normal cells.[2] Although they provide a good therapeutic effect, the severe systemic side effects induced confined applications.[3] Drug delivery system used the notion that delivery the most effective drug which means hyper-toxic drugs to the cancer cells directly without influence normal cells. This notion can be deemed as localized drug delivery using nano-micelles.[4]

The drug carrier needs to avoid protein adsorption which might induce rapid clearance from the blood after being introduced into the blood.[5] This is very important for them to finish the "trip" to cancer cells.[6] The good anti-fouling properties of PCL-*b*-(PCL-DOPA-*b*-PMPC)$_2$ was already proved in Chapter 3 and Chapter 5. This polymer can form a nano-micelle with PC shell which endows this drug carrier an "invisible cloak" to avoid the protein adsorption and further clearance.[7]

Stimuli-responsive properties are described as the micelles can selectively enrich in cancer cells or release the encapsulated drug rapidly in cancer cells.[8-9] Those properties required micelles have specific functional groups to response the different environments between normal cells and cancer cells. It is easy to understand that the more drug carried which enriched in cancer cells, could improve the therapeutic effect. Catechol group with strong adhesion properties could be used for the functionalization of micelle.[10] Recently, the superparamagnetic iron oxide nanoparticles (SIONs) endow nano-micelles with a magnetic response.[11] This functionality is expected to enrich the micelles in desirable tissues or organ through the external magnetic field.

Furthermore, the SIONs could generate the localized heat when exposed to an alternating magnetic field, which achieves the hyperthermia treatment.[12]

As described above, the drug carrier needs a long journey to the cancer cells, the loaded drug should be stable during the "trip". Since the most of the current anti-cancer drugs are hydrophobic, it is encapsulated into the hydrophobic core by hydrophobic interactions.[13] However, this hydrophobic interaction is inherent weak which induced the drug release during the circulation.[14] To address this problem, the strong interaction between hydrophobic drug and polymer is necessary.[15] The drug release exploration in Chapter 5 indicated the catechol group shows good drug capacity. As the conclusion, PCL-b-PCL-DOPA-b-PMPC is a promising material in DDS field.

6.2. Conclusion

The research described in this thesis containing a preparation of novel dual-functionalization PCL possessing degradability, biocompatibility, blood compatibility and adhesion property. A new method on the basis of nucleophilic substitution reaction was applied for the graft-modification of dopamine with high conversion rate. The end-functionalization of 2-methacryloyloxyethyl phosphorylcholine (MPC) using atom transfer radical polymerization (ATRP) was performed for different dopamine functionalized PCL to obtain polymers which designated as PCL-*b*-(PCL-DOPA-*b*-PMPC)$_2$ and (PCL-*co*-PCL-DOPA)-*b*-(PMPC)$_2$. Resultant polymers show a strong adhesion property towards SUS surface. The resultant surface showed strong hydrophilicity and anti-fouling properties. The contemporary problem of PC based amphiphilic polymer coating is the surface reorganization induced the reduction of biocompatibility. The crystalline PCL segment existed in PCL-*b*-(PCL-DOPA-*b*-PMPC)$_2$ is able to suppress the surface reorganization due to the low mobility of hydrophobic segments. To investigate the effect of

dopamine group in controlled release, the polymer/drug film was prepared with different ratios between PCL and PCL-*b*-$(PCL\text{-}DOPA)_2$. Results indicated the introduction of PCL-*b*-$(PCL\text{-}DOPA)_2$ enhanced the drug capacity, however, its inherent hydrophilicity induced faster diffusion resulted in faster drug release rate. With a PCL-*b*-$(PCL\text{-}DOPA\text{-}b\text{-}PMPC)_2$ cover or PCL cover, the drug release can be controlled significantly. The in vitro drug release curve is well-fitted to the Higuchi model, indicating the drug release is predictable and controllable.

6.3. References

1. Fournier, E.; Passirani, C.; Montero-Menei, C. N.; Benoit, J. P. Biocompatibility of Implantable Synthetic Polymeric Drug Carriers: Focus on Brain Biocompatibility. *Biomaterials* **2003,** *24* (19), 3311-3331.

2. Mura, S.; Nicolas, J.; Couvreur, P. Stimuli-responsive Nanocarriers for Drug Delivery. *Nature Materials* **2013,** *12* (11), 991-1003.

3. Sun, L.; Du, J. Revisiting the Time for Removing the Unloaded Drug by Dialysis Method Based on a Biocompatible and Biodegradable Polymer Vesicle. *Polymer* **2012,** *53* (10), 2068-2073.

4. Du, J.; Armes, S. P. Preparation of Biocompatible Zwitterionic Block Copolymer Vesicles by Direct Dissolution in Water and Subsequent Silicification within Their Membranes. *Langmuir* **2009,** *25* (16), 9564-9570.

5. Ahmad, Z.; Shah, A.; Siddiq, M.; Kraatz, H.-B. Polymeric Micelles as Drug Delivery Vehicles. *RSC Advances* **2014,** *4* (33), 17028-17038.

6. Feng, W.; Brash, J. L.; Zhu, S. Non-biofouling Materials Prepared by Atom Transfer Radical Polymerization Grafting of 2-Methacryloloxyethyl Phosphorylcholine: Separate Effects of Graft Density and Chain Length on Protein Repulsion. *Biomaterials* **2006,** *27* (6), 847-855.

7. Krishnan, S.; Weinman, C. J.; Ober, C. K. Advances in Polymers for Anti-biofouling Surfaces. *Journal of Materials Chemistry* **2008,** *18* (29), 3405-3413.

8. Wang, J.; Bhattacharyya, J.; Mastria, E.; Chilkoti, A. A Quantitative Study of the Intracellular Fate of pH-responsive Doxorubicin-polypeptide Nanoparticles. *Journal of Controlled Release: Official Journal of the Controlled Release Society* **2017,** *260*, 100-110.

9. Hruby, M.; Konak, C.; Ulbrich, K. Polymeric Micellar pH-sensitive Drug Delivery System for Doxorubicin. *Journal of Controlled Release: Official Journal of the Controlled Release Society* **2005,** *103* (1), 137-148.

10. Moulay, S. Dopa/Catechol-Tethered Polymers: Bioadhesives and Biomimetic Adhesive Materials. *Polymer Reviews* **2014,** *54* (3), 436-513.

11. Mahmoudi, M.; Sant, S.; Wang, B.; Laurent, S.; Sen, T. Superparamagnetic Iron Oxide Nanoparticles (SPIONs): Development, Surface Modification, and Applications in Chemotherapy. *Advanced Drug Delivery Reviews* **2011,** *63* (1-2), 24-46.

12. Xu, L.; Xia, J.; Wang, L.; Qian, J.; Li, H.; Wang, K.; Sun, K.; He, M. alpha-Fe2O3 Cubes with High Visible-light-activated Photoelectrochemical Activity towards Glucose: Hydrothermal Synthesis Assisted by a Hydrophobic Ionic Liquid. *Chemistry* **2014,** *20* (8), 2244-53.

15. Kim, S. M.; Park, S. B.; Bedair, T. M.; Kim, M. H.; Park, B. J.; Joung, Y. K.; Han, D. K. The Effect of Solvents and Hydrophilic Additive on Stable Coating and Controllable Sirolimus Release System for Drug-Eluting Stent. *Materials Science & Engineering. C, Materials for Biological Applications* **2017,** *78*, 39-46.

16. Patel, S. K.; Lavasanifar, A.; Choi, P. Roles of Nonpolar and Polar Intermolecular Interactions in the Improvement of the Drug Loading Capacity of PEO-b-PCL with Increasing PCL Content for Two Hydrophobic Cucurbitacin Drugs. *Biomacromolecules* **2009,** *10* (9), 2584-2591.

17. Kocak, G.; Solmaz, G.; Bütün, V. A New Approach for the Synthesis of pH-Responsive Cross-Linked Micelles from a Poly(glycidyl methacrylate)-Based Functional Copolymer. *Macromolecular Chemistry and Physics* **2016,** *217* (24), 2744-2754.

Acknowledgement

I am deeply indebted to Prof. Dr. Atsushi Takahara, my supervisors, for his patience, supervision, encouragement and thoughtful guidance towards the completion of this thesis. I wish to express special appreciation to Assoc. Prof. Dr. Ken Kojio for his help, support, interest and valuable hints. I am profoundly thankful to Dr. Tomoyasu Hirai, Dr. Yuji Higaki, Dr. Wei Ma, and Takahara Lab members in Institute for Materials Chemistry and Engineering (IMCE) for their friendship, support, advice, encouragement, and criticism. Prof. Yoshiko Miura and Prof. Keiji TANAKA are appreciated for helps and advices to complete this thesis. Last but not least, I would like to acknowledge to my beloved family and China Scholarship council, whose support enabled me to complete this research.